Precambrian Research 318 (2018) 25–69

Contents lists available at ScienceDirect

Precambrian Research

journal homepage: www.elsevier.com/locate/precamres

Strain variations across the Proterozoic Penokean Orogen, USA and Canada

John P. Craddock[a,*], David H. Malone[b], Mark D. Schmitz[c], Jennifer N. Gifford[d]

[a] Geology Department, Macalester College, St. Paul, MN 55105, USA
[b] Department of Geography-Geology, Illinois State University, Normal, IL, USA
[c] Department of Geosciences, Boise State University, Boise, ID 83725, USA
[d] The University of Mississippi, Geology & Geological Engineering, 120-A Carrier Hall, University, MS 38677-1848, USA

A B S T R A C T

Strata in the Huron (2.5–2.0 Ga) and Animikie (2.2–1.85 Ga) basins were deposited on the southern margin of the Archean Superior province. These rocks were deformed during the Penokean orogeny (~1850 Ma) followed by subsequent accretionary orogens to the south at 1750 Ma (Yavapai) and 1630 Ma (Mazatzal). Strain patterns are unique to each orogenic belt with no far-field effect: Archean Wawa terrane rocks in the Penokean foreland preserve deformation associated with Archean accretion with no younger Penokean, Yavapai or Mazatzal strain overprint. The Penokean orogeny deformed Huron-Animikie basin sediments into a north-vergent fold-and-thrust belt with no Yavapai or Mazatzal strain overprint. Yavapai orogen strains (SW-NE margin-parallel shortening) are unique when compared to the younger Mazatzal shortening (N20°W) shortening, with no strain overprint.

Penokean deformation is characterized by shortening from the south including uplifted Archean gneisses and a northerly thin-skinned fold-and-thrust belt, with north-vergent nappes and a gently-dipping foreland. Our study of finite and calcite twinning strains (n = 60) along (~1500 km) and across (~200 km) the Penokean belt indicate that this orogeny was collisional as layer-parallel shortening axes are parallel across the belt, or parallel to the tectonic transport direction (~N-S). Penokean nappe burial near the margin resulted in vertical shortening strain overprints, some of which are layer-normal. The Sudbury impact layer (1850 Ma) is found across the Animikie basin and provides a widespread deformation marker with many local, unique strain observations. We also report new geochronology (U-Pb zircon and apatite) for the gneiss-mafic dike rocks at Wissota (Chippewa Falls, WI) and Arbutus (Black River Falls, WI) dams, respectively, which bears on Penokean-Yavapai deformation in the Archean Marshfield terrane which was accreted during the Penokean orogen. Pseudotachylite formation was common in the Superior province Archean basement rocks, especially along terrane boundaries reactivated by contemporaneous Penokean, Trans-Hudson, Cape Smith and New Quebec deformation. In the hinterland (south), the younger Yavapai orogen (1750 Ma; n = 8) deformation is preserved as margin-parallel horizontal shortening (~SW-NE) in Yavapai crust and up to 200 km to the north in the Penokean thrust belt as a strain and Barrovian metamorphic overprint. Mazatzal deformation (1630 Ma; n = 16) is preserved in quartzites on Yavapai and Penokean crust with layer-parallel and layer-normal shortening strains oriented N20°W.

1. Introduction

The Penokean orogen (1850 Ma), on the southern margin of the Archean Superior province, is one of four contemporaneous Proterozoic orogens that accreted new crust to proto-Laurentia from every direction, the first significant crustal addition to proto-Laurentia since the end of the Archean (Hoffman, 1988; Whitmeyer and Karlstrom, 2007). The Penokee Mountains include a southern, thick-skinned hinterland, a central thrust belt with north-vergent nappes and a foreland in the northerly Huron and Animikie basins along a distance of ~1500 km (Holst, 1993; Schultz and Cannon, 2007; Fig. 1). These exposures afford a strain study along and across (~200 km) strike of a mountain building event that changed subduction polarity as it evolved (Schultz and Cannon, 2007) and includes a stratigraphic marker at 1850 Ma that corresponds with the proximal Sudbury impact (e.g. Fralick et al., 2002; Addison et al., 2005; Pufahl et al., 2007; Cannon et al., 2009; Fig. 2). Previous strain studies across thrust belts (Chapple, 1978) have documented the role of far-field stress and strain fields in the interpretation of subsequent thrust sheet motions (Craddock and van der Pluijm, 1989; van der Pluijm et al., 1997) demonstrating that collisional orogens have no thrust sheet rotations (Appalachians: Kilsdonk and Wiltschko, 1988; Hnat and van der Pluijm, 2011) and oblique convergence results in thrust sheet rotations during orogenic shortening (Sevier belt, Craddock, 1992, Gondwanide belt, Craddock et al. 2007). The Penokean orogeny deformed the Huron and Animikie basins which include a diverse suite of metasedimentary rocks that require a variety of strain measuring techniques to understand the deformational dynamics and unravel the tectonic history of the belt.

Our contribution is a study of strains along and across the Penokean orogen in Ontario (east), Michigan, Wisconsin and Minnesota (west) in comparison to older strain data from the Archean Wawa and Wabigoon belts to the north (i.e., Archean basement in the Penokean foreland; Card, 1990) and the younger, Mesoproterozoic Yavapai (1750 Ma) and Mazatzal (1630 Ma; Craddock and McKiernan, 2007) accretionary

* Corresponding author.
E-mail address: Craddock@macalester.edu (J.P. Craddock).

https://doi.org/10.1016/j.precamres.2018.09.004
Received 15 January 2018; Received in revised form 27 August 2018; Accepted 11 September 2018
Available online 26 September 2018
0301-9268/

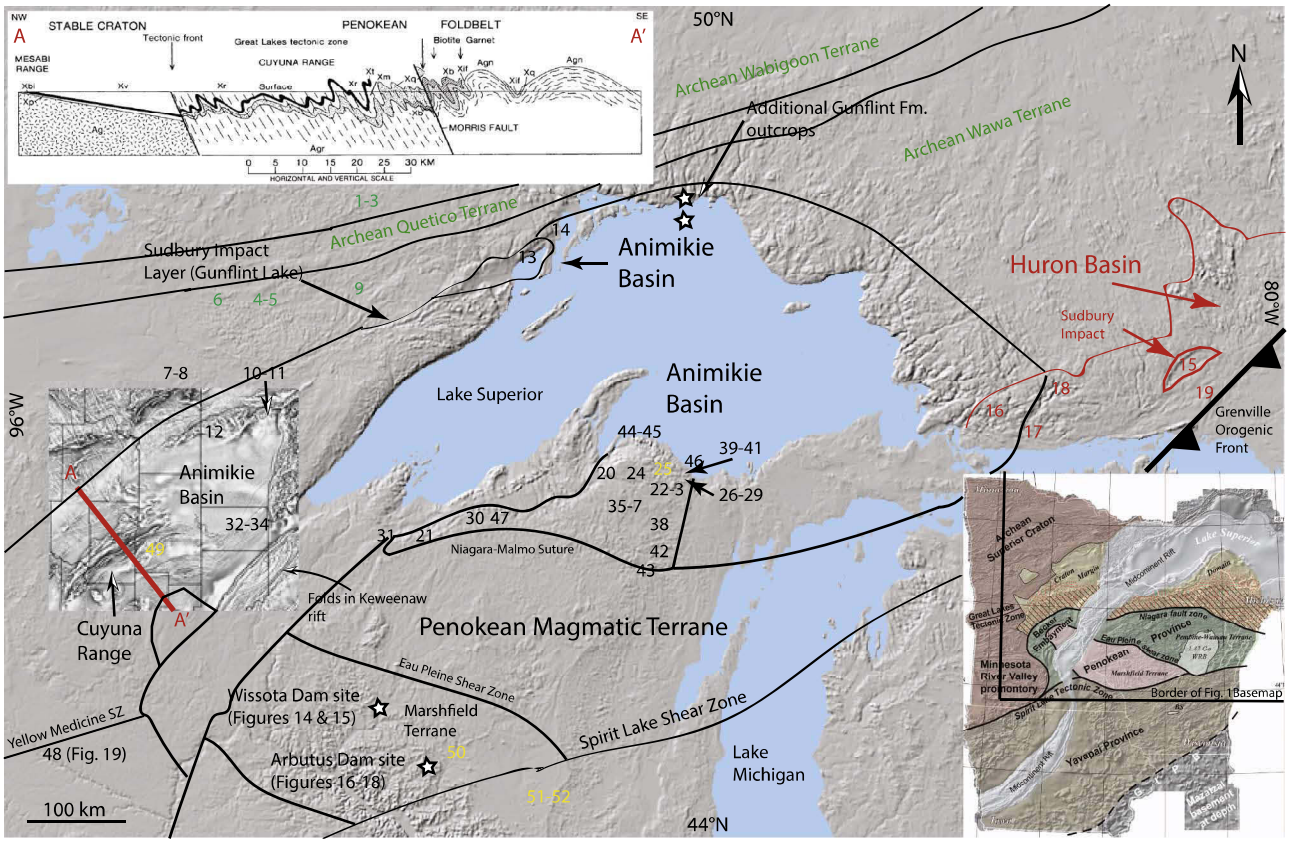

Fig. 1. Shaded relief basemap of the Lake Superior region showing the locations of Huron and Animikie basin sediments deformed by the Penokean orogen. Strain sample sites are identified (see Table 1). Inset map shows the Archean Superior province (Hoffman, 1988; Card, 1990) and accreted juvenile crust to the south (NICE, 2006). Aeromagnetic inset in Minnesota shows the Cuyuna Range and Animike foreland (Chandler, 1991), referenced to the cross section above (McSwiggen et al., 1995). Strains in Archean rocks are in green, Penokean Huron strain samples are red, Animikie basin samples are black and Yavapai-Mazatzal strain sites are yellow. (For interpretation of the references to colour in this figure legend, the reader is referred to the web version of this article.)

orogenic belts to the south (Fig. 1, see inset). With these new data we can address the variations in tectonic shortening along and across the Penokean belt to identify the orogen as oblique or collisional accretion. We can also interpret the presence of unique strain patterns in younger accreted crust and any far-field strain overprints in older crust to the north of the respective active margins between 1850 and 1630 Ma.

2. Regional geology

Within the Archean Superior province, there are ~15 convoluted SW-NE trending belts that were sutured together by north-dipping subduction, from north to south, between 2.77 and 2.73 Ga and include the 3.0 Ga Marmion terrane (e.g. Card, 1990; Percival et al., 2006; Percival, 2007). The Superior province is surrounded by orogenic crust (1.85 Ga) accreted from the south (Penokean orogen), west and north (Trans-Hudson, Cape Smith), and east (New Quebec) that preserves the Archean accretion of these granite-greenstone, gneiss and metasedimentary terranes into the protocontinent Laurentia (Hoffman, 1988; Corrigan et al., 2009). Along the curved, southern margin of Laurentia, there are Archean gneisses (3.0–3.6 Ga) of the Minnesota River valley terrane (MRV: Goldich and Hedge, 1962; Schmitz et al., 2006; Bickford et al., 2006) and the Watersmeet, MI area (3.5 Ga; Van Schmus, 1980). The Great Lakes tectonic zone (Southwick et al., 1988) separates the Wawa greenstone terrane from these older gneiss belts to the south (Fig. 1). The Watersmeet gneiss domes appear to be a cohesive terrane whereas the MRV is composed of 4 gneiss terranes that docked in succession along NW-dipping, NE-striking reverse faults (Gibbs et al., 1981; Boyd and Smithson, 1994) forming a significant tectonic promontory and embayment. Neoarchean gneiss belts are not known to underlie the Huronian basin although such gneisses may be obscured by the Grenville orogenic front. The curved shape of the southern Laurentian margin influenced the subsequent Huron-Animikie deposition and Penokean orogen terrane accretion (Van Schmus and Bickford, 1981; Bickford et al., 1986; Van Wyck and Johnson, 1997; Ernst and Bleeker, 2010).

The Huron basin contains a southward thickening wedge of sedimentary and volcanic rocks, the Huronian Supergroup, that attain a maximum thickness of about 12 km. These rocks unconformably overly the Archean Superior Province in Ontario, including the Wawa and Abitibi greenstone belts. The Huronian section is dominantly composed of siliclastic rocks with paleocurrent patterns indicating that sediment was derived from eroding highlands to the north and west (Long, 1995).

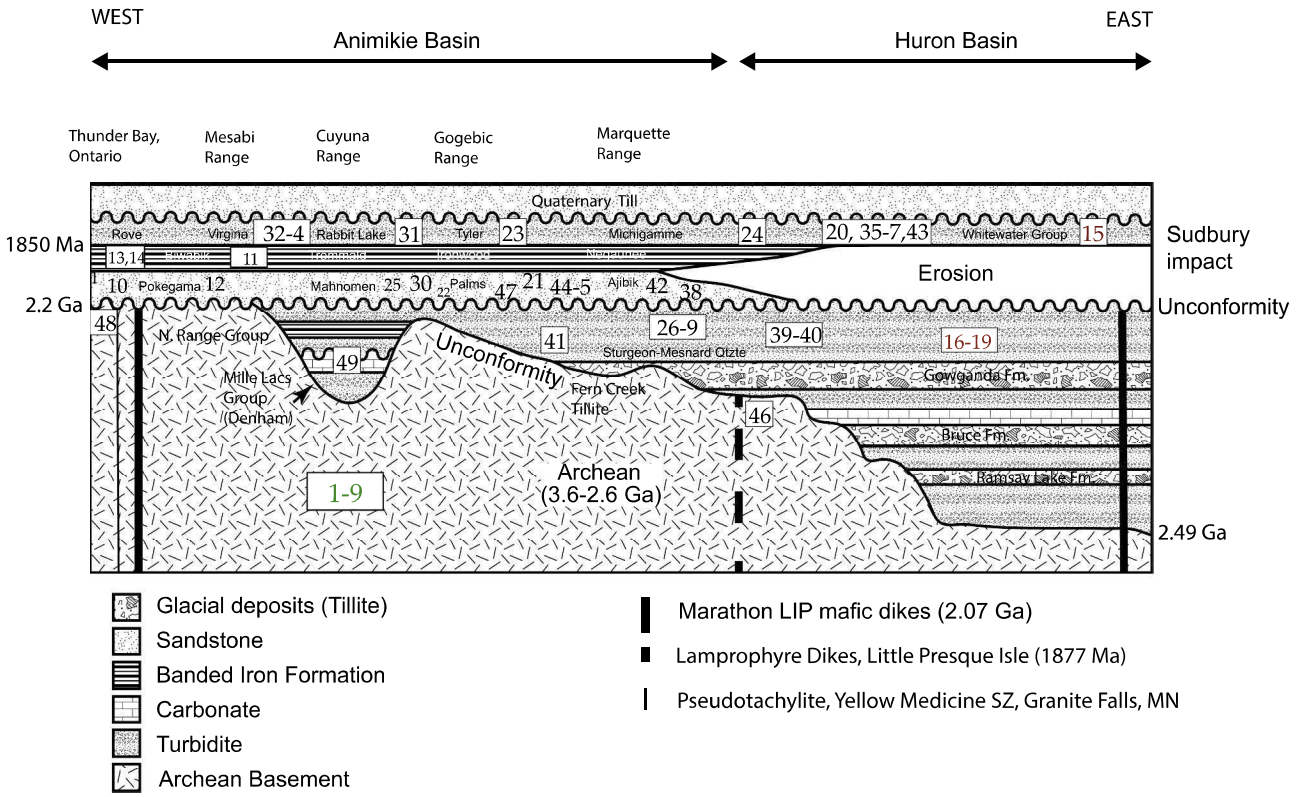

Fig. 2. Schematic cross section from ~W to E across the Animikie and Huron basins showing the regional stratigraphic relations and locations of strain samples (Table 1; Fig. 1) Adapted from Young (1983), Ojakangas (1994), Ojakangas et al. (2001), Vallini et al. (2006, 2007) and Schulz and Cannon (2007). Animikie samples are in black, Huronian samples in red, Archean footwall samples are in green (see Fig. 1). (For interpretation of the references to colour in this figure legend, the reader is referred to the web version of this article.)

The stratigraphic section comprises four unconformity-bounded successions (groups-see Roscoe, 1969; Young, 1973). The lowermost, Elliot Lake Group, is a succession of immature quartzite and metaconglomerate of the Livingstone Creek Formation that are overlain by bimodal volcanic rocks, including the Thessalon Formation in the western Huron Basin (Bennett et al., 1991) and the Elsie Mountain, Stobie and Copper Cliff formations in the southeastern Huron Basin (Roscoe and Card, 1993) and overlying and intercalated conglomerate, sandstone and mudstone of the Matinenda and McKim formations. The succeeding three successions (Hough Lake, Quirke Lake and Cobalt Groups) define climatically controlled cycles that each begin with a formation containing glacial diamictite (Ramsay Lake, Bruce and Gowganda formations, respectively), followed by a mudrock-dominated marine unit (Pecors, Espanola and Firstbrook formations, respectively) that grades upward to a sequence of fluvial sandstone (Mississagi, Serpent formations, respectively) and fluvial to shallow marine sandstone (Lorrain formation) showing evidence of deposition under humid climatic conditions (Young, 1973; Fig. 2). The uppermost Huronian is capped by peritidal and shallow marine deposits of the Gordon Lake and Bar River formations. The tectonic setting of the Huron basin is long-debated. A comprehensive summary by Long (2004) suggests that the Elliot Lake and Hough Lake groups were deposited by transverse and axial braided river systems in fault-bounded rift and strike-slip basins oriented parallel to major E-W trending faults (e.g. Murray fault). Rift-related terrestrial deposition continued through deposition of the Quirke Lake Group and was restricted mainly to the western and southeastern Huron basins. This was followed by regional thermal subsidence, possibly on a passive margin, as shown by the broader regional distribution and marine influence on deposition of the Cobalt Group (e.g. Cobalt Basin). The depositional age of the Huronian is bracketed between ca. 2452.5 ± 6.2 Ma, the age of the basal Copper Cliff flows (Ketchum et al., 2013) of the Elliot Lake Group, and circa 2219 Ma, the age of the oldest Nipissing gabbro sills, which intruded the entire succession (Corfu and Andrews, 1986). Rasmussen et al. (2013) have reported a U-Pb zircon age of 2308 Ma from an ash bed in the Gordon Lake Fm. near the top of the section. Folding is associated with intrusion of the Nipissing sills (Easton, 2006). Detrital zircons in the Huron section indicate a dominant source from the Superior province to the north as well as a small fraction of zircons that source ~1500 km from the west in the MRV (3000–3600 Ma) terranes (Craddock et al., 2013a).

Deposition of basal strata of the Animikie basin along the southern margin of Laurentia was characterized by significant stratigraphic and sedimentologic variability (Fig. 2; Young, 1973, 1983; Ojakangas, 1994; Ojakangas et al., 2001; Schultz and Cannon, 2007). This initial stratigraphic complexity was accentuated by complex Penokean deformation. The lowest units are the Mille Lacs (with the Denham section) and North Range Groups in central Minnesota which correlate with the glacial diamictite-quartzite-dolomite sequence of the Chocolay

Table 1
Strain Results, Penokean Foreland, Thrust Belt and Hinterland.

	Sample ID	Rock Unit	Orogenic	εAnalysis/Age	Orientation	Grains (n=)	ε1	ε2	ε3	ε1 (%)	NEV (%)	Vσ(MPa)	Fabric Interp.	Location	Comment
	(see Fig. 1)		Distance (km)												
Archean	1	Steep Rock	220	CTA/2.7 Ga	60°, 80°S	25	145°, 35°	306°, 338°	58°, 3°	−1.95	3	−34	LNS	Steep Rock, Atikokan, ONT	Fig. 4d
Footwall	2	Steep Rock	220	CTA/2.7 Ga	60°, 80°S	23	231°, 5°	334°, 6°	170°, 87°	−1.325	1	−31	LNS	Steep Rock, Atikokan, ONT	
(north)	3	Steep Rock	220	CTA/2.7 Ga	60°, 80°S	23	325°, 5°	251°, 14°	71°, 87°	−2.05	1	−35	LNS	Steep Rock, Atikokan, ONT	
	4	Ely Greenstone	150	CTA/2.6 Ga	70°, 90°	32	340°, 85°	273°, 11°	168°, 23°	−5.1	9	−37	LPS	Ely, MN	Pillow Rims
	5	Ely Greenstone	150	CTA/2.6 Ga	70°, 90°	38	348°, 83°	68°, 4°	162°, 7°	−6.3	7	−34	LPS	Ely, MN	Vein
	6	KK dike	150	CTA/2.06 Ga	340°, 90°	25	341°, 5°	81°, 13°	166°, 83°	−7.7	16	−28	LPS	Tower, MN	Craddock and Moshoian (1995)
	7	KK dike	150	CTA/2.06 Ga	331°, 90°	13	333°, 7°	73°, 2°	258°, 88°	−5.5	0	−31	LPS	Lake Kabetogama, MN	Craddock and Moshoian (1995)
	8	KK dike	150	CTA/2.06 Ga	331°, 90°	14	166°, 5°	252°, 14°	68°, 82°	−5.8	7	−33	LPS	Lake Kabetogama, MN	Craddock and Moshoian (1995)
	9	KK lamprophyre	150	CTA/2.06 Ga	0°, 90°	16	1°, 2°	268°, 45°	94°, 32°	−3.9	0	−27	LPS/ DPS	Saganaga Lake, MN	2.06 Ga Ar−Ar age (Fig. 6)
Thrust Belt	10	Pokegama Qtzte	100	ACF/ > 1.8 Ga	35°, 5°S		110°, 2°	191°, 46°	8°, 43°				LPS	Eveleth, Mesabi Range, MN	
Foreland	10	Pokegama Qtzte	100	AMS/ > 1.8 Ga	35°, 5°S	21 cubes	Kmin = 90°		Kmax = random				LNS	Eveleth, Mesabi Range, MN	
	11	Biwabiki BIF	100	AMS/ > 1.8 Ga	35°, 5°S	28 cubes	Kmin = 90°		Kmax = SE−NW				LNS	Eveleth, Mesabi Range, MN	Fig. 3e, f
	11	Biwabik BIF	100	CTA/ > 1.8 Ga	35°, 5°S	12	138°, 4°	49°, 84°	257°, 6°	−3.5	0	−31	LPS	Eveleth, Mesabi Range, MN	Thunderbird mine; Fig. 5e
	12	Pokegama Qtzte	100	ACF	Horizontal		330°, 6°	63°, 15°	255°, 83°				LPS	Grand Rapids, Mesabi Rge.	
	13	Gunflint Fm.	100	CTA/LS	Horizontal	18	352°, 6°	182°, 83°	292°, 8°	−1.3	5	−22	LPS	E. Thunder Bay roadcut	
	14	Gunflint Fm.	100	Vein CTA/ > 1.8 Ga	90°, 90°	14	3°, 47°	273°, 4°	191°, 55°	−7.7	28	−37	LPS	Sibley Pen., Ontario	Pass Lake Traverse (Figs. 5d, 8)
	14	Gunflint Fm.	100	LS CTA/ > 1.8 Ga	Horizontal	12	188°, 12°	281°, 7°	12°, 77°	−2.1	0	−24	LPS	Sibley Pen., Ontario	Pass Lake Traverse (Fig. 8)
	14	Gunflint Fm.	100	Vein CTA/ > 1.8 Ga	50°, 90°	13	351°, 9°	284°, 5°	221°, 87°	−5.7	7	−31	LPS	Sibley Pen., Ontario	Pass Lake Traverse (Fig. 8)
	14	Gunflint Fm.	100	Vein CTA/ > 1.8 Ga	90°, 90°	19	183°, 6°	267°, 3°	327°, 88°	−7.9	7	−35	LPS	Sibley Pen., Ontario	Pass Lake Traverse (Fig. 8)
	14	Gunflint Fm.	100	LS CTA/ > 1.8 Ga	Horizontal	20	178°, 6°	272°, 3°	68°, 84°	−2.3	0	−26	LPS	Thunder Bay	
	14	Gunflint Fm.	100	LS CTA/ > 1.8 Ga	Horizontal	17	183°, 23°	312°, 47°	112°, 36°	−3.1	0	−27	LPS	Thunder Bay	

(*continued on next page*)

Table 1 (*continued*)

	Sample ID	Rock Unit	Orogenic	εAnalysis/Age	Orientation	Grains (n =)	ε1	ε2	ε3	ε1 (%)	NEV (%)	Vo(MPa)	Fabric Interp.	Location	Comment
Thrust Belt	15	Sudbury Impact	90	Impact Shape			340°, 0°	vertical	70°, 0°	2:1			LPS		Fig. 1
	15	Sudbury Impact	90	Concretions	Horizontal	n = 54	340°, 0°	vertical	70°, 0°	2:1			LPS	Chelmsford Fm., Sudbury	Fig. 3b
	16	Huronian Quartzite	90	ACF	Horizontal		171°, 7°	77°, 4°	350°, 84°				LPS	Lorrain Fm.; Batchawana	Fig. 3c
	17	Huronian Quartzite	90	ACF	90°, 65°S		178°, 58°	84°, 6°	347°, 37°				LPS	Lorrain Fm.; Desbarat	
	18	Huronian Quartzite	90	ACF	Horizontal		342°, 9°	265°, 6°	135°, 84°				LPS	Lorrain Fm.: Elliot Lake	
	19	Huronian Quartzite	90	ACF	Horizontal		338°, 5°	42°, 6°	182°, 84°				LPS	Grenville footwall, Sudbury	
	19	Espanola Fm.	90	CTA	Horizontal	No Twins								Elliot Lake area	
	20	Michigamme Fm.	120	CTA/vein	90°, 60° S	34	177°, 8°	305°, 23°	57°, 33°	−3.5	5	−37	LPS	L'Anse, MI	
	21	Bad River Dolomite	20	CTA/ > 1.8 Ga	Horizontal	14	36°, 5°	116°, 7°	277°, 86°	−2.3	28	−27	LPS	Quarry, Namekagon, WI	
	22	SIL lapilli	140	ACF	0°, 30°E		327°, 55°	217°, 11°	132°, 41°				LNS	Connors Creek, MI	Figs. 3a & 5b
	23	Mesnard Quartzite	120	ACF	80°, 60° S		168°, 58°	77°, 5°	338°, 51°				LPS	Negaunee, MI	
	24	Siamo Slate	120	CTA/vein	90°, 60° S	28	183°, 55°	93°, 5°	344°, 83°	−5.6	11	−33	LPS	Negaunee, MI	
	25	Hemlock volcanics	130	CTA/replacement	110°, 90°	38	278°, 5°	211°, 9°	33°, 85°	−6.6	0	−41	LPS/ VPS	Clarksburg, MI	Fig. 5c
	25	Hemlock volcanics	130	CTA/replacement	90°, 90°	36	87°, 8°	177°, 9°	351°, 82°	−7.1	0	−40	LPS/ VPS	Clarksburg, MI	
	26	Sturgeon Qtzte	120	ACF	90°, 90°		181°, 88°	1°, 2°	270°, 6°				LPS	Marquette, MI	
	27	Kona Dolomite	120	CTA/veins	90°, 90°	23	355°, 86	88°, 3°	178°, 4°	−2.1	30	−28	LPS	Marquette, MI	
	28	Kona Dolomite	120	CTA/veins	90°, 90°	14	62°, 8°	181°, 82°	342°, 12°	−10.1	21	−24	LPS/ VNS	Marquette, MI	
	29	Kona Dolomite	120	CTA/veins	0°, 90°	27	355°, 31°	131°, 44°	262°, 5°	−8.6	21	−18	LPS/ VNS	Marquette, MI	
	30	Palms Fm.	30	ACF	90°, 90°		85°, 6°	183°, 86°	351°, 8°				LPS	Wakefield, MI	
	31	Tyler Fm.	20	ACF	60°, 61° NW		2°, 88°	266°, 6°	173°, 5°				LPS	Hurley, WI	
	32	Thomson Fm.	40	CTA/ > 1.8 Ga	72°, 52° S	17	116°, 57°	213°, 8°	306°, 22°	−7.9	17	−24	LPS	Carlton, MN	Fig. 5a
	33	Thomson Fm.	40	AMS	Horizontal	29 cubes	Kmin = 90°		Kmax = 0°				LPS	Carlton, MN	
	34	Thomson Fm.	40	Concretions	Variable	23 locales	Prolate		Oblate				LPS/ LNS	Carlton & Pine counties, MN	Holst (1985); Holm et al. (1988)
	35	Michigamme Fm.	60	CTA/veins	90°, 90°	24	332°, 12°	222°, 13°	86°. 87°	−5.1	25	−17	LNS	N. Crystal Falls, MI	
	36	Michigamme Fm.	40	CTA/veins	90°, 90°	35	352°, 6°	266°, 11°	99°, 85°	−14.1	22	−19	LNS	N. Crystal Falls, MI	
	37	Michigamme Fm.	70	ACF/ > 1.8 Ga	Horizontal		205°, 7°	1°, 87°	133°, 3°				LPS	Canyon Falls. MI	
	38	Randville Dolomite	110	CTA/veins	0°, 90°	18	6°, 3°	83°, 4°	182°, 88°	−3.2	37	−22	LPS	Fumee Wayside, MI	
	39	Mesnard Qtzte.	100	SEM/dislocations	Steep dips							−33 to −73	n/a	Republic syncline	Kappmeyer and Wiltschko (1984)
	40	Kona Dolomite	70	ACF/reduction spots	Variable		1°, 5°	90°, 88°	271°, 3°					Marquette County, MI	Westjohn (1978)

(*continued on next page*)

Table 1 (*continued*)

	Sample ID	Rock Unit	Orogenic	εAnalysis/Age	Orientation	Grains (n =)	ε1	ε2	ε3	ε1 (%)	NEV (%)	Vo(MPa)	Fabric Interp.	Location	Comment
	40	Kona Dolomite	70	ACF/reduction spots	Variable		320°, 1°	220°, 1°	140°, 88°					Marquette County, MI	Meyer (1983)
	41	Enchant. Lake Fm.	70	ACF	Variable		187°, 5°	272°, 4°	46°, 88°					Marquette County, MI	Carter (1989)
	42	Sturgeon Qtzte	10	ACF	90°, 90°		70°, 65°	161°, 6°	242°, 21°				LPS	Loretto, MI	
	43	Michigamme Fm.	10	ACF	90°, 90°		4°, 82°	353°, 7°	82°, 14°				LNS	Falls Canyon, WI	
Basal Thrust	44	Basal Marquette	100	CTA/LS	Horizontal	28	164°, 3°	84°, 13°	302°, 84°	−3.3	12	−34	LPS	Big Erich Falls, MI	DNAG ref.
Belt	45	Basal Marquette	100	CTA/vein	Horizontal	32	342°, 8°	263°, 13°	72°, 78°	−3.7	4	−36	LPS/ VPS	Big Erich Falls, MI	DNAG ref.
	46	Lamprophyres	110	CTA/1.77 Ga	0°, 90°	83	26, 12°	144°, 87°	334°, 38°	−2.5	0	−37	LNS	Little Presque Isle	Craddock et al. (2007)
	46	Lamprophyres	110	CTA/1.77 Ga	0°, 90°	24	301°, 84°	88°, 21°	167°, 22°	−4.1	100		LNS	Little Presque Isle	Craddock et al. (2007)
	46	Lamprophyres	110	CTA/1.77 Ga	90°, 90°	65	38°, 9°	126°, 62°	338°, 57°	−2.2	0	−35	LNS	Little Presque Isle	Craddock et al. (2007)
	46	Lamprophyres	110	CTA/1.77 Ga	90°, 90°	24	157°, 82°	342°, 47°	243°, 26°	−3.4	100		LNS	Little Presque Isle	Craddock et al. (2007)
	46	Lamprophyres	110	CTA/veins	0°, 90°	273	43°, 14°	337°, 11°	181°, 88°	−8.6	0	−34	LNS	Little Presque Isle	Craddock et al. (2007)
	46	Lamprophyres	110	CTA/veins	90°, 90°	29	47°, 5°	131°, 32°	313°, 86°	−9.2	0	−34	LNS	Little Presque Isle	Craddock et al. (2007)
	46	Lamprophyres	110	CTA/veins	Combined	74	166°, 84°	235°, 41°	324°, 59°	−8.8	100		LNS	Little Presque Isle	Craddock et al. (2007)
	47	Basal Palms Fm.	30	CTA/fibers	Horizontal	22	186°, 5°	6°, 86°	268°, 5°	−13.1	25	−33	LPS	Wakefeld, MI	
	47	Basal Palms Fm.	30	CTA/fibers	Horizontal	46	202°, 26°	31°, 46°	131°, 6°	−3.65	23	−35	LPS	Wakefeld, MI	
	47	Basal Palms Fm.	30	CTA/fibers	Horizontal	18	1°, 23°	182°, 86°	273°, 3°	−13.3	0	−35	LPS	Wakefeld, MI	
	48	Pseudotachylite	50	CTA/1.8 Ga/Amyg.	60°, 90°	14	305°, 10°	201°, 1°	15°, 81°	−7.4	7	−44	VNS	Granite Falls, MN	Craddock and Magloughlin (2005)
	48	Pseudotachylite	50	CTA/1.8 Ga/vein	60°, 90°	18	312°, 9°	52°, 4°	161°, 82°	−2.4	16	−37	VNS	Granite Falls, MN	Craddock and Magloughlin (2005)
	48	Pseudotachylite	50	CTA/1.8 Ga/vein	60°, 90°	18	82°, 12°	12°, 9°	245°, 83°	−2.7	16	−34	VPS	Granite Falls, MN	Craddock and Magloughlin (2005)
Hinterland	49	Denham LS	−10	CTA/2.2 Ga	90°, 80° S	32	162°, 7°	72°, 8°	305°, 86°	−4.3	12	−29	LNS	Denham, MN	
	50	Veedum Qtzte	−200	ACF/?	90°, 65°S		181°, 5°	7°, 58°	273°, 3°				LPS	Veedum, WI	Spirit Lake Shear Zone; Fig. 13
	51	Seven Sisters Qtzte	−300	ACF/ < 1.76 Ga	Horizontal		343°, 12°	248°, 85°	78°, 11°				LPS	Hamilton Mound, WI	Craddock and McKiernan (2007)
(south)	52	H. Mound Qtzte	−300	ACF/ > 1.76 Ga	Horizontal		78°, 5°	169°, 7°	311°, 86°				LPS	Hamilton Mound, WI	

Key: CTA is calcite twin analysis; ACF is a finite strain technique (see Craddock and McKiernan, 2007); AMS is anisotropy of magnetic susceptibility. E1 is the shortening strain axis, E2 intermediate and E3 the extension axis.

LPS: Layer-parallel shortening; LNS: Layer-nornal shortening; VPS: vein-parallel shortening; VNS: vein-normal shortening.

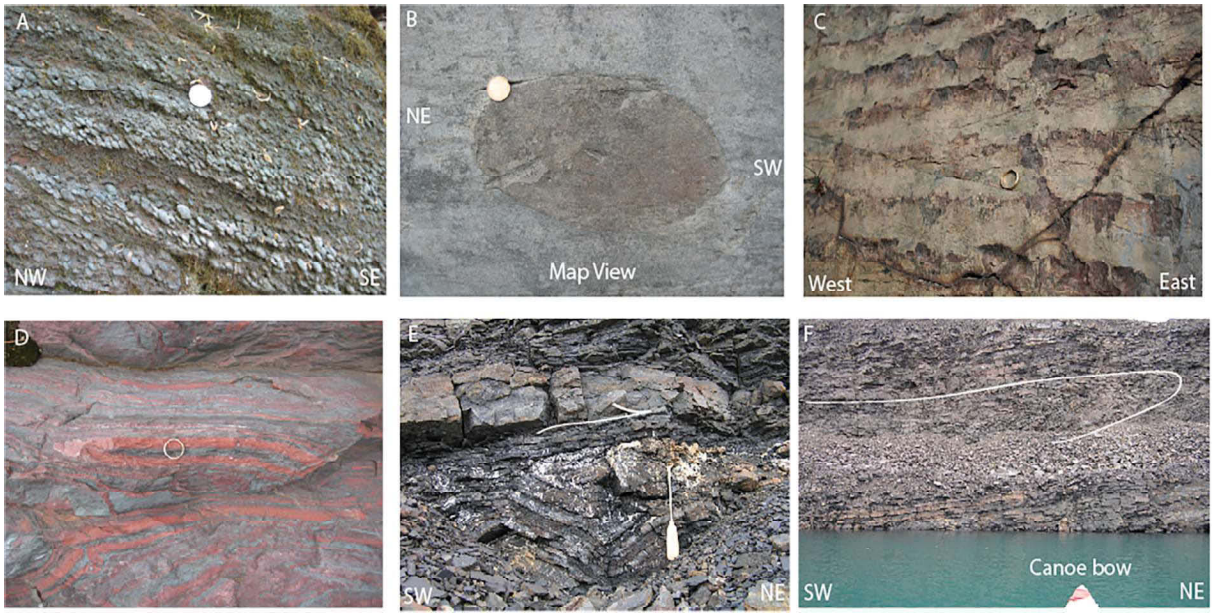

Fig. 3. Field photos of outcrop-scale deformation: A. Sudbury impact airfall lapilli (Connors Creek, MI), B. Ellipsoidal concretions in the Chelmsford Fm. within the Sudbury structure, C. Dip-slip striations on the limb of a Penokean anticline preserved in the Huronian Lorraine Fm. (2.4 cm diamter ring for scale), D. Complex folds in banded iron formation, Ishpeming, MI (2.4 cm diameter ring for scale), E. complex contractional folds in Biwabik iron formation, Virginia, MN, F. sheath fold in Biwabik iron formation, Virginia, MN (canoe for scale).

Group in the Marquette range, Michigan, which correlates with the Gowganda-Bar River (Cobalt Group) of the western Huron section (Pettijohn, 1943; Young, 1973). The upper Chocolay Group is separated from the lower Animikie (Menominee) Group by a regional unconformity that represents a depositional hiatus of ~300 Ma and the Animikie Group includes passive continental margin deposition: basal sandstone, Superior-type banded iron formation, and upper turbidite (Ojakangas et al., 2001) in unconformable contact with various Archean gneiss and greenston (2.6–3.6 Ga) starting at ~1930 Ma. Ojakangas et al. (2001) report local paleosols and calcite replacement of evaporite minerals suggesting lots of topographic variation across the Animikie basin in the lower Animikie Group. In the Animikie foreland, basal units unconformably overlie the Kenora-Kabetogama mafic dikes (2.07 Ga; Schmitz et al., 1995) which are part of the Marathon large igneous province (LIP; Halls et al., 2008). The Sudbury meteorite impact deposits (1.85 Ga; Addison et al., 2005) overly the Huronian section to the east (Sudbury basin) and are preserved across the southern margin in the Animikie basin as a tsunami and/or base-surge deposit, and appear to correlate with the demise of the depositional system that favored banded iron formations (Pufahl et al., 2007; Cannon et al., 2009), followed by Animikie turbidite deposition, including the Whitewater Group that overlies the Sudbury impact to the east. The Sudbury deposit, in conjunction with U-Pb ages of ash beds in the turbidites (Fralick et al., 2002) and Nd model ages from mudrocks have greatly aided in unraveling the complex history of Penokean deformation toward a clearer regional stratigraphy (see Craddock et al. 2013a, Fig. 5). The Animikie basin received a steady supply of Superior province zircons (2.6–2.7 Ga). The older strata also contain some zircons in the 3.5–3.8 Ga age spectra while the zircon populations in the upper turbidites are mostly of Penokean (arc) ages, including some late Penokean ages (1818 and 1826 Ma, Craddock et al., 2013a).

The Penokean orogen (e.g. Van Schmus, 1980; Sims et al., 1981; Schulz and Cannon, 2007 and references therein) spanned a period of 1.85–1.82 Ga based on Ar-Ar reset ages in Archean gneiss domes (Holm and Lux, 1996; Schneider et al., 1996; Holm et al., 1998; Tohver et al., 2007) and regional monazite U-Pb ages (Schneider et al., 2004). Van Schmus (1976) brackets the Penokean orogeny between 1890 and 1830 Ma using U-Pb zircon ages. Deformation along the Niagara-Malmo suture, where there are ophiolitic remnants, preserves evidence of north-directed thrusting and dextral penetrative fabrics (Klasner et al., 1993). Gross et al. (2006) provides detailed kinematic data for the Niagara-Malmo suture and interprets a complex deformational history that includes both normal and reverse motion. The Niagara-Malmo suture separates the Penokean orogen on the north from Penokean accreted terranes on the south (NICE, 2006) where Wunderman et al. (2018) report magnetotelluric (MT) imaging that identifies one SE-dipping subduction remnant. Most of the hanging-wall folds indicate north-directed thrust transport with finite strains (Brocum and Dalziel, 1974; Holst, 1982, 1984, 1985; Holm et al., 1988) preserving margin-normal (N-S) sub-horizontal shortening and a younger sub-vertical shortening (Craddock et al., 2007). Animikie strata in the Cuyuna and Mesabi ranges and near Thunder Bay preserve compressional, thrust-related, Penokean structures (McSwiggen et al. 1995; Jirsa et al., 2005; Hill and Smyk, 2005) and there are numerous small, mafic-ultramafic intrusions in the Penokean foreland that are attributed to decompression melting (1850–1900 Ma; Holm et al., 2007). It is now known that the regional BIF-hosted Barrovian metamorphic isograd patterns reported by James (1955; Rebublic, Peavy nodes) in the Animikie Group are the result of widespread Yavapai (~1.75 Ga) subduction to the south (Holm et al., 1998; Schneider et al., 2004; Tohver et al., 2007; Vallini et al. 2007). Huronian strata were also overthrust during the Grenville orogeny (Carr et al., 2000), and extended during

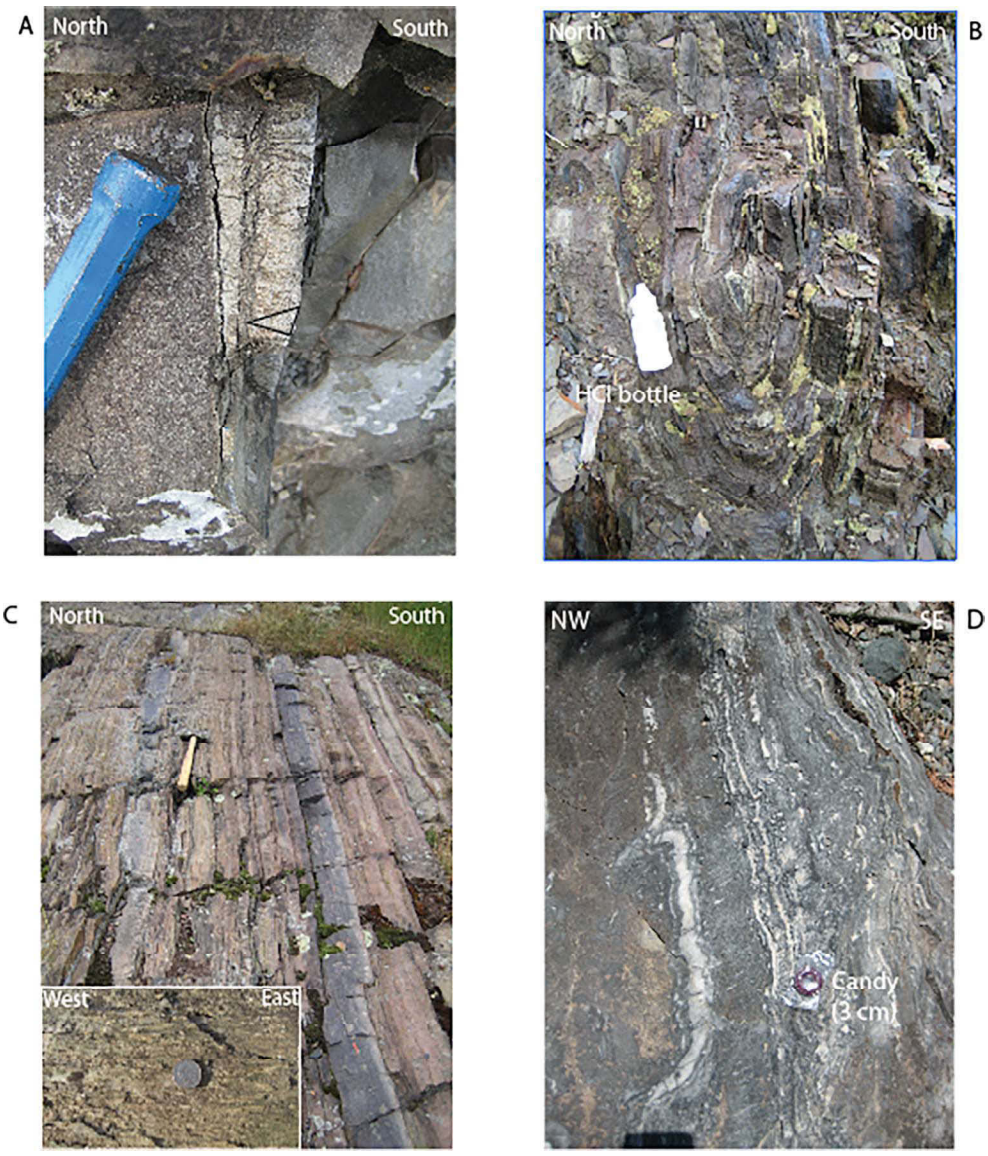

Fig. 4. (A) Cone-in-cone (apex to North) structures in the vertical Tyler Fm., Hurley, WI. (B) Isoclinal minor folds in the Riverton Iron Fm., Canyon Falls, MI. (C) E-W, vertical Palms Fm. with E-W, horizontal, sinistral striations (inset), Wakefield, MI. (D) Archean carbonate in the Steep Rock quarry, Atikokan, Ontario.

Midcontinent rift tectonism (1.1 Ga; Craddock et al., 2013b; Stein et al., 2014; Malone et al., 2016; Craddock et al., 2017a,b). This extension further complicates correlations between the Huronian and Animikie stratigraphic successions and Penokean structures (Fig. 2).

3. Methods

Appendix 1 includes the details of analytical methods used in this study for calcite twinning, finite strains, X-ray fluorescence, Ar/Ar (biotite) and U-Pb (zircon and apatite) geochronology and paleomagnetism.

4. Results

4.1. Field relations

Results are presented from oldest (Archean Wabigoon terrane) to youngest (Proterozoic Mazatzal quartzites; Fig. 1, Table 1). The regional stratigraphy of the Huron-Animikie basins is found in Fig. 2 with strain samples identified (Table 1); all the Huron-Animikie strata were deposited on Archean Wawa (Abitibi) crust and, locally, Archean MRV and Watersmeet gneisses. The variety of outcrop-scale sedimentological and structural observations are presented in Fig. 3 (folds, faults, strain elements) and 4 (cone-in-cone structure, minor folds, marble and strike-

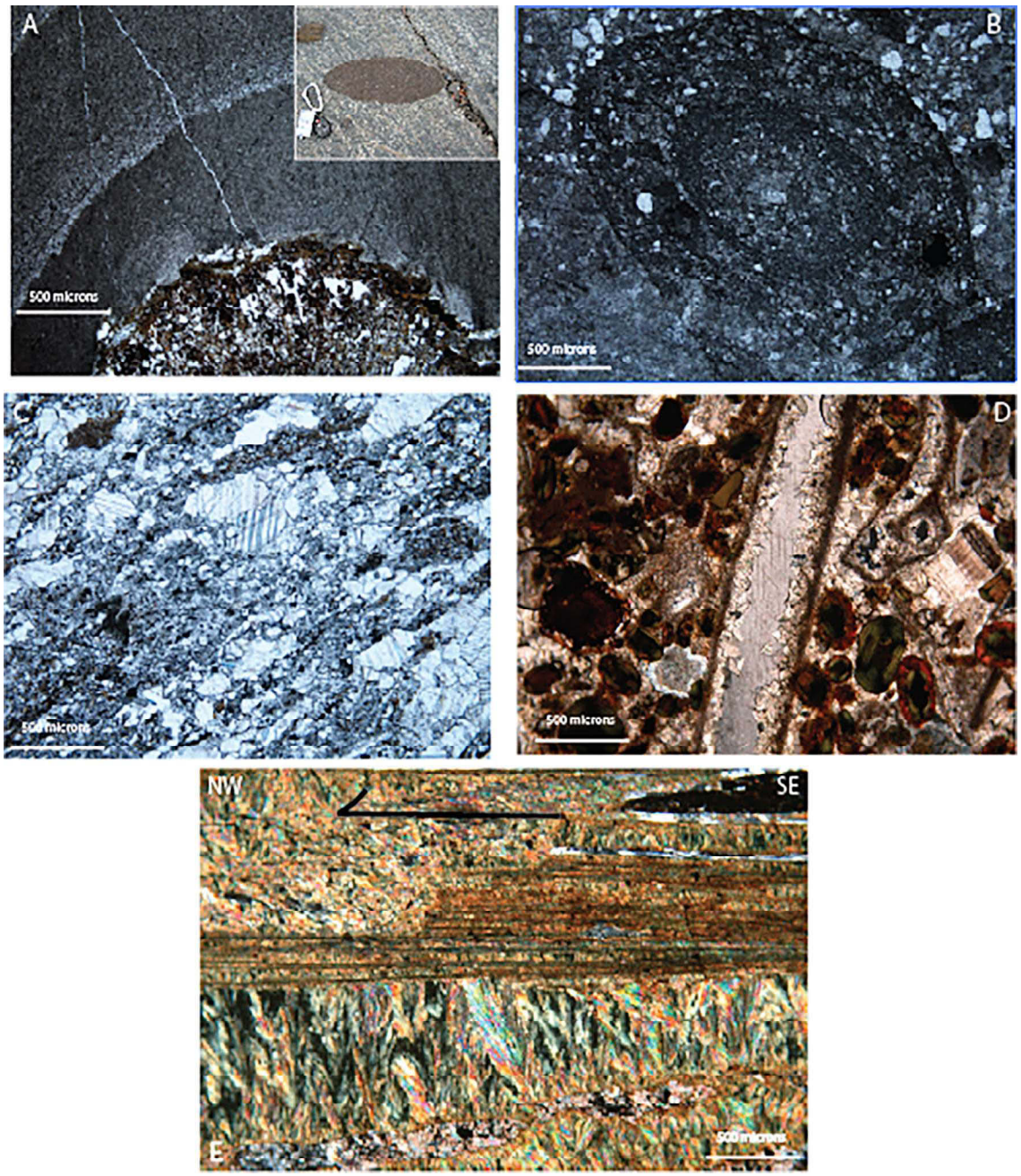

Fig. 5. Photomicrographs of various strain measuring elements in Animikie basin rocks: A. Zoned calcite-siderite rim of a carbonate concretion (XP; inset field photo), Thomson Fm., Minnesota, B. Sudbury impact ashfall lapilli (XP) found at Connors Creek, MI, C. Twinned replacement calcite (PL) in Hemlock Volcanics, Clarksburg, MI, D. Twinned calcite (PL) in Gunflint Fm., Ontario, E. Serpentinite-calcite (XP) steps in Biwabik iron formation, Eveleth, MN.

slip faults) and photomicrographs of strain elements and fault kinematics are shown inFig. 5. We also report a variety of strain results from Archean-hosted, pre-Penokean sites to the north (Fig. 6) and post-Penokean rocks that represent Yavapai and Mazatzal deformations which may be useful in interpreting younger strain overprints on Penokean rocks. Strain data is presented in Fig. 7a–f. Penokean footwall and foreland deformation is found in Figs. 8, 9 and 12, and the Sudbury impact relations in Figs. 10 and 11. Deformation in the Archean Marshfield terrane, at the Wissota, Arbutus and Veedum sites, is found in Figs. 13–18. Penokean pseudotachylite is presented in Figs. 19 and

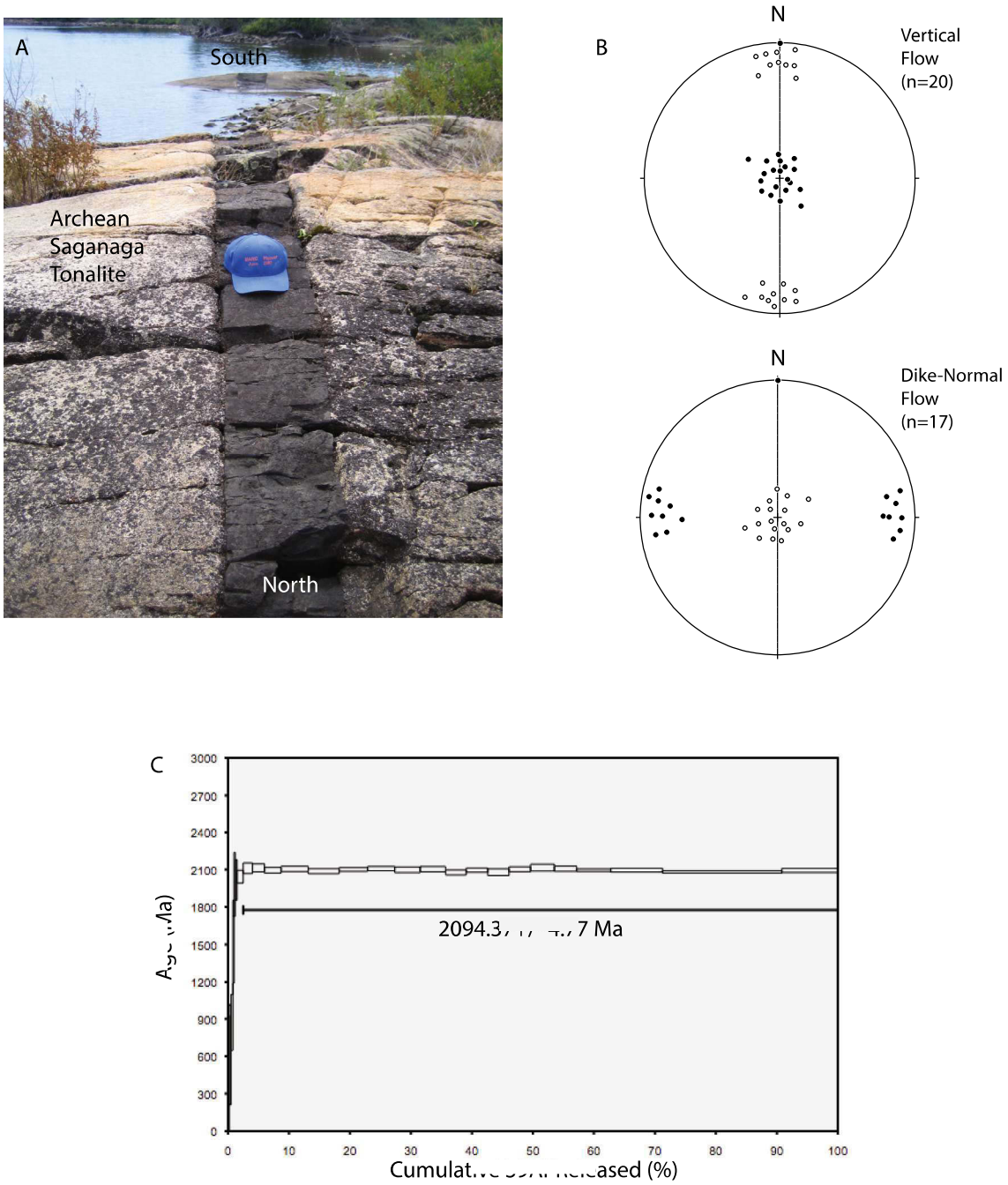

Fig. 6. Marathon LIP lamprophyre dike crosscutting the Archean Saganaga Lake tonalite near the end of the Gunflint Trail, MN (A). AMS results for two lamprophyre dikes in the same swarm (B; upper, vertical flow; lower, dike-normal flow. Kmax-filled circle, Kmin-open circles), and Ar/Ar age from lamprophyre biotites (C).

20. Regional strain shortening axes are summarized stereographically in Fig. 21. Tectonic schematics are found in Figs. 22–26.

4.2. *Pre-Penokean footwall deformation*

Three sites are described here and represent pre-Penokean deformations in the Archean foreland to the north of the Penokean foreland in Ontario (Fig. 1; Table 1, samples 1–9). These sites are included to demonstrate the uniqueness of Archean deformation in proximity of deformed Penokean rocks and to document the absence of a Penokean (or younger) strain overprint (see Discussion on pseudotachylite) that has been documented in the distal forelands of other

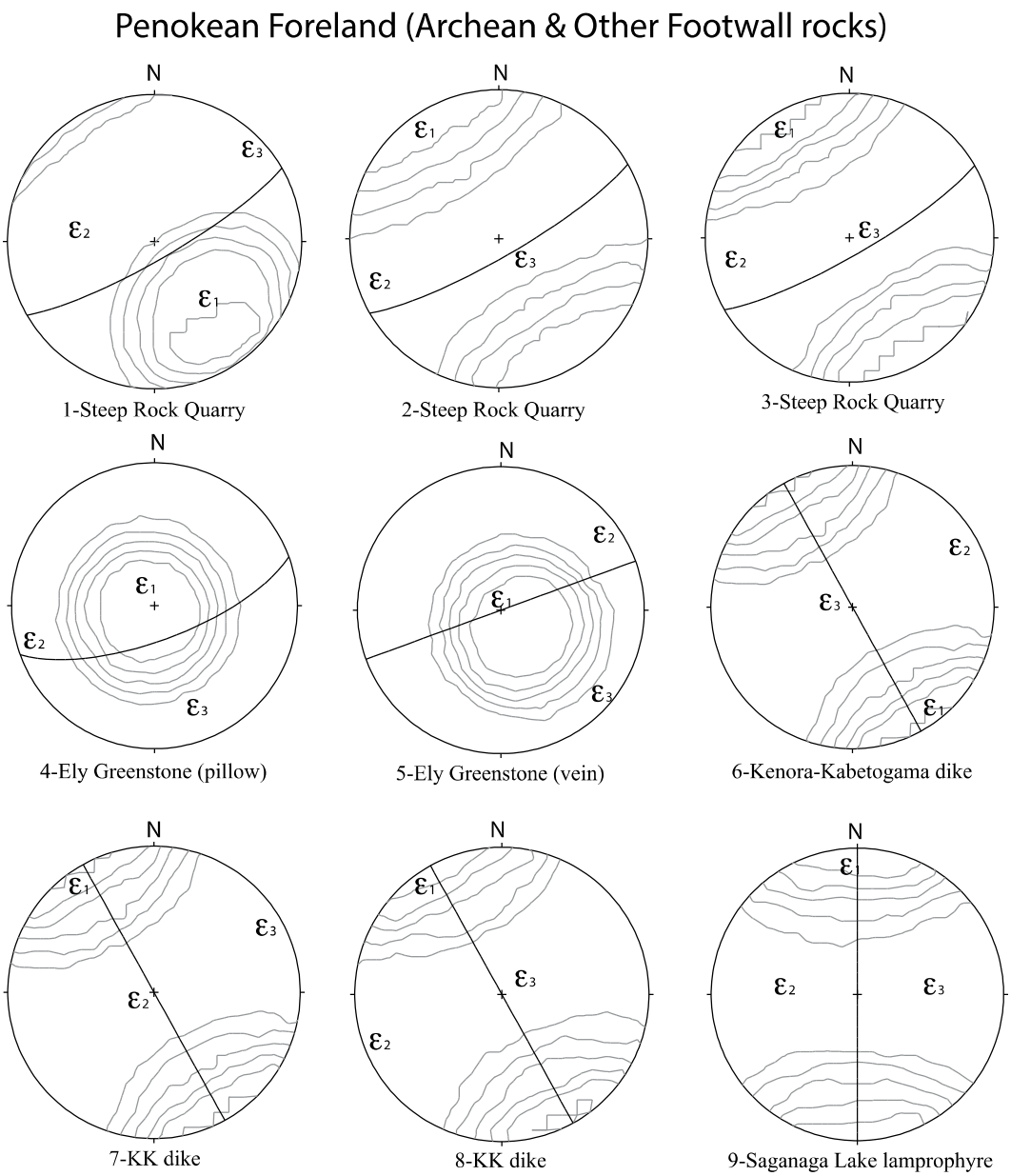

Fig. 7. Strain data (see Table 1, Fig. 21). Shortening axis is e1, intermediate axis is e2 and extension axis is e3. Turner (1953) compression axes are contoured for calcite strain data. Great circles are bedding, vein or dike orientations. Sample 33: AMS = filled circle is Kmax, open circle is Kmin.

orogenic belts (van der Pluijm et al., 1997).

Within the Archean Wabigoon terrane is the 3.0 Ga Marmion tonalite inlier which was the depositional site of one of the rare examples of an Archean marble and includes the world's largest stromatolites (Wilks and Nisbet, 1988). The carbonate Mosher Fm. (500 m) is the lower part of the Archean Steep Rock Group and is adjacent to the Fe-rich Jolliffe ore zone which was mined from 1891 to 1979 (Kusky and Hudleston, 1999). Steep Rock Lake is the growing reservoir in the dormant mine pit north of Atikokan, Ontario and is a park. We sampled marble, breccia and calcite veins in steeply-dipping strata on the east side of the mine and each calcite type records a SE-NW shortening strain normal to bedding (Fig. 4d; Table 1; Fig. 7a). No twinning strain overprint was observed.

The Ely Greenstone is part of the Archean Wawa (Abitibi) belt and is exposed in a SW-NE trending belt of heterogeneous metasedimentary and metavolcanic rocks (Bauer et al., 1992) between Soudan and Ely,

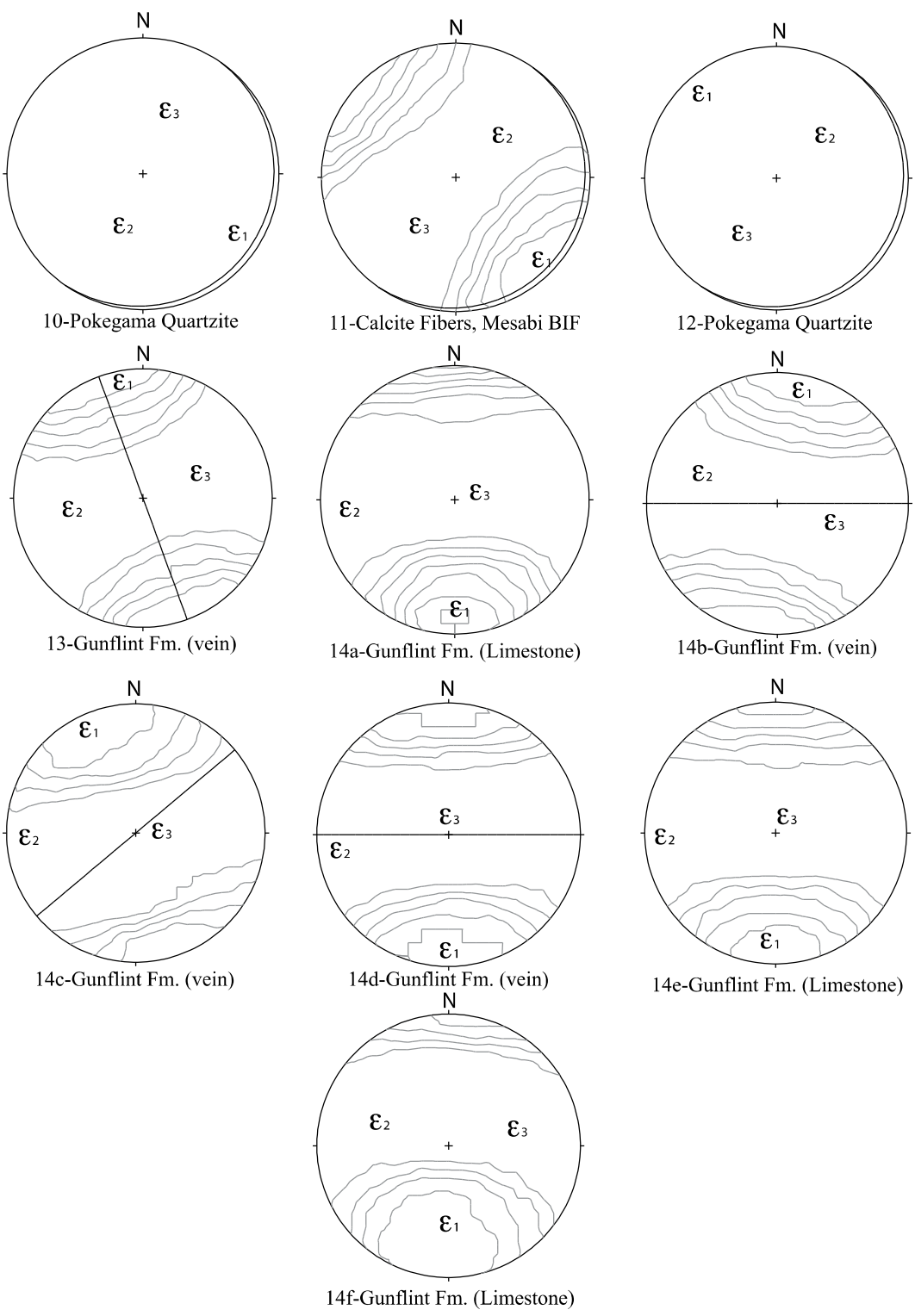

Fig. 7. (*continued*)

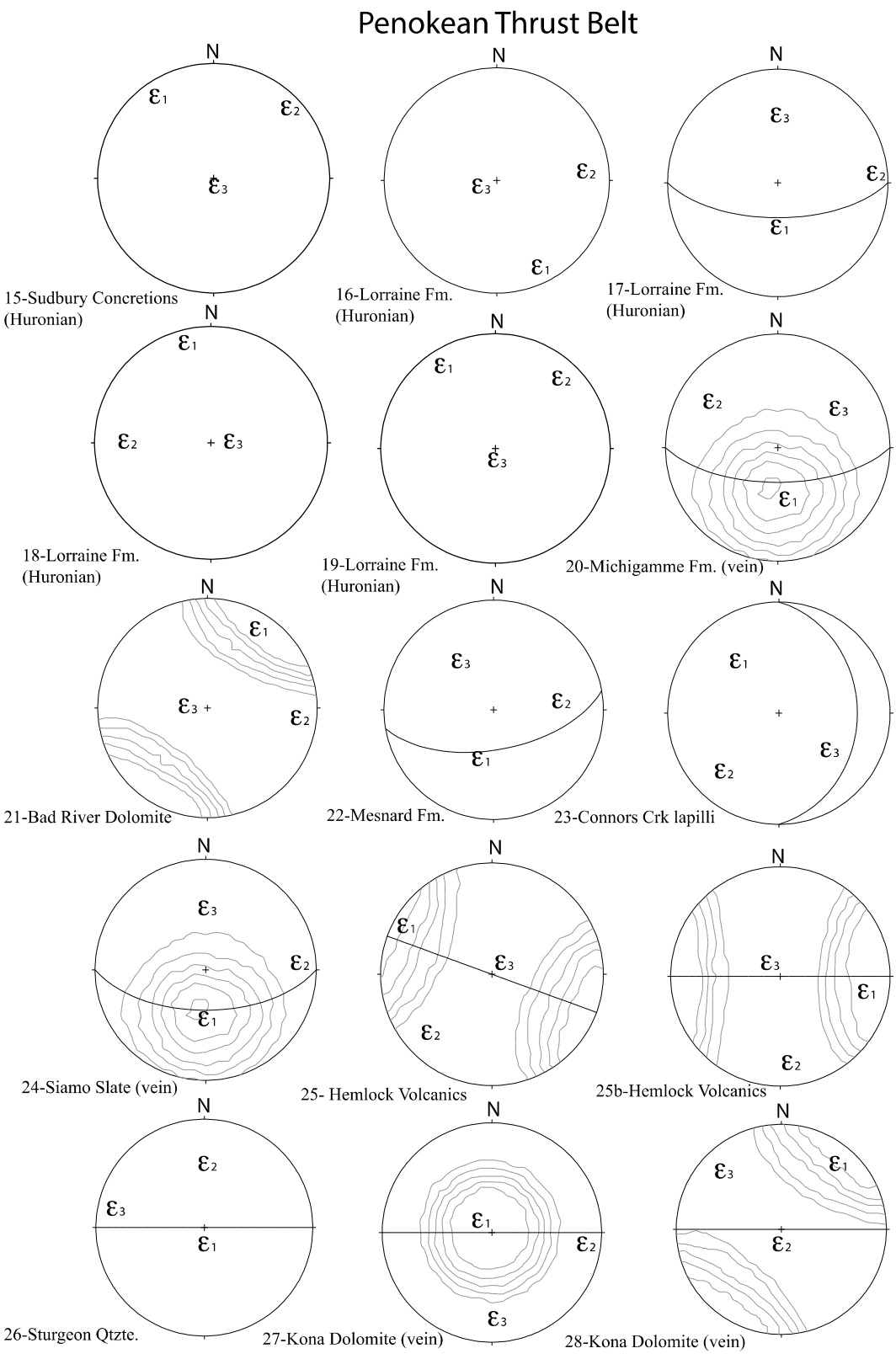

Fig. 7. (*continued*)

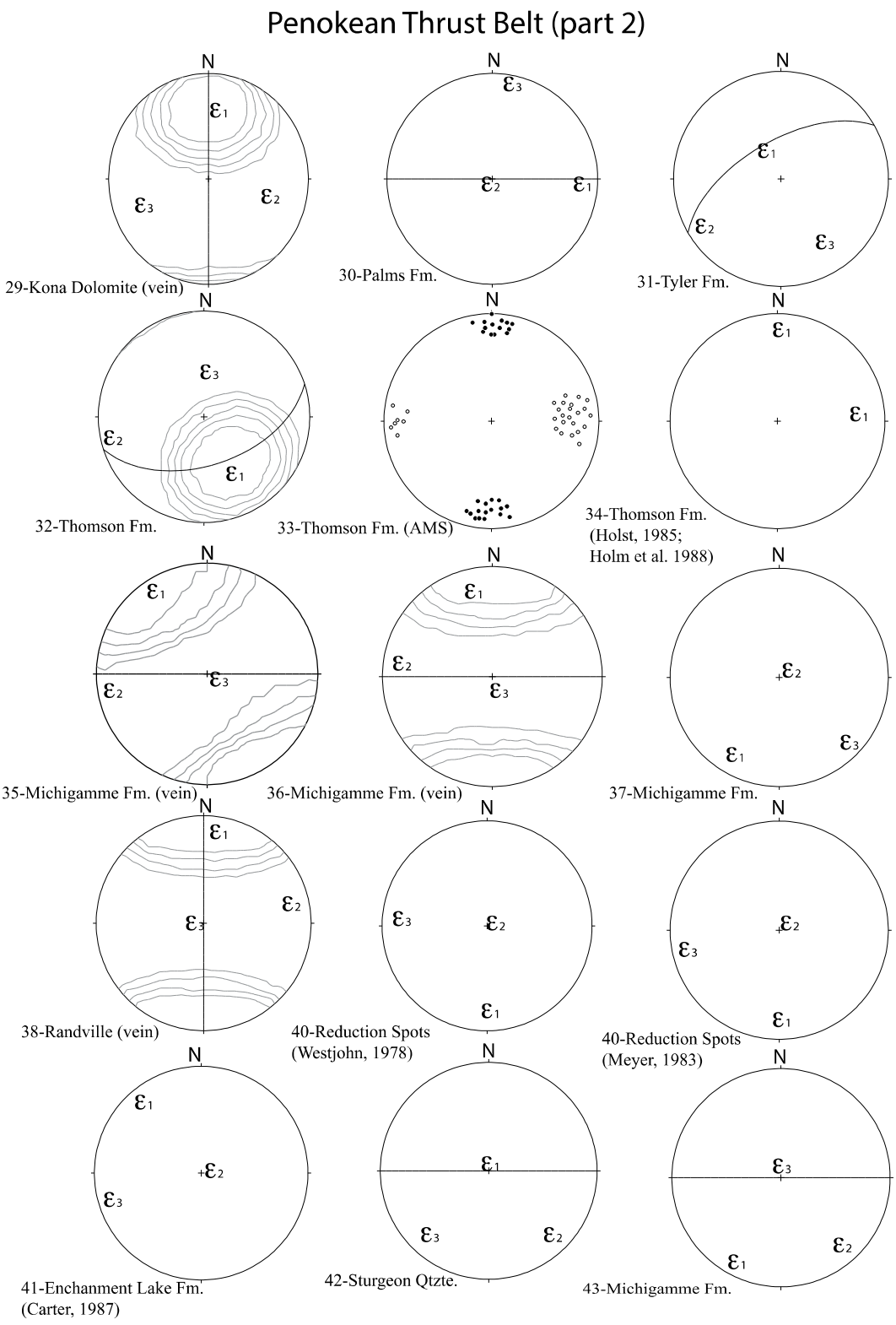

Fig. 7. (*continued*)

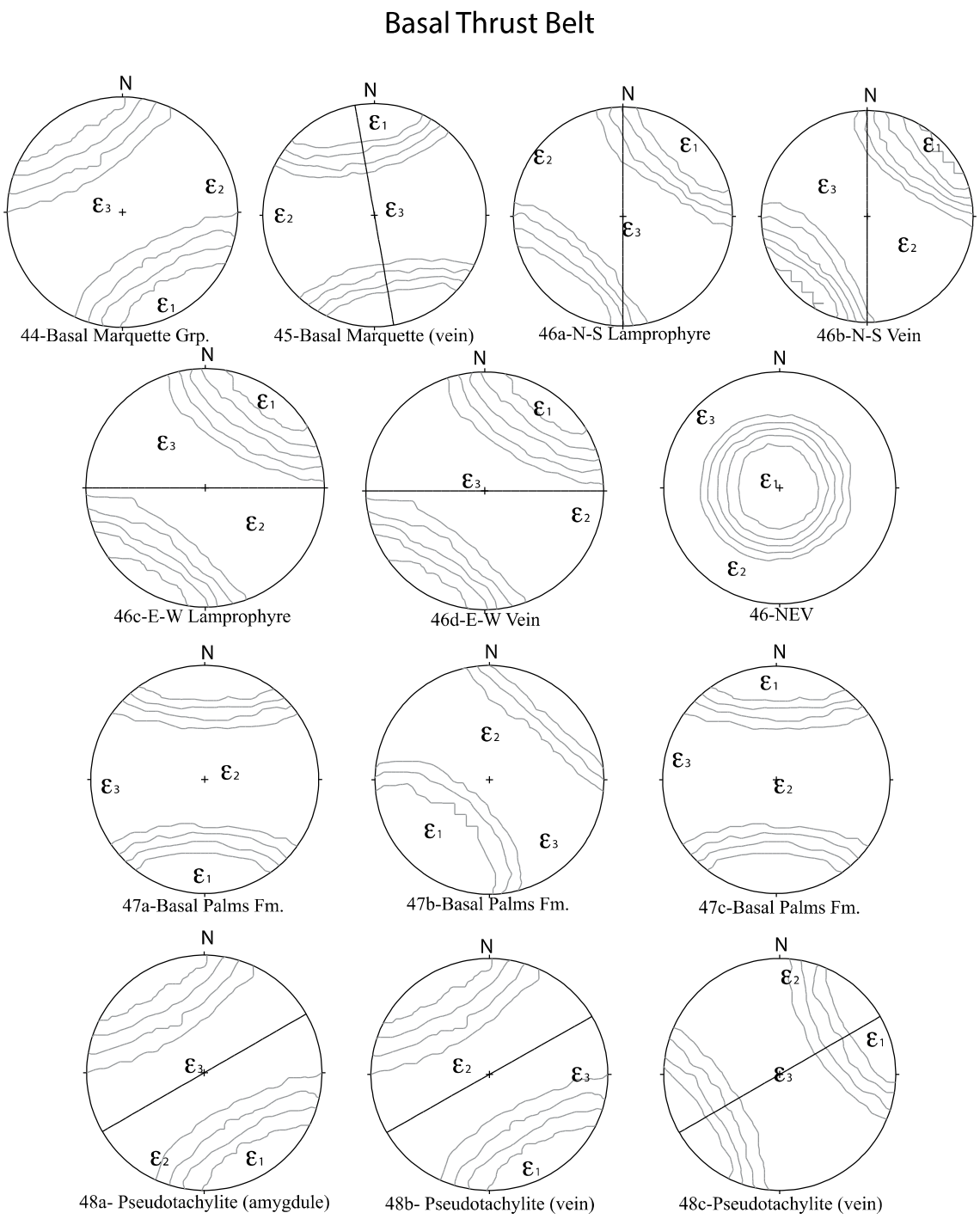

Fig. 7. (*continued*)

MN. Pillows in the Ely Greenstone are vertical and north-facing and contain calcite between pillows and in pillow-margin calcite veins. Twinning strains in both types of calcite preserve a layer-parallel shortening strain: ε_1 is vertical and so is bedding (Fig. 7a; Table 1) and there is no twinning strain overprint (see also Bauer, 1985; Schultz-Ela and Hudleston, 1991).

North-striking lamprophyre dikes that crosscut the Archean Saganaga tonalite (Goldich and Hedge, 1962) in the Wawa terrane in northern Minnesota (Fig. 1). These dikes contain primary magmatic calcite which is common in lamprophyres (Table 2, Craddock et al., 2007). Calcite twinning strains preserve a horizontal, dike-parallel shortening strain, a result similar to the dike-parallel faults in the

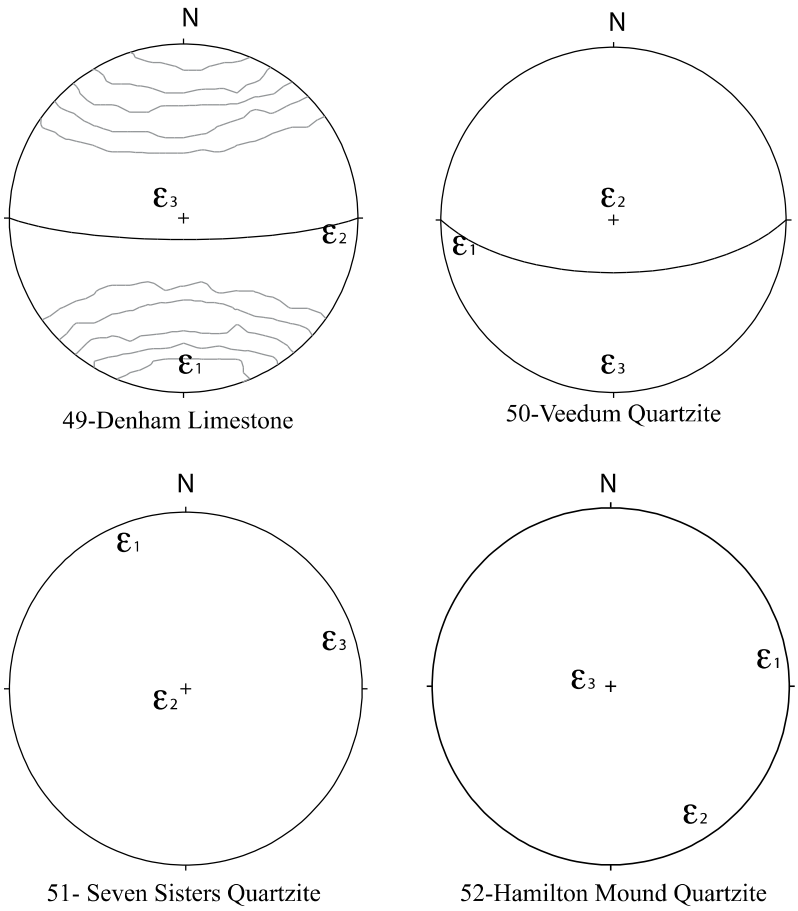

Fig. 7. (*continued*)

nearby Wawa terrane (Craddock and Moshoian, 1995; Fig. 7a; Table 1). AMS results are mixed with one of the two dikes indicating dike-parallel, horizontal flow and the other vertical flow (Craddock et al., 2005). Biotites from the lamprophyres yield an Ar-Ar plateau age of 2094 ± 4 Ma (Fig. 6), making these dikes consistent in age and orientation to be included in the Kenora-Kabetogama dike swarm as part of the Marathon LIP (Halls et al., 2008) although lamprophyre is uncommon in the swarm (Southwick and Day, 1983; Southwick and Halls, 1987; Schmitz et al., 1995).

4.3. Foreland deformation

Hill and Smyk (2005) were the first to propose that the Gunflint Formation near Thunder Bay and Pass Lake, Ontario represents both the flat-lying foreland of the Penokean thrust belt and the foreland thrust belt transition (Fig. 1; Table 1, samples 10–14). These structures are ~200 km north of the Penokean margin if the younger Keweenaw (Midcontinent) rift is removed. Along Pass Lake Rd. (Highway 587) there is a transect of a north-vergent fold-and-thrust sequence (E-W folds with shallow plunges) that becomes flat-lying Gunflint Formation resting unconformably on Archean Wawa terrane rocks over a distance of ~3 km (Figs. 8 and 9a). The lower Gunflint Fm. contains primary calcite (Fig. 5d) and numerous veins and, in both the foreland and Pass Lake transect, twinned calcite records a sub-horizontal, N-S layer-parallel shortening strain (Figs. 1 and 7b; Table 1, sample sites 13 and 14). The Gunflint Fm. is also exposed at a higher topographic and structural level, and here, the Gunflint Fm. is folded in complex (isoclinal in places) N-S folds with a steeply-dipping N-S cleavage (Baird, 2015) and a local breccia composed of Gunflint Fm. clasts (Fig. 9b inset); we did not recover any calcite for strain analysis.

Also ~200 km inboard of the Penokean margin is the Pokegama Quartzite-Biwabik iron formation section that makes up the Mesabi Range (Figs. 1 and 2). This is the northwest extent of the Animikie basin and the strata dip ~5°–10° to the southeast except where they wrap

Fig. 8. The Gunflint Fm., as exposed along Pass Lake Rd. east of Thunder Bay, with N-vergent think-skinned folds (top) that formed along a S-dipping thrust fault with ramp-anticlines and an axial-planar cleavage and veins (A, B) and small-scale folds (C–E).

around the Virginia Horn (Jirsa et al., 2005) and there are many local, contraction structures (Fig. 3e,f). The basal Pokegama Quartzite (~100 m thick) preserves a layer-parallel shortening strain oriented SW-NE (Samples 10, 12; Fig. 7b), similar to the twinning strains in bedding-parallel, sheared calcite in the Thunderbird Mine (Sample 11; Fig. 5e).

4.4. Thrust belt deformation

Strain markers are common but vary across both basins, and field and microscopic examples are highlighted in Figs. 3–5; this grouping of strain results (Samples 15–43; Figs. 1, 2, 7c & d; Table 1, Fig. 1) is from the structural setting north of the Niagara suture and within the Huron-Animikie section that is faulted and folded. This two dimensional, map-view strain ellipse is duplicated in three dimensions by the ellipsoidal shapes of carbonate concretions in the post-impact Chelmsford Fm. of the Whitewater Group (Fig. 3b; Table 1). Shortening was horizontal, parallel to bedding, and oriented at N20°W.

The Huron section contains abundant quartzite and is thus ideal for finite strain measurement. We collected four samples of the Lorrain Fm. (Fig. 2), three across the western end of the basin, and a single sample south of Sudbury near the footwall of the Grenville orogen. All the strain results indicate a layer-parallel shortening strain oriented ~N-S (Table 1; Samples 15–19), roughly parallel to the Penokean transport direction and normal to the various folds in the Huron section (Bennett et al., 1991) which is consistent with slip surfaces along bedding planes parallel to the shortening direction and normal to the local fold axis (Fig. 3c).

Samples 20–43 (Figs. 1 & 2; Table 1) represent a variable assemblage of metasedimentary and metavolcanic (Samples 24, 25) rocks across the Animikie Basin analyzed by a variety of strain techniques. Layer-parallel shortening is the rule, with a wide range of bedding orientations and the shortening directions plot as a girdle ± 20° from the inferred Penokean thrust transport direction (see Discussion). Exceptions to this observation include the following: Sudbury impact lapilli found near Connors Creek, MI (Sample 23) are deformed into ellipsoidal shapes (Fig. 3a) with the shortening axis at a high-angle to bedding (layer-normal shortening) and plunging to the NW. The Hemlock Fm. volcanics near Clarksburg, MI are full of replacement calcite (Fig. 5c), which is twinned and both steeply dipping samples

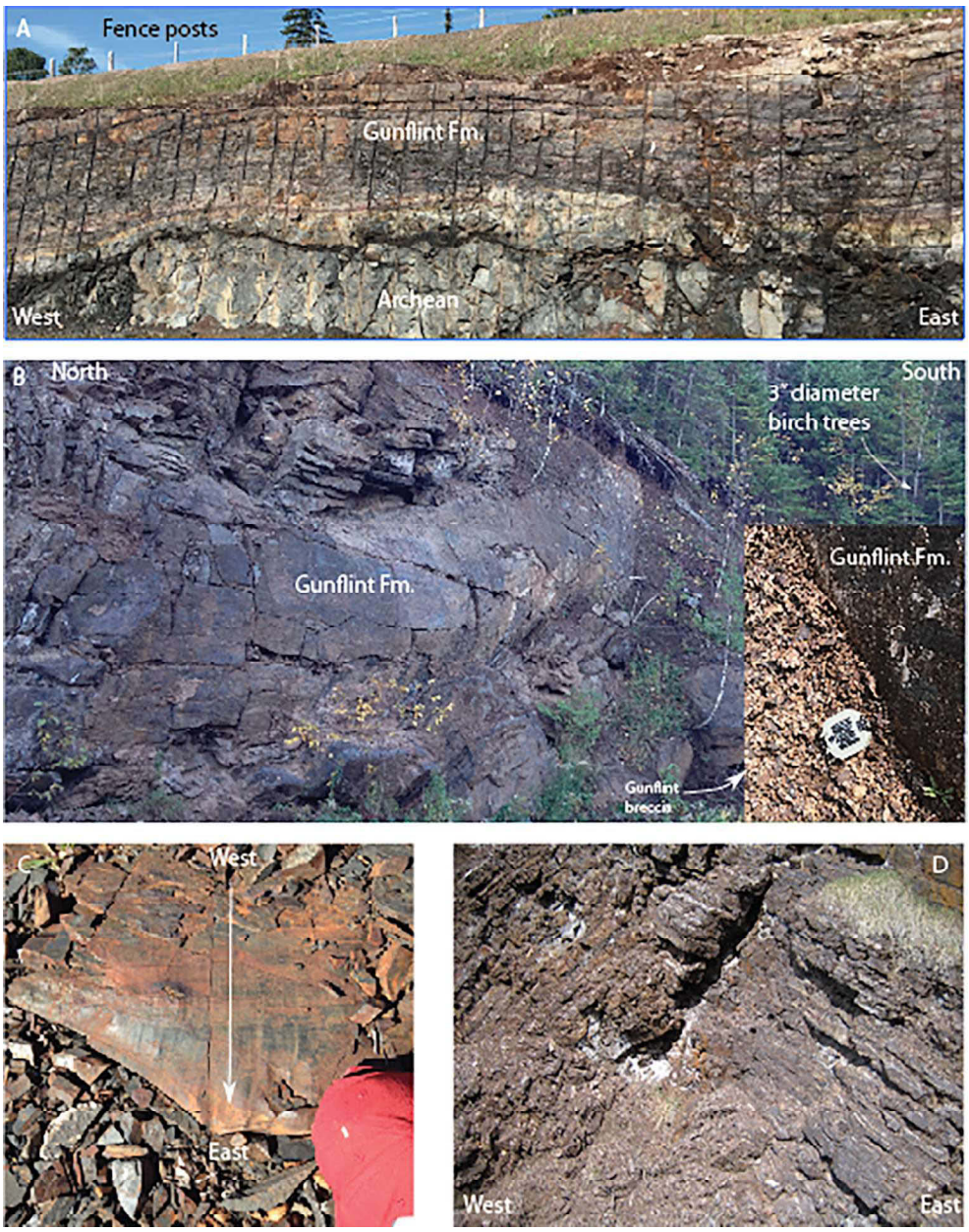

Fig. 9. The Gunflint Fm.-Archean unconformity along the Transcanadian Highway at the Pass Lake junction (A), which has occasional layer-parallel E-W striations (no steps; C), and is up-dip (north) of N-S folds (B, D; outcrop width ~ 30 m). The N-S folds are stratigraphically and structurally higher than the E-W fold-and-thrust sequence in Fig. 8 and include sub-vertical Gunflint Fm. breccia (B, inset at Mirror Lake campground).

record an E-W, horizontal shortening strain. The same strain result is observed in the vertical Palms Fm. in Wakefield, MI (sample 30; Fig. 4c) where sinistral, E-W fault motion is documented. Strains in the Thomson Fm. in east-central Minnesota have been measured by Schwartz (1942) and Holst (1985) and two strain ellipsoid orientations are observed: horizontal shortening oriented N-S and E-W (Sample 34) although the earlier studies do not reference strain axes to local bedding (i.e., oblate or prolate ellipsoids; Holst, 1982, 1984). AMS measurements of the Thomson Fm., with K_{min} oriented horizontal and E-W and K_{max} oriented horizontal and N-S suggest E-W shortening in turbidites that have two cleavages and are refolded, west-vergent nappes (Holst, 1982, 1984). Finite strain studies of Westjohn (1978), Meyer (1983) and Carter (1989) are included (Samples 40, 41, Table 1 and Fig. 7).

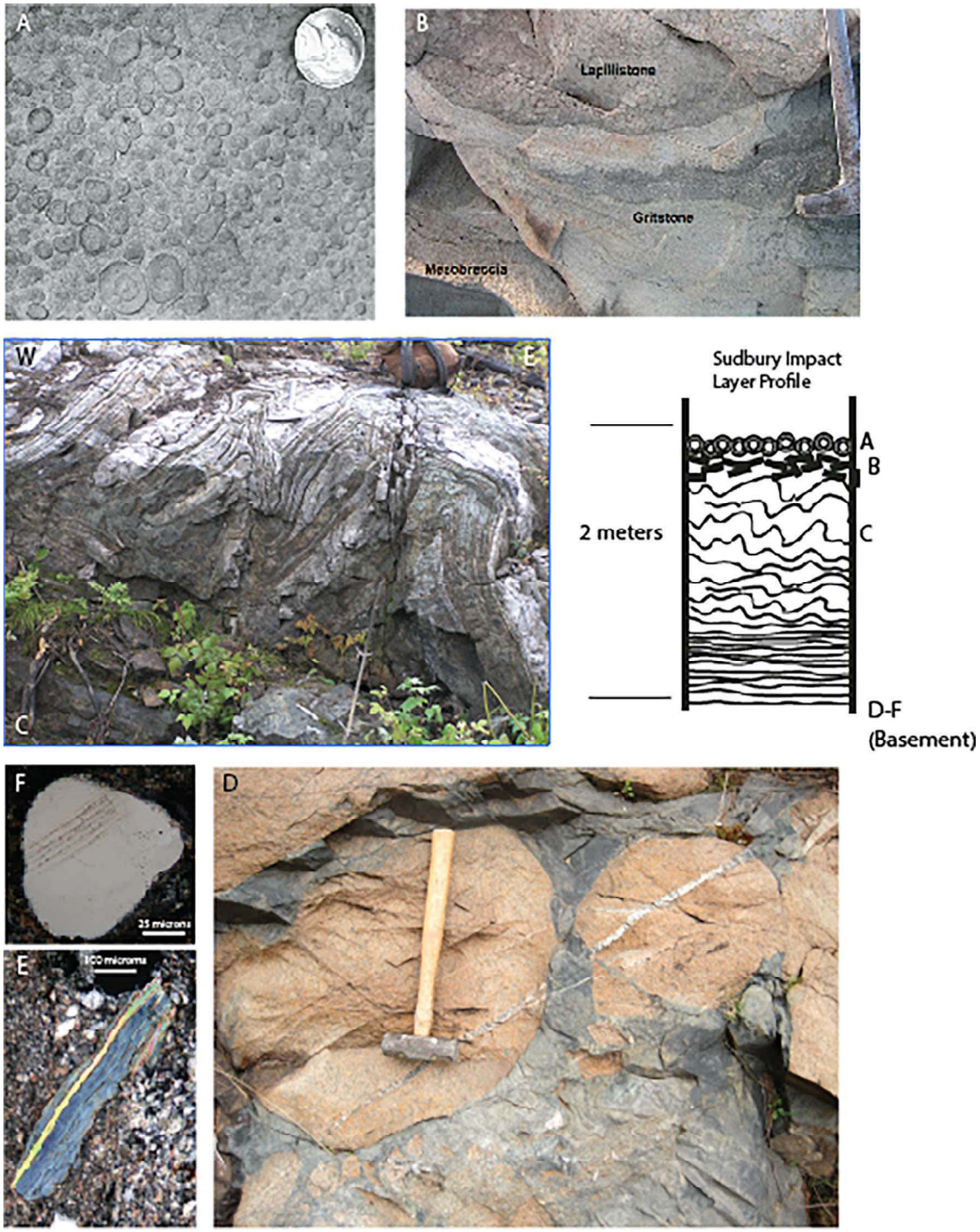

Fig. 10. Representative profile of the Sudbury impact layer near Gunflint Lake, MN (Jirsa, 2011). with ashfall lapilli (A, B) above the folded Gunflint Fm. (C) ~800 km from Sudbury. Archean gneisses with shale "seismite" at Silver Lake, MI (D), including brecciated mylonite fragments and shocked quartz (E, F).

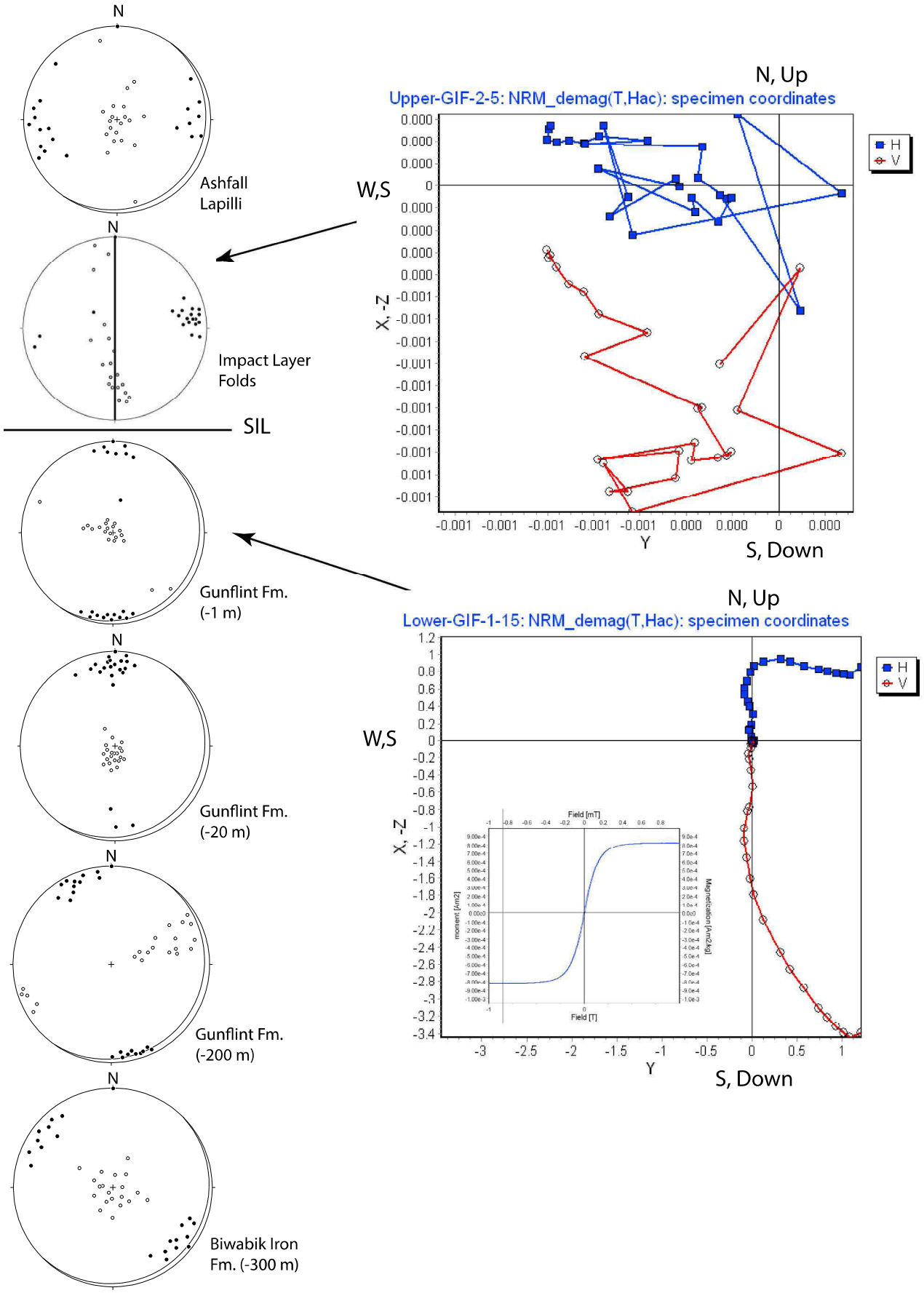

(caption on next page)

Fig. 11. Paleomagnetic study of the Gunflint Fm. near Gunflint Lake where the AMS Kmax fabric is parallel to the inferred Penokean thrust transport direction and local bedding below the Sudbury impact layer (SIL; left column, lower hemisphere projections; Kmax = black circle; Kmin = open circle). The AMS fabric in, and above, the SIL is rotated 90° which corresponds to a well-preserved magnetic paleopole below the impact layer (lower right; hysteresis inset documents magnetite as the magnetic mineral) and a chaotic result in the ashfall lapilli above the SIL. The lower Biwabik Fm. result is a distal sample from the Thunderbird Mine, Virginia, MN.

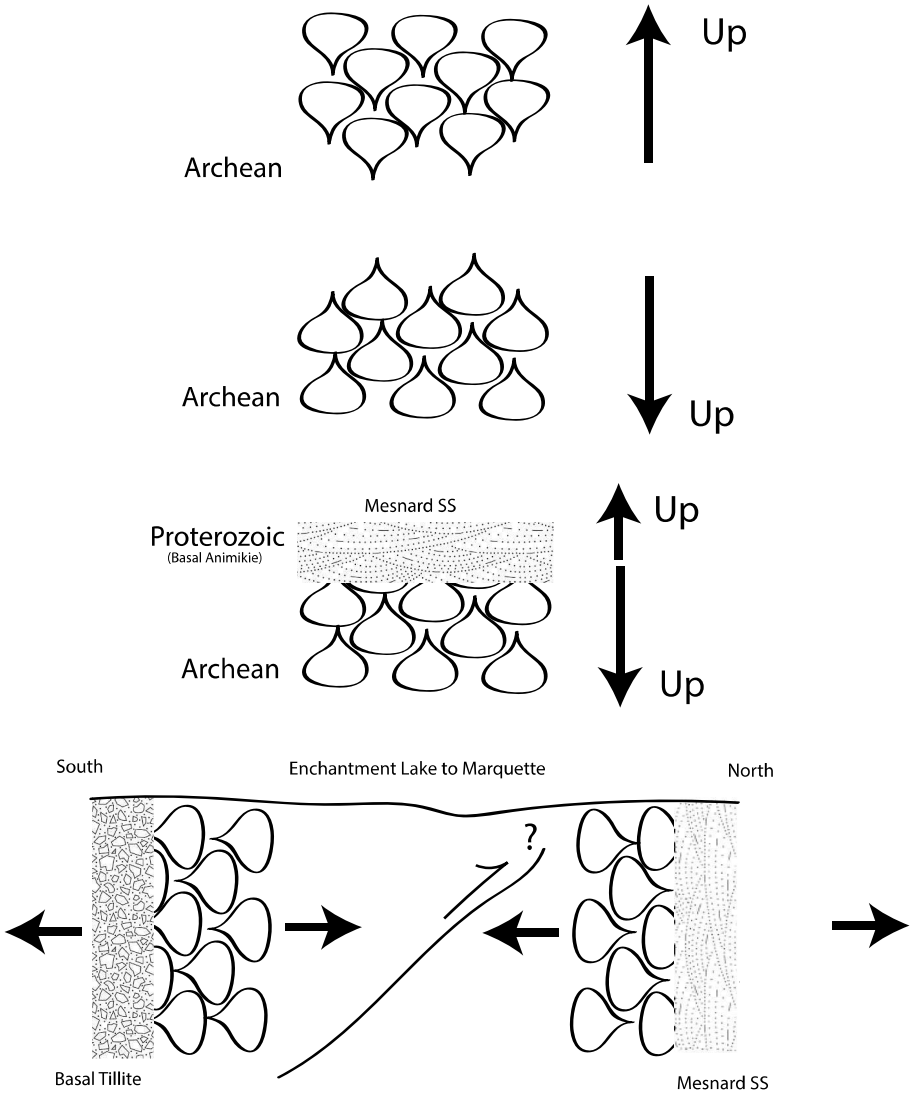

Fig. 12. Deformation of a "bottom-on-bottom" structure (Van Hise and Leith, 1911) that involved pre-Penokean inversion of Archean pillow basalts, deposition of basal Animikie basin Mesnard Fm. sandstone, which is locally equivalnet to the basal Fern Creek tillite, both of which are now sub-vertical and face in opposite directions and indicate Penokean offset of Archean basement and the overlying Animike section.

4.5. Distal Sudbury impact deformation

The Sudbury bolide (1850 Ma) landed in the Huron basin and was back-filled by the Whitewater Group which is equivalent to the shales in the upper Animikie section (Rove, Thomson, Virginia Fms.; Figs. 1 and 2; Table 1, Sites 15 and 22). At Silver Lake, MI, 400 km from the impact site, seismic vibrations in Archean gneisses allowed Animikie turbidites to settle into dilational spaces in the gneisses (Fig. 10d), deposits referred to as "seismites" (Cannon et al., 2009). These seismites include shocked quartz and exotic fragments, like marble mylonites (Fig. 10e,f). There is also a regional breccia zone on the top of the banded iron formations found ~800 km from the impact site referred to as

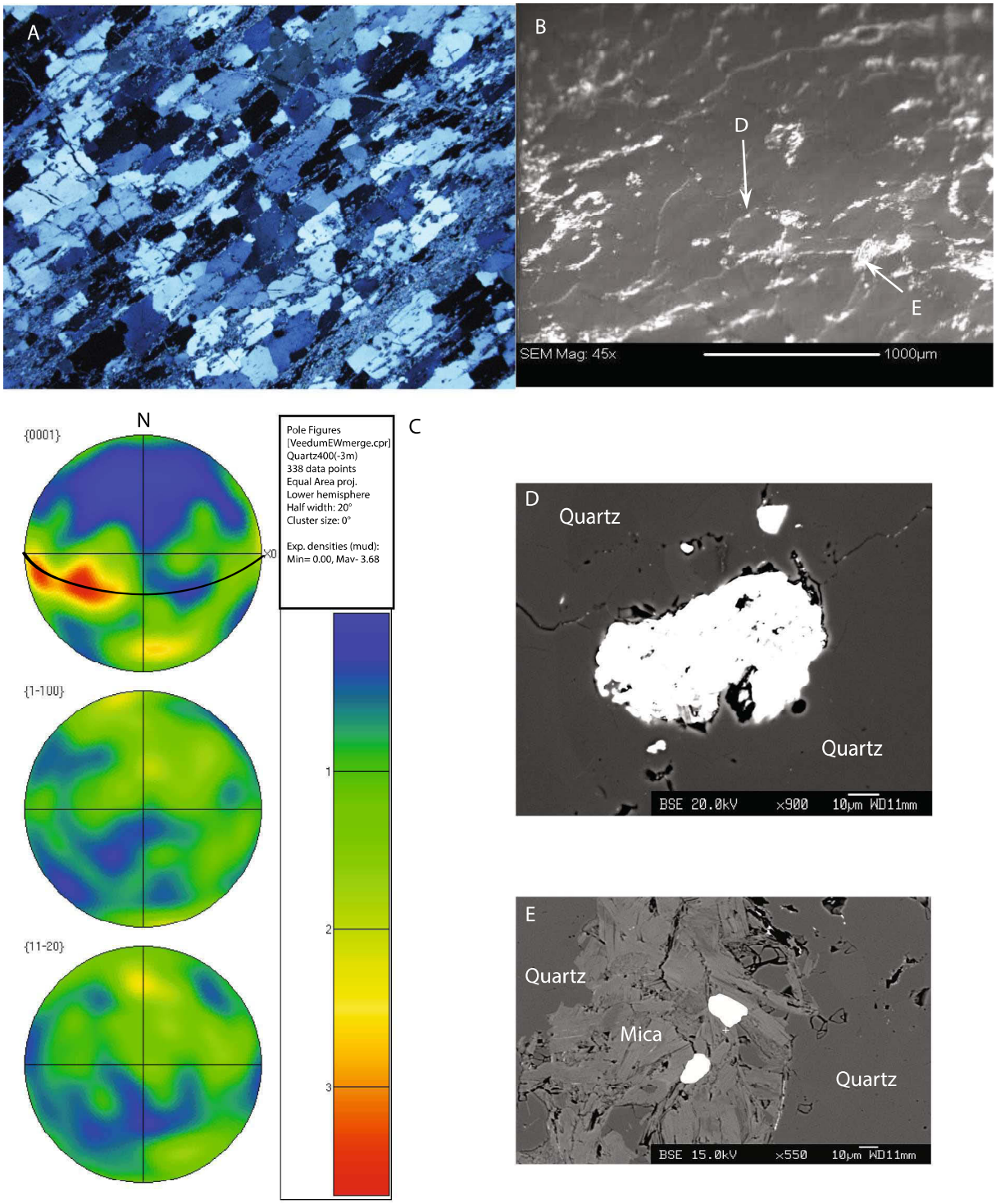

Fig. 13. Veedum Quartzite (Veedum, WI) in polarized light (A) with an SEM close-up (B) of a polished surface used for EBSD pole figures (C; great circle is bedding). Both detrital (D) and metamorphic (E) monazite (white) is common.

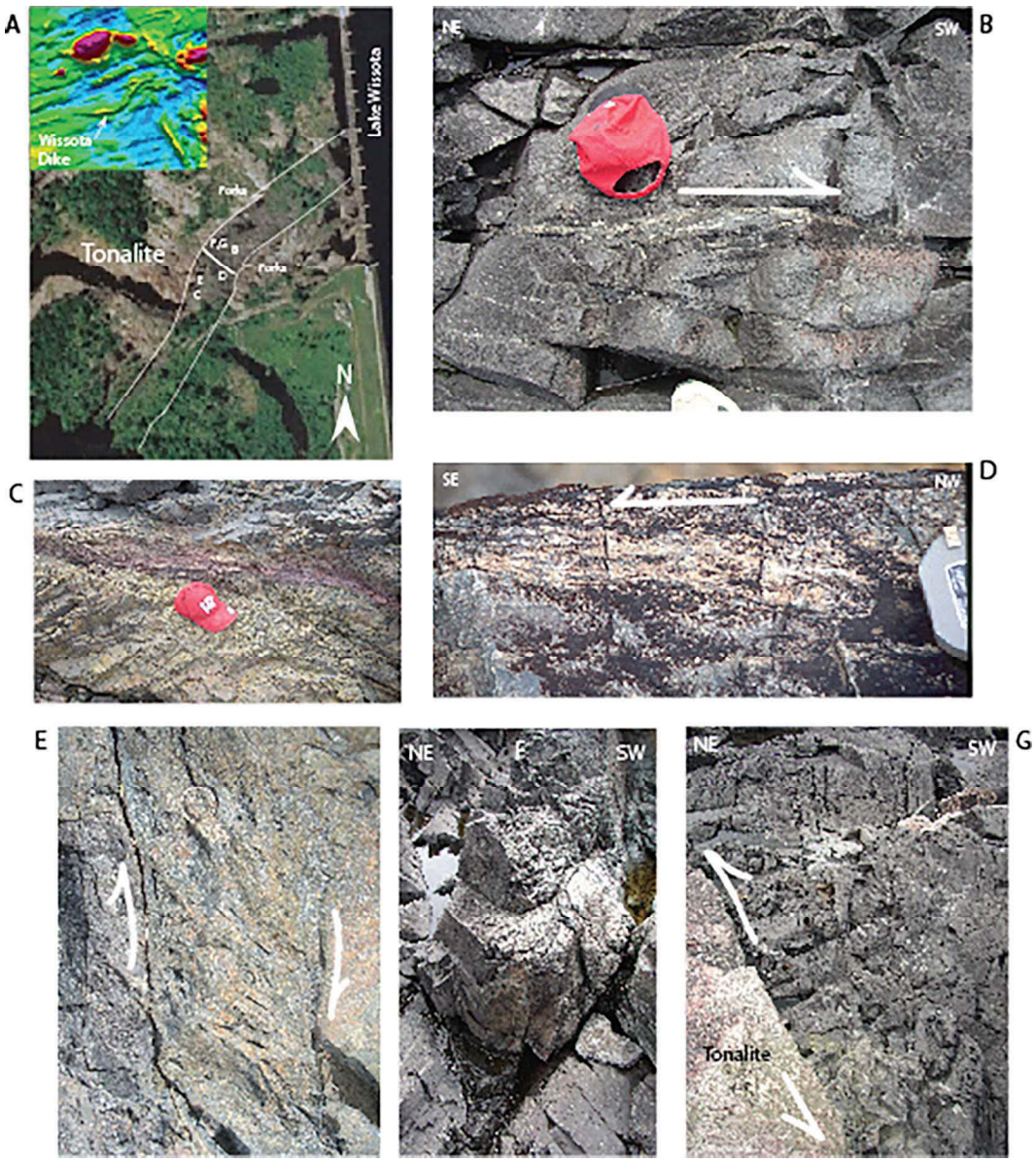

Fig. 14. A. Aerial photograph of Proterozoic tonalite and folded mafic dike below the Wissota Dam, Chippewa Falls, WI, with aeromagnetic inset. B. Dike margin-parallel sinistral sigma structure (E-W) in dike center; C. Trondjemite intrusion, D. Dike-normal (SE-NW), vertical, sinistral mylonitic zone (Brunton compass for scale); E. Dextral, sigmoidal shear zone (ring for scale); F. Sigmoidal joints (outcrop width ~ 1 m) offset along SE-NW vertical strike-slip faults that become listric along the dike-tonalite contact (G; outcrop width ~ 2 m).

"tsunamites" that are overlain by turbidites. In northern Minnesota, near Gunflint Lake, the Gunflint Fm. rests unconformably on Archean tonalite and the tonalite-Gunflint-Rove Fm. section is faulted and gently folded (see below). The Gunflint Fm. contains minor folds that increase in amplitude up-section (Fig. 10c) with fold amplitudes (1 m) increasing just below the Sudbury impact layer (SIL). Sudbury lapilli are mixed throughout the local chaos zone and are undeformed (circular; Fig. 10a,b). The Gunflint Fm. is 120 m thick and we took oriented samples 200, 100, 10 and 1 m below the SIL and from the local SIL folds and the overlying lapilli layer. We also include an AMS result from the lower Biwabik iron formation near Eveleth, MN as a distal comparison. Banded iron formations contain Fe-oxides, Fe-carbonates and Fe-silicates (Morey, 1999) but the magnetic carrier has a soft coercivity (~5 mT) and is magnetite (hysteresis loop inset; Fig. 11). AMS

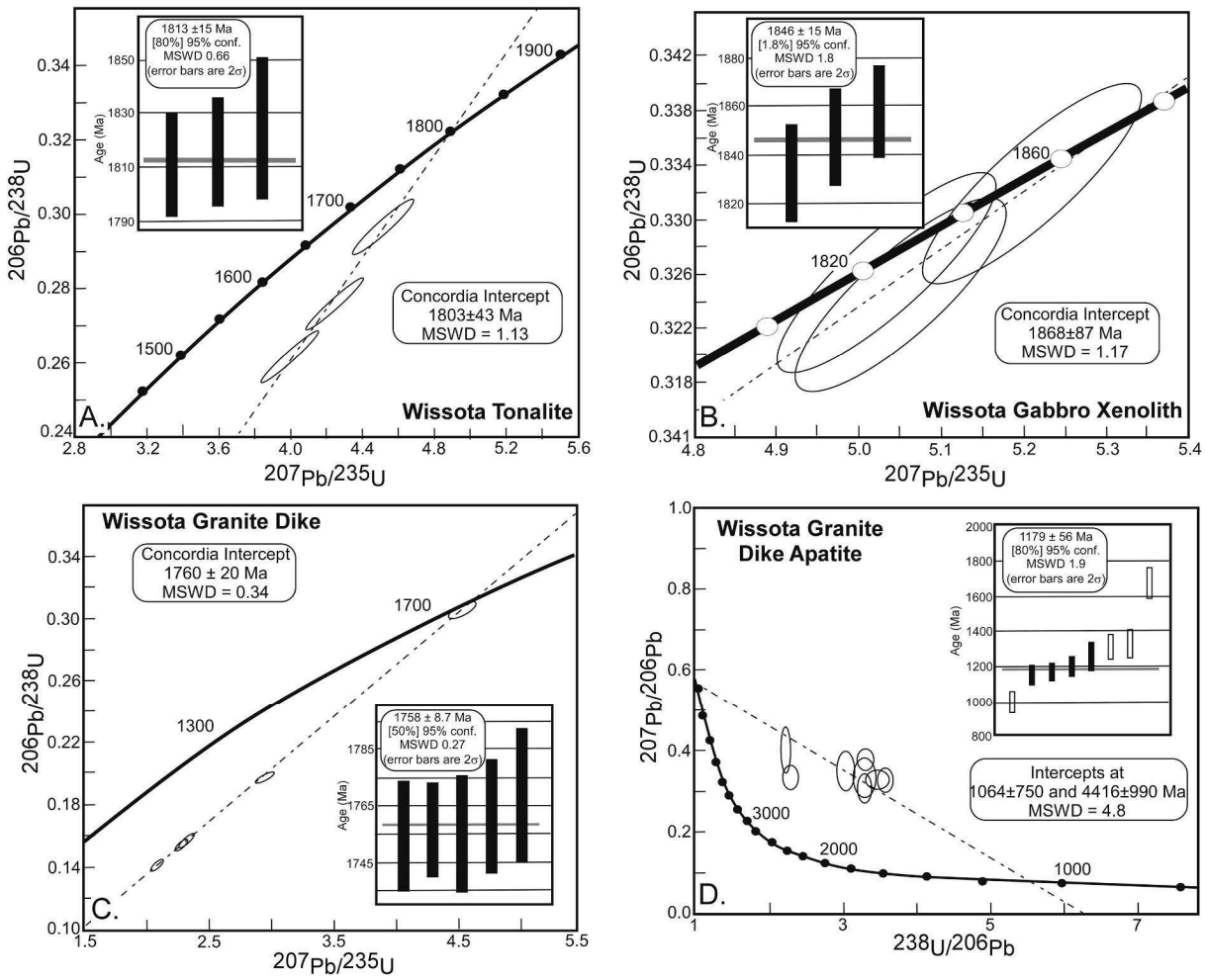

Fig. 15. Geochronology results for the Wissota dam area, Marshfield terrane. A: Wissota tonalite, B. the xenolithic gabbro dike, C. the granitic (formerly trondjemite) dike iin the gabbro xenolith and D., U-Pb apatite from the xenolithic gabbro. See Fig. 14 (field relations) and Table 4.

measurements record a clear depositional fabric (K_{max} is SE-NW and horizontal, K_{min} is vertical) below the SIL (Table 3). Folds that define the SIL, and the overlying lapilli, preserve a very different AMS fabric orientation with K_{max} rotated 90° and normal to the SIL fold axes and bedding. Demagnetization studies also record a stable paleopole 1 m below the SIL and magnetic chaos in the deformed zone (Fig. 11).

4.6. Basal thrust belt deformation: Animikie basin basal strata

There are four sites where it was possible to measure strains in either basal Animikie strata in contact with Archean basement (Fig. 1; Table 1, samples 44–47). East of L'Anse, MI and on the west side of the Huron Mountains is an exposure of a flat-lying carbonate with calcite veins that rests on Archean gneiss at Big Erich Falls, MI. This site has been interpreted as a paleosol at the base of the Animikie Basin (Kalliokoski and Lynott, 1987). Calcite twinning strains in the host carbonate and calcite veins record a horizontal shortening strain oriented at N10°W with no strain overprint (Fig. 7e; Samples 44, 45). East of Wakefield, MI is an exposure of basal Palms Formation resting unconformably on Archean Ramsey Volcanics (LaBerge et al., 1992). Striated calcite fault gouge is prevalent along the contact and is presumed to represent fault motions associated with the basal Penokean thrust. Striations are horizontal and step to the north; twinning strains also record a horizontal N-S shortening strain (Sample site 47). Nearby, the Palms Formation is vertical and many bedding planes preserve horizontal, sinistral striations; strains here record sub-horizontal shortening parallel to bedding (E–W; Fig. 4c).

4.7. Basal thrust belt deformation: footwall deformation

Four sites include Penokean deformation hosted in Archean crust that are now exposed and represent the footwall beneath the Animikie basin strata and the contact with the overlying thrust belt (Fig. 1; Table 1, samples 44–48). Little Presque Isle is a small island in Lake

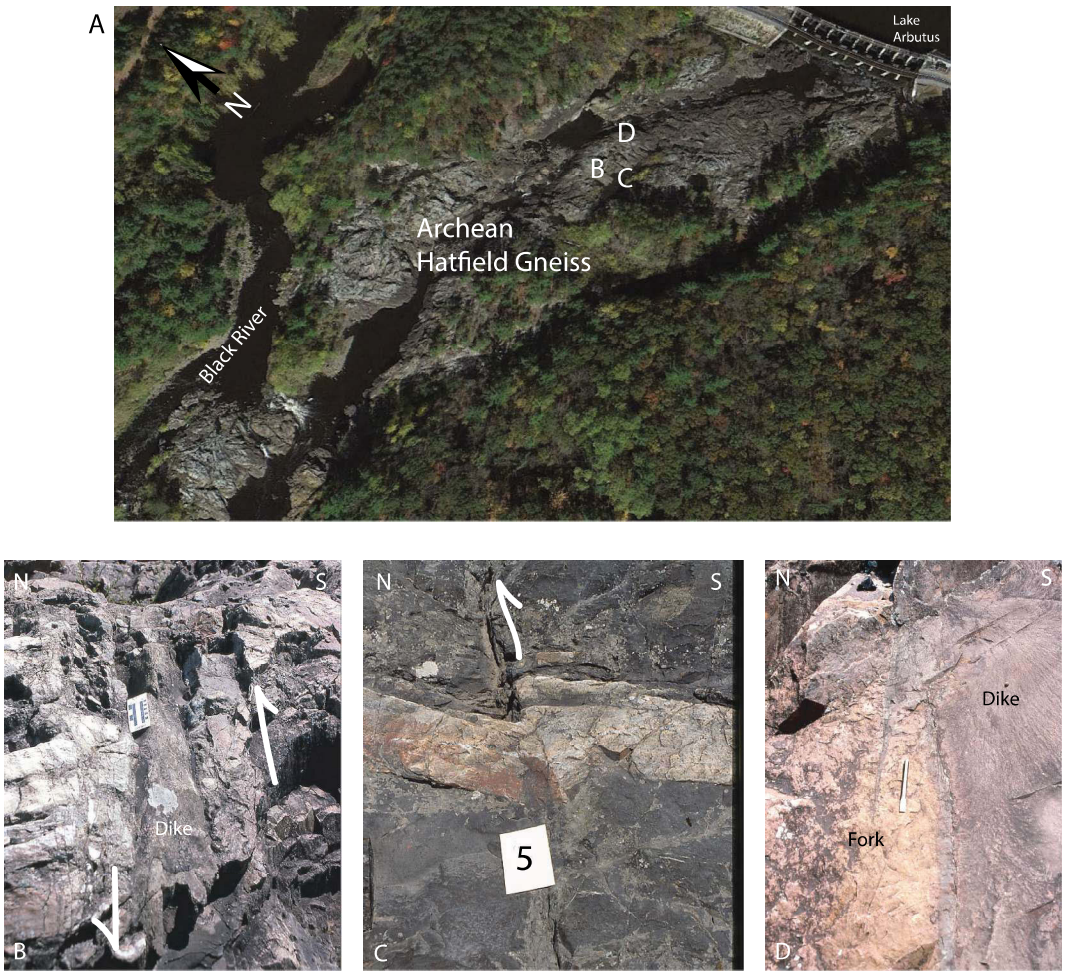

Fig. 16. Airphoto of Archean Hatfield Gneiss intruded by dikes below the Arbutus Dam, Black River Falls, WI (A); B. Offset fault-dike; C. Offset gneissic layer; D. Westward-forking mafic dike. See Fig. 17 (geochronology) and 18 (structure map paired with Table 4).

Superior, north of Marquette, MI where Penokean lamprophyric dikes (E-W and N-S; 1877 Ma Ar-Ar age on phlogopite) intrude the Archean Compeau Creek Gneiss and both are crosscut by Keweenaw-aged mafic dikes. The magmatic calcite in the lamprophyres, and the calcite veins parallel to their margins, preserve a horizontal shortening strain ~ parallel to Penokean thrust translation (N 30°E) and record a vertical shortening strain overprint (Fig. 7e; Craddock et al., 2007).

Along a N-S traverse from Enchantment Lake, MI toward Marquette one encounters a series of outcrops (bedding: 90°, 90°) with many opposing, younging directions in the basal Animikie Mesnard Sandstone, Fern Creek Tillite and pillows in the Archean basement (Fig. 12). Specifically, the Archean pillows were overturned at the time of deposition of the basal Animikie strata yet the Fern Creek is now vertical and youngs to the south while the Mesnard Sandstone is vertical and youngs to the north. This was described by Van Hise and Leith (1911) as a "bottom-on-bottom" structure as the bottoms of Archean pillows are in depositional contact with the bottom of the Fern Creek and Mesnard formations. The traverse described here also requires Penokean faulting of the Archean basement to rotate the Animikie basal units to a vertical orientation as the structure is duplicated normal to strike.

In the Minnesota River valley near Granite Falls, MN Archean gneisses and granulites were reactivated between the Morton and Montevideo terranes by Penokean shortening. Pseudotachylite was generated along the Yellow Medicine shear zone, crosscutting Marathon LIP dikes (2.06 Ga; Schmitz et al., 2006), and is presumed to be Penokean in age (Fig. 1; Craddock and Magloughlin, 2005). Calcite amygdules in pseudotachylite and calcite veins interwoven with pseudotachylite preserve a twinning strain that is N30°W and horizontal or, normal to the Yellow Medicine shear zone. A younger, crosscutting calcite vein (N70°E, 90°) preserves a horizontal, dike-parallel shortening strain (Fig. 7e; Table 1).

4.8. Hinterland deformation

4.8.1. Denham

The Marshfield and Wisconsin magmatic terranes collided with the

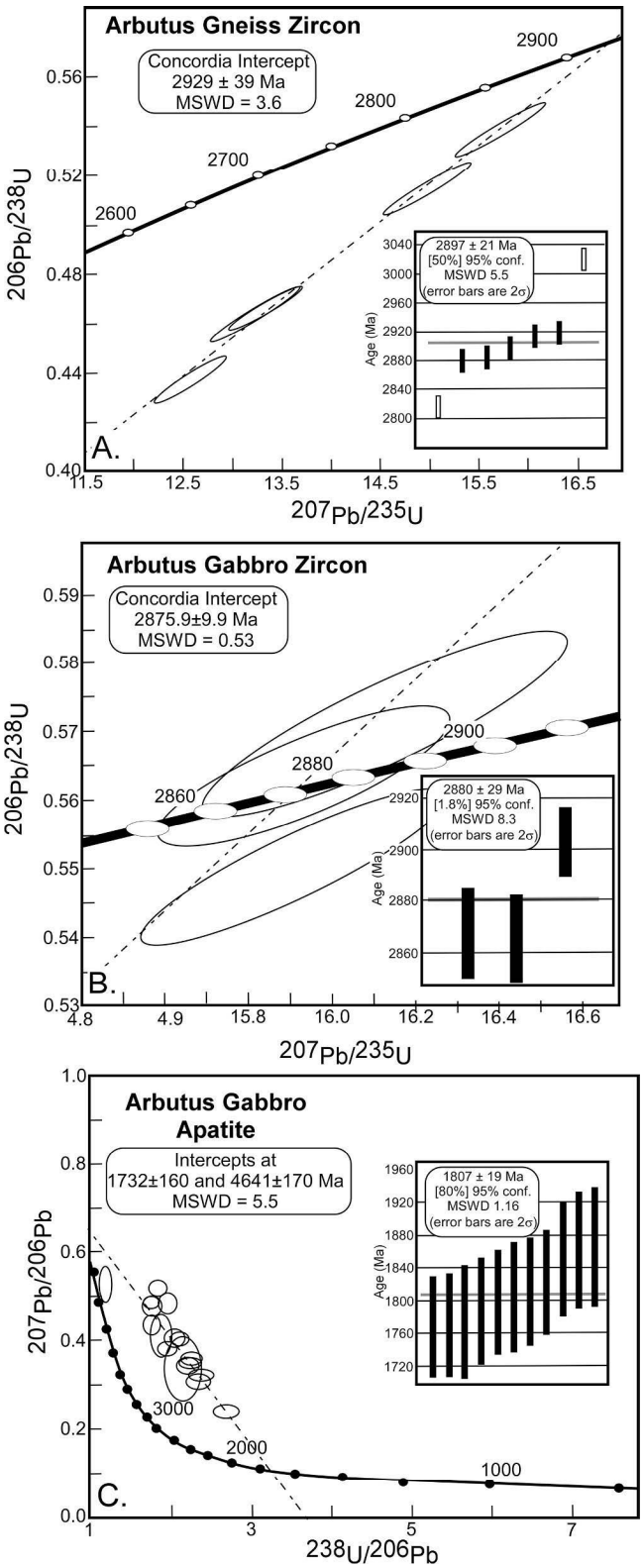

Fig. 17. Geochronology for the Hatfield Gneiss area below Arbutus dam, Marshfield terrane. A. U-Pb concordia plot for Hatfield gneiss zircons, B. for zircons in the intrusive gabbro, and, C. U-Pb apatite ages from the gabbro. See Figs. 16 and 18 for field relations and Table 4 for data tables.

southern Superior craton forming the Penokean orogeny that included the Denham sequence in central Minnesota. Marble is present in the Denham section and is largely dolomitic; one sample was calcite-rich and preserves a shortening strain that is horizontal, layer-normal, and oriented toward N18°W (Fig. 7f; Table 1; Fig. 1, Sample 49).

4.8.2. *Veedum*

Near the berg of Veedum, WI there are a few small outcrops of upright, purple-pink quartzites in proximity to a small quarry with a sheared quartzite. This quartzite is in the vicinity of the Spirit Lake shear zone (Table 1, Fig. 1, sample 50) and could be part of the southern Marshfield terrane and thereby sheared by Yavapai or Mazatzal deformation. The quartzite foliation strikes N80°E and dips 65°S (Fig. 13) with mica growth between quartz grains and both detrital and metamorphic monazites. Zircons were recovered (n = 18) and eleven ages were concordant LA-ICPMS ages: core ages (n = 7) were: 2531, 2542, 2560, 2692, 3459, 3473 and 3553 Ma with rims (n = 4) of 1126, 1141, 1153, and 1401 Ma (Table 4). Finite strains preserve a horizontal shortening axis normal to strike with quartz 001 axes within the plane of the foliation with shallow westerly plunge (Figs. 7f and 13).

4.8.3. *Wissota Dam, Marshfield terrane*

The Marshfield terrane is composed of a variety of Archean crystalline rocks that range in age from 2.5 to 3.0 Ga (Van Schmus, 1976, 1980). The Marshfield terrane is crosscut by mafic rocks of the "central Wisconsin dike swarm" (Green et al., 1987). The Marshfield terrane is bounded on the north by the Eau Pleine shear zone and Wisconsin magmatic terrane (1850 Ma); to the south is the Spirit Lake shear zone with Yavapai (~1750 Ma) granites and rhyolites further south (Fig. 1, inset).

The geology of the Chippewa River valley was mapped by Myers et al. (1980) and includes a number of E-W striking mafic intrusions. These intrusions are not related to the Keweenaw rift, which is ~100 km to the west. At the mouth of Lake Wissota near Chippewa Falls, WI, Myers et al. (1980) reported three lithologies, all of which were previously undated: 1) a weakly foliated tonalite body; 2) a 50-m wide gabbroic dike; and 3) a small pink trondjemite (herein reclassified as granite; Fig. 14c) dike. The gabbro was interpreted by Myers et al. (1980) as a dike that intruded the tonalite. The structure of the gabbroic body is an open fold (vertical plunge) with limbs that change strike ~20°and are truncated along vertical shear zones that strike ~N70°E. There are numerous joints, some of which are curved and truncated along the dike-tonalite contact. There are two orthogonal ductile kinematic indicators (Fig. 14b) and, at the hinge of the fold (N40°W) there is a strike-normal sinistral mylonite zone (Fig. 14b,d) one that is parallel to a series of closely spaced strike-slip faults (N40°W) that are dextral and sinistral based on the sigmoidal shapes of joints (Fig. 14e–g). None of the faulting is observed in the host tonalite and some joints and faults become asymptotic at the margin (Fig. 14g).

Zircons from each of these lithologies were separated and analyzed by LA-ICPMS methods. We also determined U-Pb cooling ages of apatite grains extracted from the granite. Geochronologic data is provided in Tables 5 and 6, and are portrayed graphically in Fig. 15. The Wissota tonalite has a Concordia age of 1803 ± 43 Ma and a weighted mean age of 1813 ± 15 Ma, which indicates that the tonalite is very late Penokean (or perhaps very earliest Yavapai) in age. The gabbroic body has a Concordia age of 1868 ± 87 Ma and a weighted mean age of 1846 ± 15 Ma, and includes some Archean xenocrystic zircons. Thus, the gabbroic body is not a dike that cross cuts the tonalite, rather it is a Penokean-aged xenolith that is part of the younger tonalite. The complex array of structures discussed above that pervade the dike but not

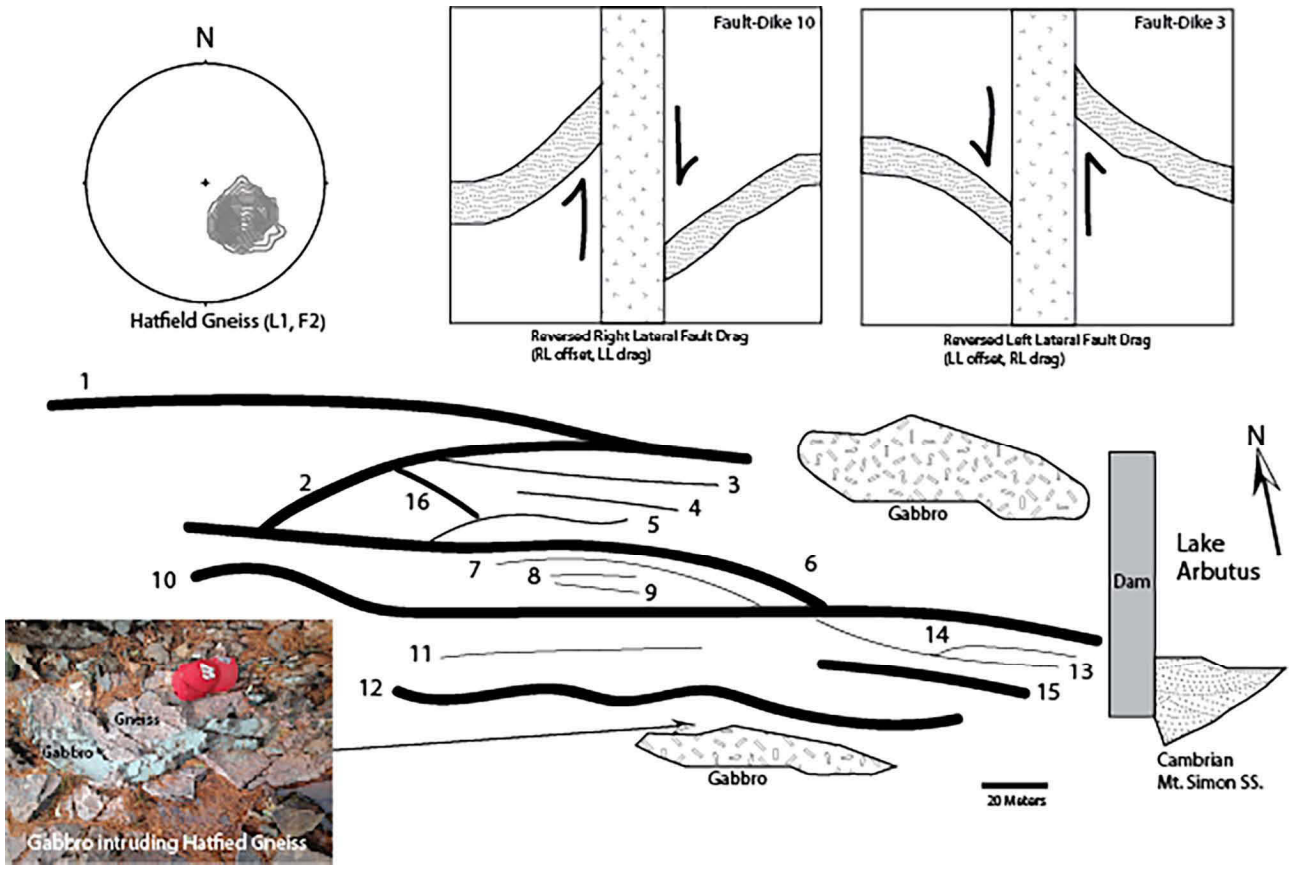

Fig. 18. Schematic geologic map of faults and dikes that crosscut the Archean Hatfield gneiss below the Lake Arbutus dam near Hatfield, WI. Thick black lines are dike-faults, thin black lines are faults. Lower hemisphere stereonet is for folds and lineations in the host gneiss.

the host tonalite and likely formed before or during tonalite ascent. Zircons extracted from the granite dike are strongly discordant, but fall nicely on an isochron that has a Concordia age of 1760 ± 20 Ma. The weighted mean age is 1758 ± 8.7 Ma. Thus, the granite dike is Yavapai in age. Apatite grains in the Wissota granite have a lower Concordia intercept of 1064 Ma and a weighted mean age of 1179 Ma indicated that these rocks were reheated during the opening of the Midcontinent rift (Table 6).

4.8.4. *Arbutus Dam, Marshfield terrane*

The principal lithology below the Lake Arbutus dam, which is the largest Archean exposure in Wisconsin, is the Archean quartzofeldspathic Hatfield Gneiss and interlayered amphibolite (Sims, 1990), which is dated at ~2.8 Ga (Maas and Brown, 1987). The gneiss is intruded by mineralized gabbro at the north and south ends of the exposure. The structural grain of the gneiss does not pervade the gabbro, which suggests that the gabbro was emplaced after Archean deformation concluded. Mafic dikes and fault-dike arrays cross cut the gneiss, and are vertical and strike ~N90°E, which is approximately normal to the strike of the country rock foliation (dip is 65° SE); both mineral lineations (L_1) and fold axes (F_2) plunge about 50°-65° to the southeast (Maas and Brown, 1987; Fig. 18). Medaris and Singer (2004) have reported an Ar-Ar re-set age from amphiboles within a similar mafic dike near Wisconsin Rapids of 1654 Ma that is interpreted to be a Mazatzal thermal overprint; they also report a widespread reset event at 1450 Ma in central Wisconsin related to intrusion of the Wolf River batholith (Fig. 1; Medaris et al., 2003, 2009). All basement rocks are overlain by the middle Cambrian Mt. Simon Sandstone (Konstantinou et al., 2014; Fig. 18).

Zircons extracted from the Hatfield Gneiss yield a Concordia age of 2929 ± 39 Ma, and a weighted mean age of 2897 ± 21 Ma (Fig. 17). A subset (n = 3) of xenocryst zircons yield ages of > 3000 Ma. The ~2900 Ma age for the Hatfield gneiss is about 100 Ma older than what was previously reported. The Arbutus gabbro has a Concordia age 2875 ± 9.9 Ma and a weighted mean age of 2880 ± 29 Ma. Thus, the gabbroic dike is Archean in age, and about 20 Ma younger than the host gneiss (Fig. 17; Table 4). Apatite separated from the gabbro has a Concordia age of 1732 ± 160 Ma and a weighted mean age of 1807 ± 9 Ma (Fig. 17, Table 4), which indicates reheating during the Penokean/Yavapai orogenies.

The 16 fault-dikes present a unique opportunity to study fault kinematics in detail over ~500 m^2 of complete exposure. The results are

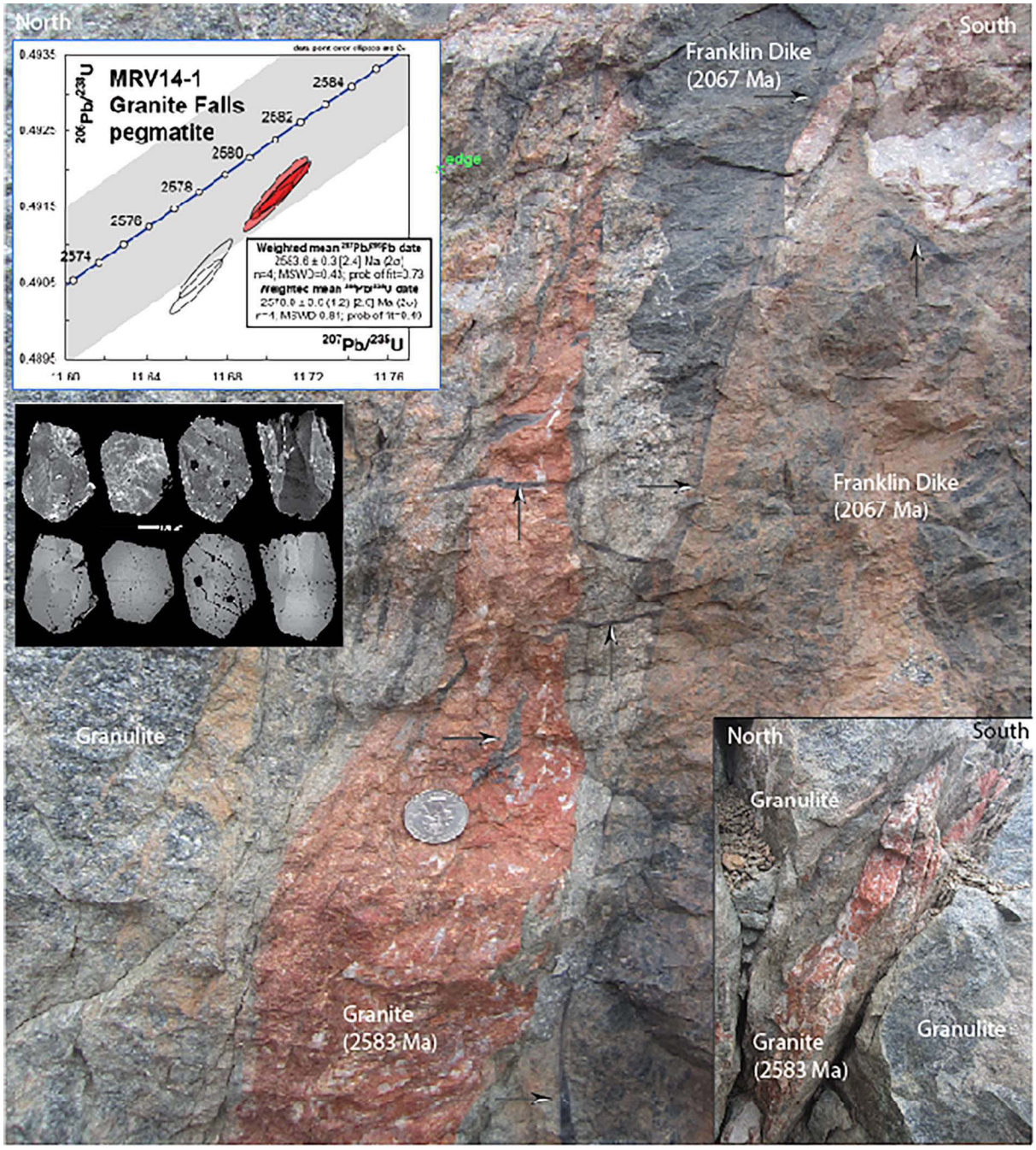

Fig. 19. Field relations of the Yellow Medicine shear zone in Granite Falls, MN. Archean granulite was intruded by a pegmatitic granite (2583 Ma; Insets: Concordia diagram and zircon CL images) then the Franklin dikes (2067 Ma) and everything was deformed during the Penokean orogen and generated pseudotachylite (arrows).

complex, with brittle features overprinting ductile kinematic structures, with changes in fault offset along strike and none of the deformation being translated to the host gniesses and amphibolites (Figs. 16 & 18; Dean and Craddock, 1993). These results will be explored, with all the Marshfield terrane geochronology (Figs. 15 & 17), in a future contribution.

4.8.5. Hamilton Mound

Greenberg and Brown (1984) reported the occurrence of ~300 outliers of purple-pink quartzite across Wisconsin that are unstudied as compared to the well-known Baraboo, Flambeau, McCaslin, Sioux and Barron quartzites where there are detrital zircon age constraints (Holm et al., 1998; Fig. 1; Table 1, samples 51–52). Most of these isolated

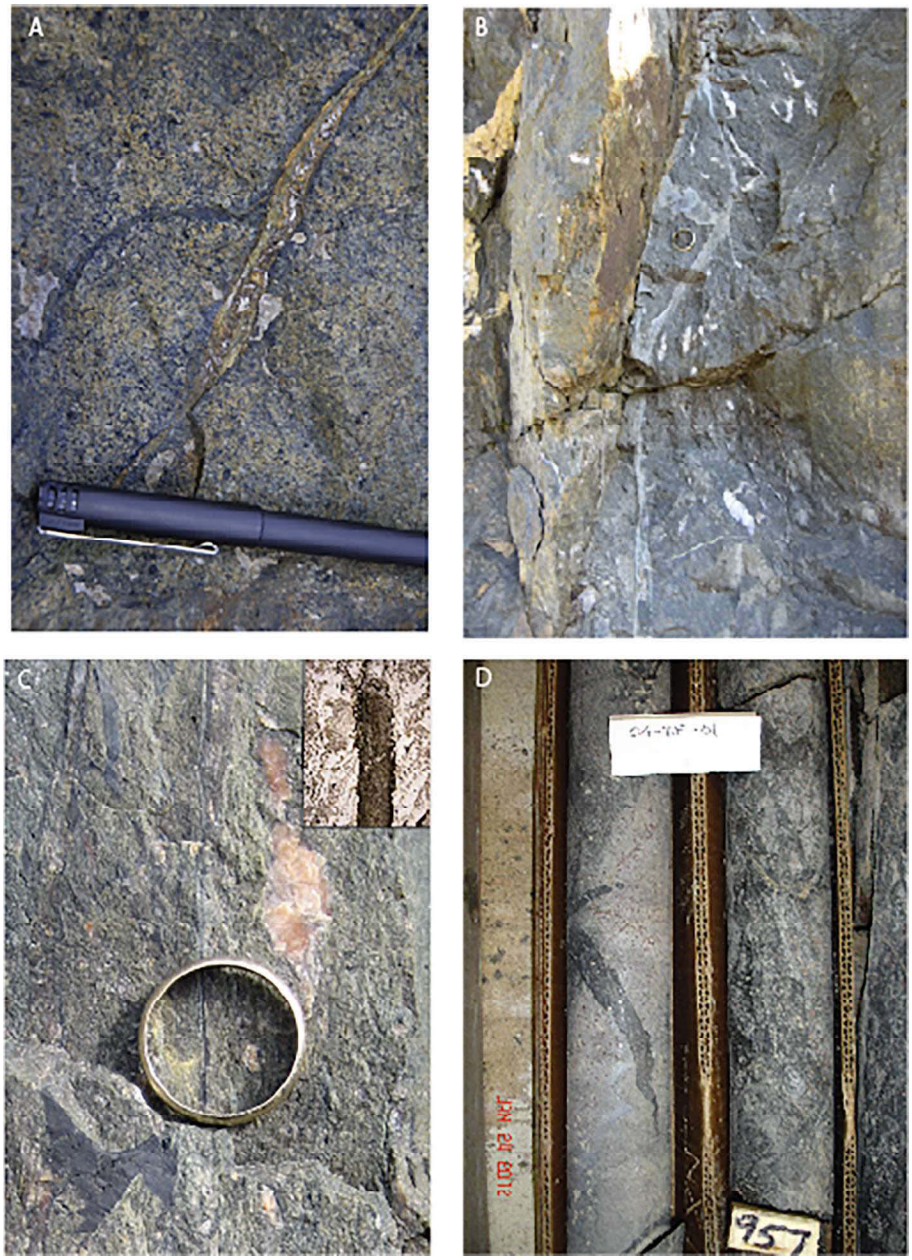

Fig. 20. Pseudotachylite related to the Penkean orogen: A. crosscutting a Franklin (2.06 Ga) mafic dike, B. along the Wawa-Quetico terrane boundary, C. along the Quetico-Wabigoon terrane boundary (thin section insert, plane light; photo width 500 μm) and, D. from drill core in the Yellow Medicine shear zone, which separates Archean gneisses of the Morton and Montevideo terranes (Fig. 19).

quartzite outliers are found in the Marshfield terrane or on Yavapai crust. Hamilton Mound is one such outlier in central Wisconsin where a lower arkosic quartzite is intruded by a granite (1.76 Ga), overlain by the Baraboo Quartzite and deformed during the Mazatzal orogen (Van Wyck and Norman, 2004; Wartman et al., 2007). Hamilton Mound shortening is layer-parallel and oriented at N60°E. The overlying, folded Seven Sisters quartzite (Baraboo-equivalent) preserves a layer-parallel shortening strain oriented at N10°W (Fig. 7f; Table 1) consistent with other Mazatzal shortening (Craddock and McKiernan, 2007).

4.8.6. *Mazatzal quartzites*

The Baraboo syncline is the best-studied of the many Mazatzal quartzite localities in Wisconsin and Minnesota (e.g Medaris et al., 2011 and references therin) and the detrital zircon work of Holm et al. (1998)

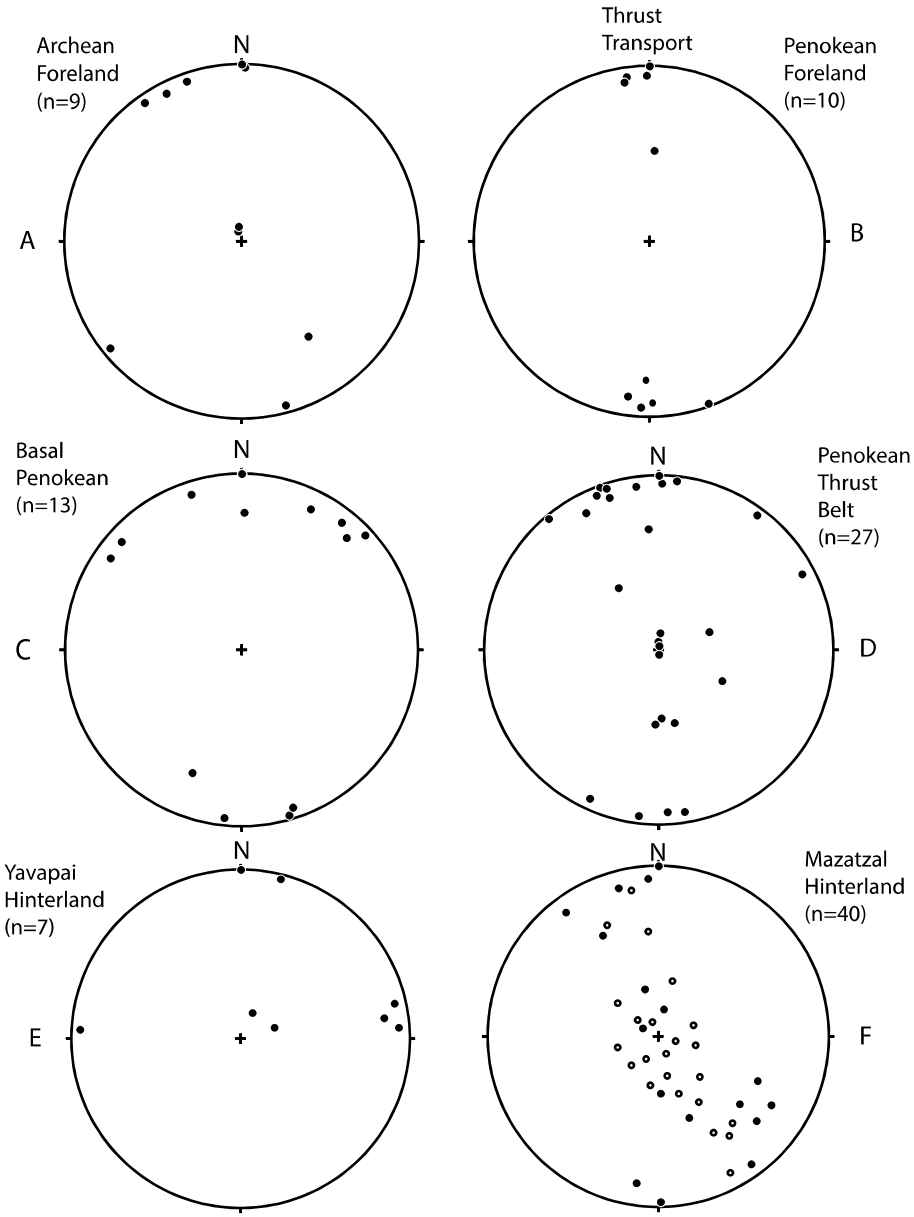

Fig. 21. Summary lower hemisphere plots of strain shortening axis data. A. Calcite twinning strains in Archean rocks in the Penokean foreland, B. Shortening strains in autochthonous Penokean foreland rocks, C. Shortening strains in the base of the Animikie basin section, D. Shortening strains in the Penokean thrust belt, E. Shortening strains related to the Yavapai orogen south of the Penokean orogen and F. Mazatzal deformation (open circles = compression axes from Riley, 1947; black = finite strain data from Craddock and McKiernan, 2007). See Table 1.

and Van Wyck and Norman (2004) better defined which purple-pink quartzites can be correlated. The quartzites in Baraboo, Flambeau and McCaslin are part of the north-vergent Mazatzal thrust belt (Romano et al., 2000) and the Sioux and Barron quartzites are part of the foreland to the north. Measurements of paleo-stress orientations (Riley, 1947) and finite strains indicate a shortening direction toward N20°W along a stereographic great circle girdle that indicates a mix of layer-parallel and layer-normal shortening. Strain gradients decrease from south to north and there was no rotation during creation of the Baraboo syncline (Craddock and McKiernan, 2007).

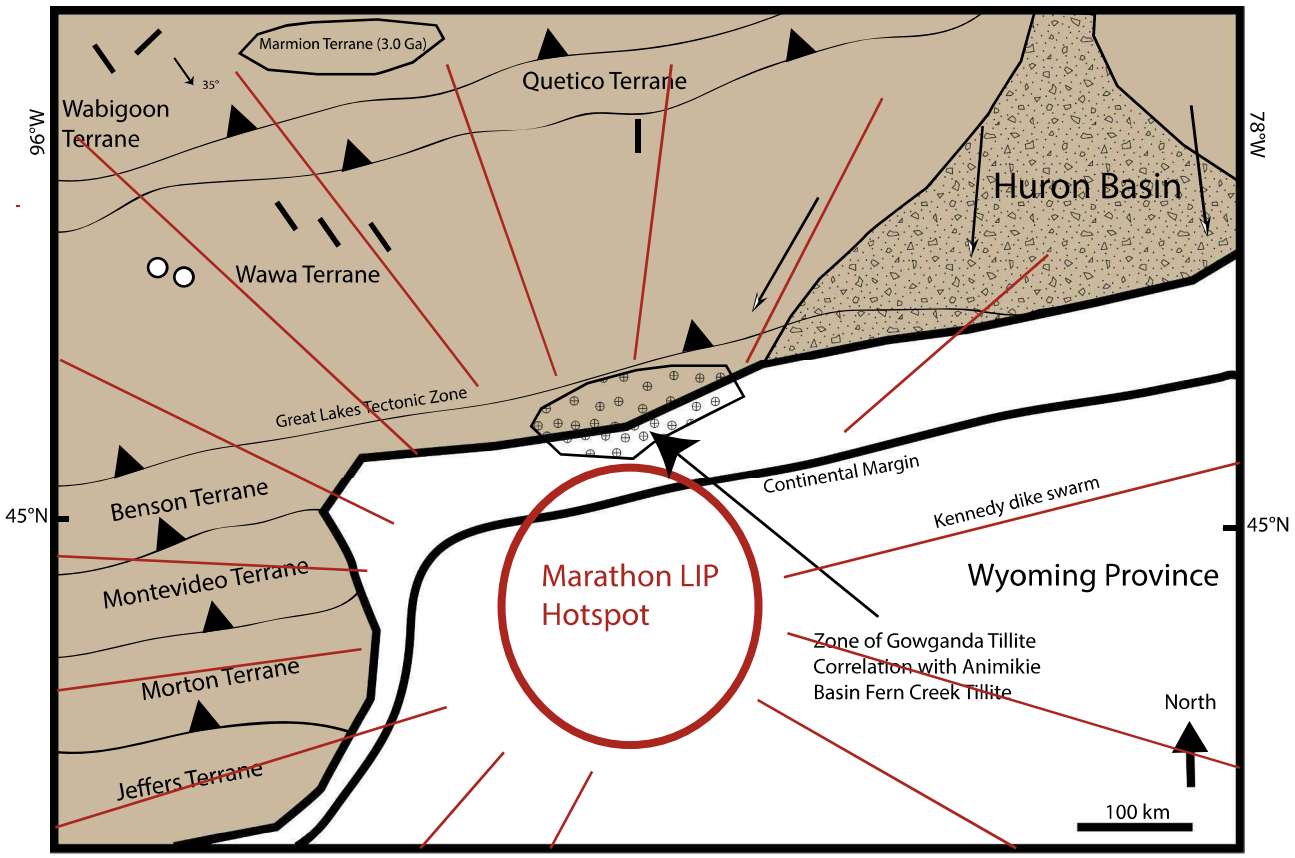

Fig. 22. Southern margin of Archean Superior province (~2.1 Ga) with the Marathon LIP hotspot and radial dike swarm and the projected southern extent of the end-Huronian Gowganda glaciation. Shortening strain data (Sites 1–9, Fig. 1 and Table 1) plotted as black lines and open circles (vertical shortening) for the Archean foreland.

4.9. Penokean pseudotachylite

Peterman and Day (1989) reported the occurrence of Penokean-aged pseudotachylite (1947 ± 27 Ma; Rb-Sr) hosted in metasedimentary rocks of the Archean Quetico belt. The frictional fault melts are in foliation planes (N45°E, 90°) parallel to the Quetico-Wawa (Abitibi; south) and Quetico-Wabigoon (north) terrane boundaries (Figs. 19 and 20). Archean basement under, or adjacent to, the Penokean thrust belt contains numerous occurrences of fault-related pseudotachylite.

Pseudotachylite is also found within the Yellow Medicine shear zone, both in the field and in drill core, which separates the Archean Morton and Montevideo terranes (Southwick and Chandler, 1996; Craddock and Magloughlin, 2005). This terrane boundary was re-activated by Penokean deformation as pseudotachylite cross cuts Archean granulites and two Proterozoic mafic dikes swarms, the 2.06 Ga Fort Francis (Schmitz et al., 2006) and 1.8 Ga hornblende andesite swarms (Himmelberg, 1968) and a previously undated granite. Zircons were separated from this granite for CA-TIMS analysis (Fig. 19; Table 5). We selected six crystal fragments that represent the clearest, most transparent, low-U, oscillatory growth zones. Two fragments exhibit some residual Pb loss and are discordant. The remaining four analyses are concordant (with decay constant uncertainties represented in Fig. 19 as the shaded band along concordia) and equivalent, with a weighted mean $^{206}Pb/^{238}U$ date of 2578.0 ± 0.6(1.2)[2.6] Ma), and weighted mean $^{207}Pb/^{206}Pb$ date of 2583.6 ± 0.3[2.4] Ma). The latter $^{207}Pb/^{206}Pb$ date is interpreted as the age of igneous crystallization (the choice of $^{207}Pb/^{206}Pb$ date maintains consistency with other published Archean geochronology). This age is younger than the 2603 ± 1 Ma ages for voluminous, late-kinematic monzogranites (e.g. Ortonville and Sacred Heart granites) that intrude the Mesoarchean gneisses of the Minnesota River Valley. It is more similar to the 2591 ± 2 Ma ages for postkinematic syenogranites and aplitic dikes, and thus helps to further constrain the final penetrative deformation of the Minnesota River Valley subprovince (Schmitz et al., 2006; Bickford et al., 2006). Additional pseudotachylite locales hosted in Archean basement are detailed in Table 6 and may be related to Penokean tectonism, like the decompression melts (1847 Ma) found 300 km into the foreland in the Wabigoon terrane at Pickle Lake (Holm et al., 2007).

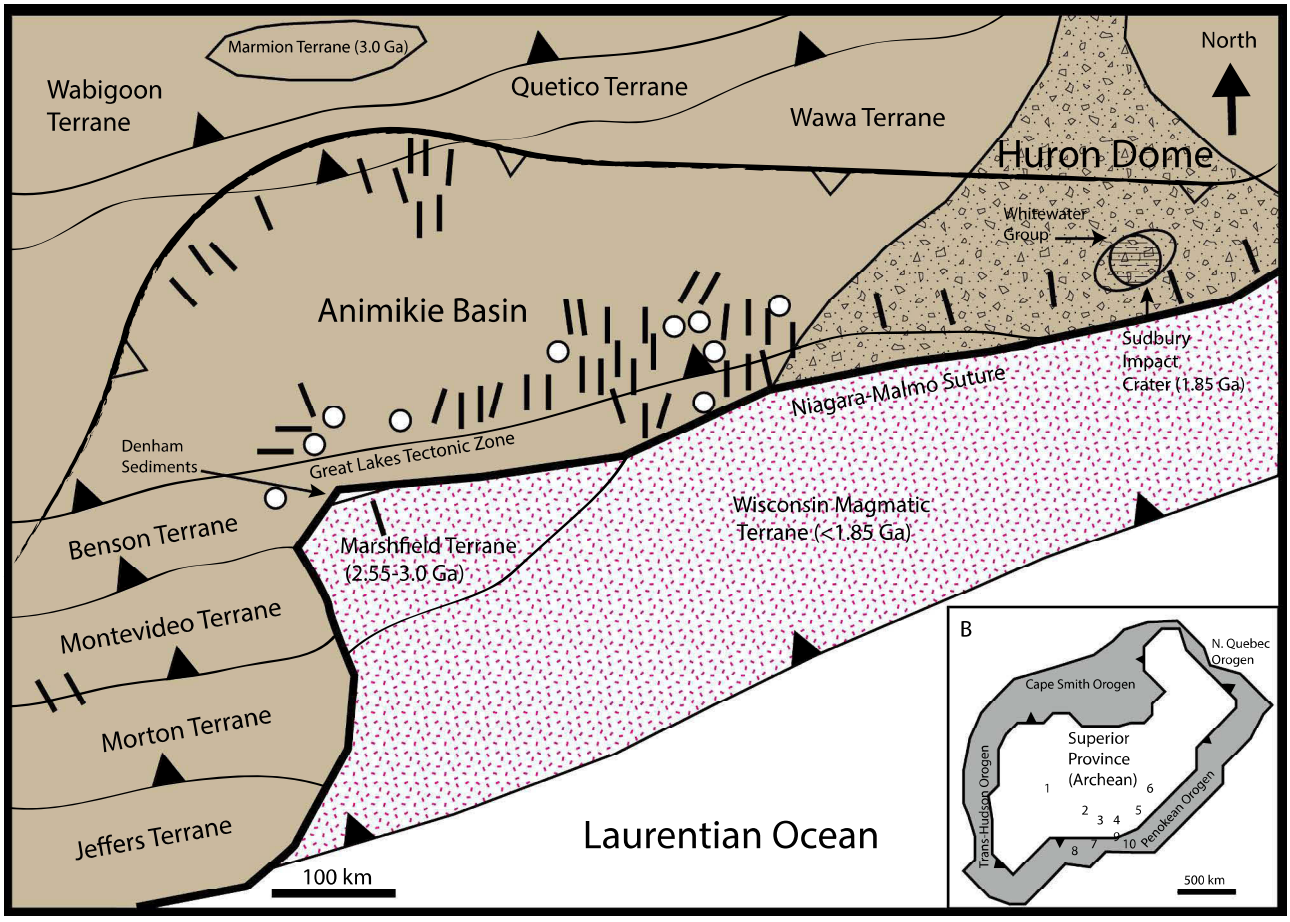

Fig. 23. Shortening strain axes for Penokean deformation in Huronian and Animikie basin strata (Sites 15–50, Table 1, Figs. 1 and 21; open circles are vertical shortening strains). Presumed Penokean-aged pseudotachylite (see insert B, Table 6) are the result of orogenic convergence everywhere around the Superior province ~ 1850 Ma.

5. Discussion

5.1. Penokean thrust belt and foreland strains

The Animikie-Huron basin sections do not present a uniform stratigraphy where, for example, any one carbonate or siliciclastic unit was deposited and deformed uniformly across the region. Even the SIL is very heterogeneous (impact pseudotachylite, seismites, tsunamites, ashfall lapilli) across the region. As a result, our strain data is from a variety of techniques on a variety of strain markers (Table 1; Figs. 1 and 2), compiled and plotted in structural or orogenic groupings (Fig. 21) and in a series of schematic figures that represent changes in the stress–strain field through the interval ~2100 (pre-Penokean) to 1630 Ma (Figs. 23–25; oldest to youngest) with a schematic tectonic cross section (Fig. 26).

The southern margin of the Superior province was an extensional boundary when the Wyoming province rifted at 2.1 Ga leaving a passive margin for deposition of the Huron and Animikie sections (Ernst and Bleeker, 2010; Craddock et al. 2013a). Strains within the Archean Wawa and Wabigoon terranes are complex and these rocks do not record a Penokean overprint despite being only ~100 km inboard of the northernmost Penokean deformation (Figs. 21, 22). Normal faults along the Superior margin led to an irregular surface upon which Animikie strata were deposited (Fig. 2) and some of these normal faults were reactivated, forming the Amasa dome and the Felch trough, as examples, as the Penokean orogen evolved. Consequently, there are thick-skinned structures close to the Niagara suture underlain by south-dipping thrust faults with complex folds and refolded folds with multiple cleavage orientations (Schultz and Cannon, 2007). Thirty to fifty km north of the Niagara suture is a margin-parallel zone of north-vergent folds, including nappes (Animikie, not Huron), and south-dipping thrust faults. Strains in this zone are dominantly layer-parallel shortening, normal to the Penokean margin (Fig. 23). Fifty to sixty kilometers from the Penokean margin is a narrow zone of strain overprints with mixed layer-normal and layer-parallel shortening, including layer-parallel shortening in vertical beds (open circles, Fig. 23). Twinned calcite does not record a strain overprint except in Sample 44 (Little Presque Isle; high NEVs) where the strain overprint is vertical shortening. The

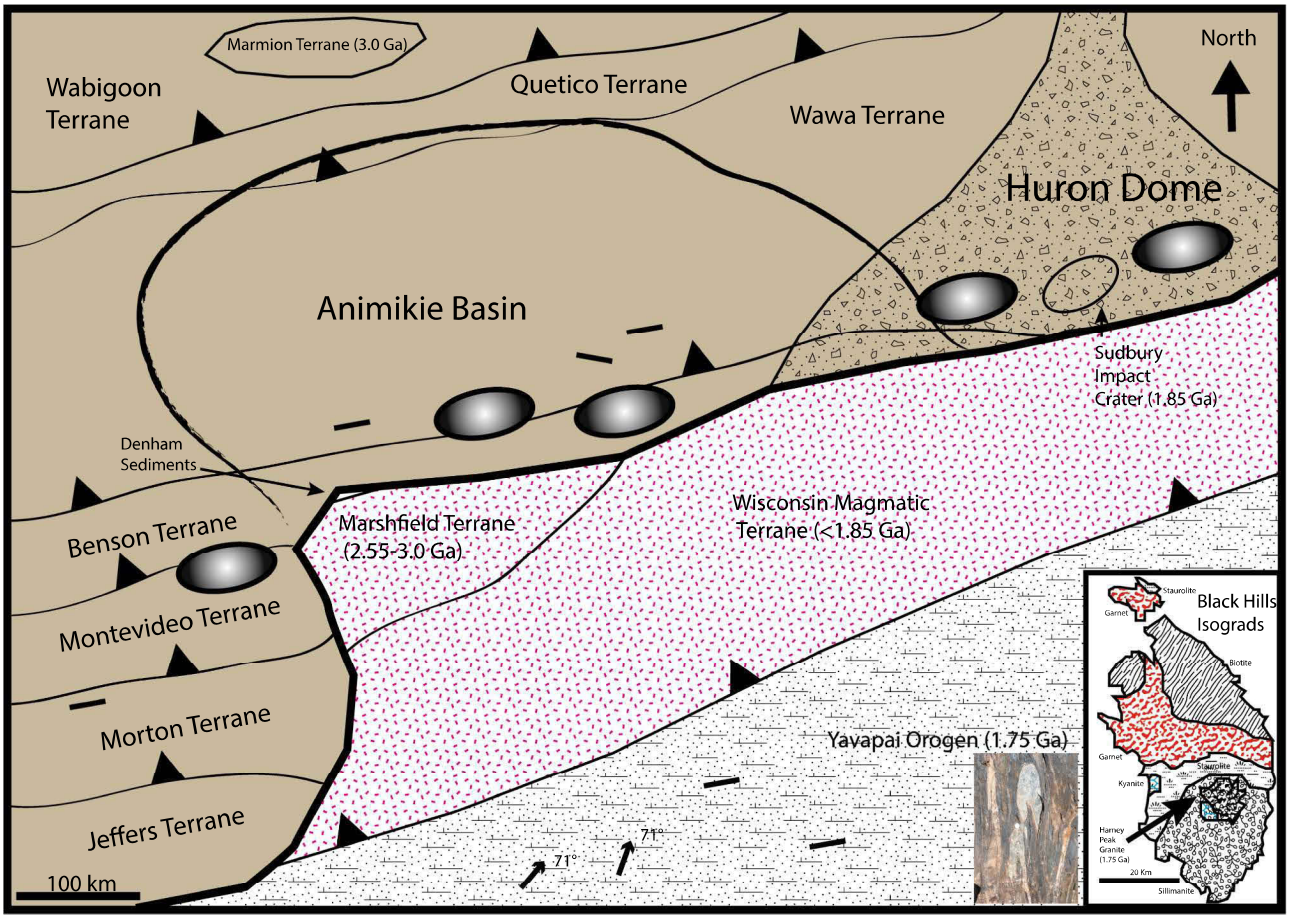

Fig. 24. Accretion of Yavapai crust from the south resulting in margin-parallel shortening both in Yavapai crust and in older Penokean rocks. Shaded ellipses represent Barrovian metamorphic isograds (James, 1955; Holm et al., 1988) known to be Yavapai in age and often associated with Yavapai intrusions-400 km inboard of the Yavapai margin. Inset: Yavapai isoclinal folds and isograds around the Harney Peak (1.715 Ga) granite in the Black Hills, SD.

Sudbury impact lapilli provide a unique strain marker as ellipsoids in the thrust belt (Sample 33; Figs. 3a and 5b; layer-normal shortening at Connors Creek) and spheres in the foreland (Fig. 10a). This strain fabric is indicative of nappe burial (Craddock et al. 2007). From 60 to 200 km north of the margin, all the shortening is layer-parallel and normal to the Penokean margin (Fig. 23). All the strain shortening axes plot as a girdle parallel to the inferred Penokean thrusting direction, with better resolution if the Penokean margin curvature is removed (Fig. 21d), or referenced to the "stable craton" site (flat-lying Gunflint Fm. in Thunder Bay with N-S layer-parallel shortening; Sites 14e,f). This regional strain fabric is identical to the collisional Appalachians where the layer-parallel shortening strain is parallel in individual thrust sheets across the belt and parallel with the same pre-thrusting strain fabric in the foreland (Kilsdonk and Wiltschko, 1988; Craddock and van der Pluijm, 1989; Hnat and van der Pluijm, 2011). The diversity of deformation mechanisms, strain measuring techniques and rock types does not lend our data set to a comparison of differential stresses (~300 MPa) and strain magnitudes (highly variable) across the belt (van der Pluijm et al., 1997).

The N-S Pass Lake transect near Thunder Bay (Fig. 8) requires additional interpretation. In analyzing the structurally lower E-W thrust-related hangingwall folds (N-S transport) and the upper N-S folds in the Gunflint Fm. (Fig. 9), there is clearly a major sub-horizontal structural complication (Baird, 2015). The upper folds could have formed as part of a very large slump along the NW margin of the Animikie basin, deformation related to a Penokean lateral thrust ramp, or distal shortening from the Trans-Hudson orogeny far to the west (Corrigan et al. 2009). The later interpretation could help explain young detrital zircons (1818, 1826 Ma) in the Rove Fm. reported by Craddock et al. (2013a). We favor an interpretation that includes slumping on the NW margin of the Animikie basin caused by the Sudbury impact (~800 km to the east) as these folds have a similar orientation to the SIL folds in the Gunflint Fm. ~150 km to the SW (Figs. 10 and 11). The N-S folds in the Gunflint Fm. near Thunder Bay are structurally and stratigraphically above the leading edge of the Penokean thrust belt (Fig. 8) and below the SIL 1 km to the north (exposed at new roadcuts at Terry

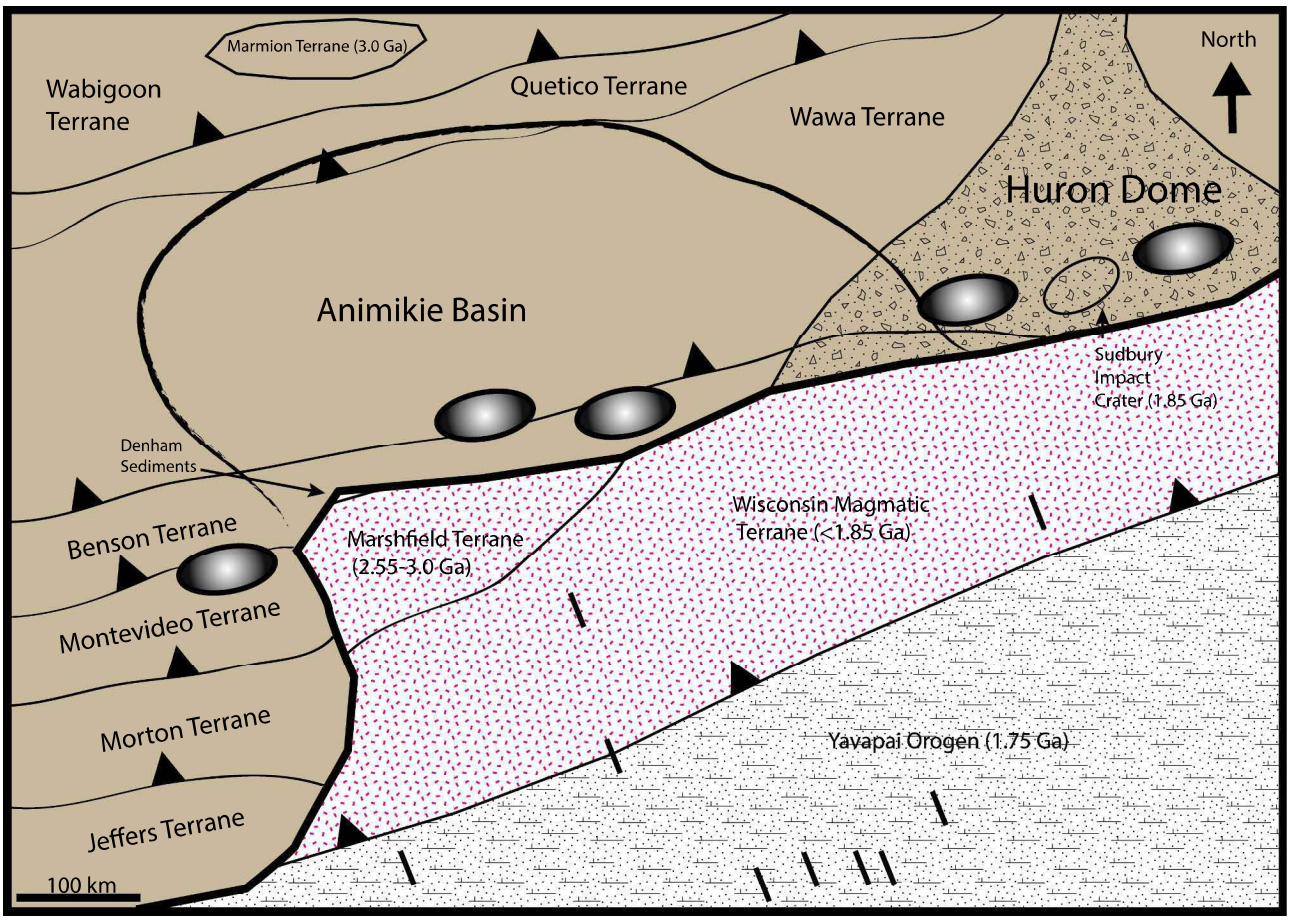

Fig. 25. Shortening strain axes in Baraboo-equivalent quartzites deformed by the Mazatzal orogen (Holm et al., 1998; Craddock and McKiernan, 2007; Medaris et al., 2011). See Table 1, Figs. 1 and 21.

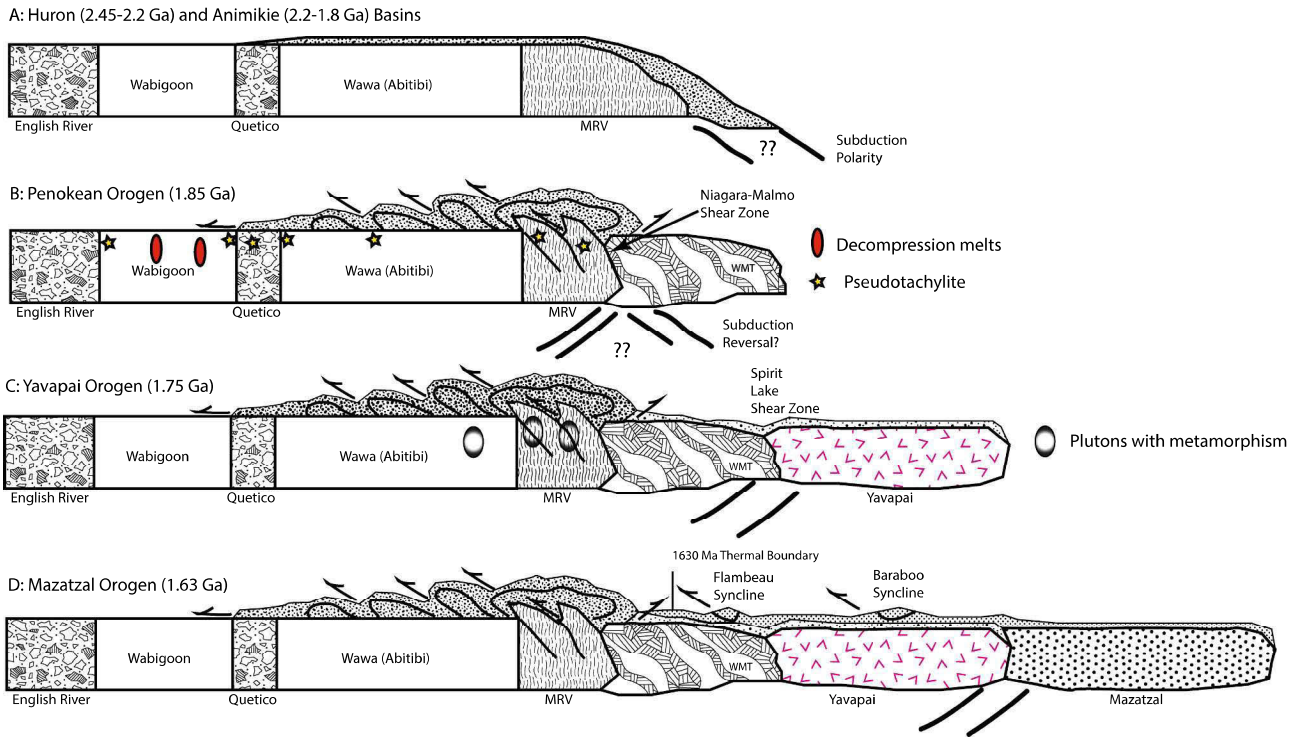

Fig. 26. Schematic, cross sectional tectonic representation of a) Huron-Animikie basin sedimentation (MRV: Archean Minnesota River Valley terranes), b) accretion of the Wisconsin Magmatic terrane (WMT, includes Marshfield terrane) to form the Penokean thrust belt, c) accretion of Yavapai crust with associated intrusions and metamorphism, and d) accretion of Mazatzal crust with foreland thermal overprint (1630 Ma; Romano et al. 2000).

Table 2
XRF Results, Saganaga Lake Lamprophyres (Site 9).

	LAMP-1 %	LAMP-2 %
SiO_2	50.05	44.29
TiO_2	2.486	3.768
Al_2O_3	9.94	11.13
Fe_2O_3	12.97	16.80
MnO	0.194	0.200
MgO	8.95	9.23
CaO	8.06	7.41
Na_2O	1.78	2.86
K_2O	0.82	1.52
P_2O_5	0.312	0.634
LOI	4.30	2.50
	ppm	ppm
Sc	22	17
V	292	305
Cr	721	418
Co	76	77
Ni	437	347
Cu	162	84
Zn	100	123
Ga	20	27
Rb	18	58
Sr	410	589
Y	18	27
Zr	173	358
Nb	21	40
Ba	512	971
La	24	45
Ce	39	65
Pb	26.1	7
Th	3	4
U	bd	1

Values reported are average of 2 analyses; Fe analyzed at total Fe_2O_3.
All samples dried > 2 h at 110 deg. Celcius prior to LOI.
Loss on Ignition (LOI) reported as percent weight change of pre-dried samples after sintering for one hour at 1000 deg. C.

Fox wayside) thereby dating the distal Penokean thrusting at 1849 Ma.

5.2. Yavapai and Mazatzal strain

The regional tectonic scenario shows the Archean Superior province terranes with progressive addition of crust from the south (Fig. 26). Animikie basin strata were deposited on the passive margin then deformed by the accretion of the Wisconsin Magmatic and Marshfield terranes forming the Penokee Mountains fold and thrust belt and decompression melts and pseudotachylite in the Archean foreland. The Yavapai orogen then generated widespread Barrovian metamorphism (James, 1955) preserved best in the deformed Huron-Animikie strata of the Penokee Mountains (Holm et al. 1988; Tohver et al., 2007; Fig. 24). The Penokee Mountains remained a highland and a source siliciclastic sediment shed to the south, with the exception being at Hamilton Mound, WI although the outcrop has been quarried out of existence. Yavapai shortening was parallel to the margin (~N60°E) and includes the sheared, vertical Palms Fm. (Sample 44) and the twinning strains in the Hemlock Fm. volcanics that are largely replacement calcite (Sample 23) in the Penokean thrust belt, and the quartzites at Veedum and Hamilton Mound in the hinterland (Fig. 20). Mazatzal accretion was next with the regional thermal peak at 1630 Ma (Romano et al., 2000) roughly along the boundary between quartzites deformed by the Mazatzal orogen (Flambeau, McCaslin) and the flat-lying Barron Quartzite in the foreland. Mazatzal shortening was oriented ~N20°W with both layer-parallel and layer-normal shortening, indicative of the stacking of nappes (Craddock and McKiernan, 2007; Fig. 25). Mazatzal quartzites also were derived from a northerly source and include Proterozoic BIF clasts from the Penokee Mountains (Dott, 1983; Medaris et al 2003).

5.3. Penokean and Yavapai metamorphism

From the Penokean margin north ~50 km there are well-known metamorphic nodes (Republic, Peavy) where the isograds are discordant in deformed Huron (Bennett et al., 1991) and Animikie (James, 1955) strata. Dating of plutons in this structural setting (Holm et al.,

Table 3
AMS Results.

			Anisotropy					
Sample	Orientation	n =	Kmax	Kint	Kmin	Lineation	Foliation	Plane
Saganaga Lamprophyre (Site 9)	0°, 90°	20	1.1	1.02	0.94	1.04	0.97	1.07
Saganaga Lamprophyre (Site 9)	0°, 90°	17	1.1	1.01	0.96	1.008	1.012	1.022
Gunflint Fm. (lapilli)[#]	35°, 7°SE	20	1.003	1.001	0.994	1.001	1.006	1.008
Gunflint Fm. (impact folds)[#]	35°, 7°SE	20	1.038	0.996	0.965	1.04	1.032	1.075
Gunflint Fm. (−1 m)[#]	35°, 7°SE	19	1.004	0.998	0.997	1.005	1.001	1.007
Gunflint Fm. (−20 m)[#]	35°, 7°SE	22	1.002	0.999	0.997	1.003	1.001	1.005
Gunflint Fm. (−200 m)[#]	35°, 7°SE	21	1.01	1.005	0.98	1.006	1.02	1.03
Gunflint Fm. (−300 m)[*]	35°, 7°SE	20	1.01	1.004	0.98	1.005	1.001	1.006

Explanation: anisotropy (Kmax = long axis, Kmin = short axis); lineation (Kmax − Kint /Kmean); foliation (Kint − Kmin /Kmean); P is the total anisotropy kmax/kmin.
[*] Thunderbird Mine, Eveleth, MN (Site 11).
[#] 5 samples from a profile near Gunflint Lake, MN (see Jirsa, 2011; Figs. 10 and 11).

Table 4
U-Pb Isotopic Data for Zircon for Wissota Dam, Arbutus Dam and Veedum, WI.

				Radiogenic Isotopic Ratios							Isotopic Dates						
Grain	U ppm	U Th	$^{206}Pb/^{204}Pb$	$^{207}Pb/^{206}Pb$	% err	$^{207}Pb/^{235}U$	% err	$^{206}Pb/^{238}U$	% err	corr. coef.	$^{207}Pb/^{206}Pb$	±	$^{207}Pb/^{235}U$	±	$^{206}Pb/^{238}U$	±	discordance (%)
Gabbro (Lake Arbutus; Figs. 16–18)																	
Spot 4	236	3.6	73,336	0.2049	1.1	16.12	2.2	0.5710	2.0	0.88	2912	46	2884	21	2866	17	−1.6
Spot 3	253	2.3	100,099	0.2052	1.1	15.93	1.8	0.5633	1.5	0.81	2880	34	2873	17	2868	17	−0.4
Spot 5	197	2.4	48,611	0.2097	0.8	15.91	1.9	0.5504	1.7	0.90	2827	39	2871	18	2903	13	2.6
Hatfield Gneiss (Lake Arbutus; Figs. 16–18)																	
BRFG_2b				0.2647	0.4	25.39	1.1	0.6958	0.8	0.96	3323	11	3405	20	3275	7	0.0
BRFG_2a				0.2413	0.5	22.31	1.3	0.6707	0.9	0.94	3197	12	3309	22	3129	9	−0.1
BRFG_4a				0.2254	0.4	16.11	1.1	0.5185	0.8	0.96	2884	10	2693	17	3020	7	0.1
BRFG_4b				0.2115	0.5	15.70	1.2	0.5386	0.8	0.95	2859	11	2777	18	2917	8	0.0
BRFG_5a				0.2111	0.4	14.98	1.2	0.5149	0.9	0.96	2814	11	2678	19	2914	7	0.1
BRFG_1a				0.2071	0.4	13.32	1.1	0.4666	0.8	0.96	2703	11	2469	16	2883	7	0.1
BRFG_3b				0.2065	0.5	13.14	1.1	0.4615	0.8	0.95	2690	11	2446	16	2878	8	0.2
BRFG_1b				0.2086	0.4	12.57	1.2	0.4372	0.8	0.96	2648	11	2338	16	2895	7	0.2
BRFG_3a				0.1986	0.4	11.85	1.1	0.4327	0.8	0.96	2593	10	2318	15	2815	7	0.2
Wissota Dike (Xenolith; Figs. 14 & 15)																	
Spot 9	683	2.3	58,300	0.1895	1.0	14.48	1.6	0.5543	1.3	0.79	2843	29	2781	15	2738	16	−3.9
Spot 5	417	3.5	23,707	0.2013	0.8	14.94	1.7	0.5385	1.5	0.87	2777	34	2811	16	2837	13	2.1
Spot 13	124	1.0	281,452	0.1813	0.9	12.95	2.0	0.5182	1.8	0.90	2692	39	2676	19	2665	14	−1.0
Spot 8 r2	304	1.1	14,154	0.2036	0.8	10.83	2.0	0.3858	1.9	0.92	2103	34	2508	19	2855	13	26.3
Spot 3	74	1.3	39,897	0.1136	1.0	5.208	2.1	0.3326	1.8	0.87	1851	29	1854	18	1858	19	0.4
Spot 1	67	0.9	50,457	0.1120	1.1	5.035	2.1	0.3262	1.9	0.86	1820	29	1825	18	1832	20	0.7
Spot 12	227	1.5	196,883	0.1129	1.1	5.051	2.1	0.3245	1.8	0.84	1812	28	1828	18	1847	21	1.9
Wissota Trondjhemite (Figs. 14 & 15)																	
Spot 43	118	97.5	38,390	0.1075	1.2	4.525	2.0	0.3055	1.6	0.80	1719	24	1736	16	1757	22	2.2
Spot 53	2099	17.3	7156	0.1082	1.3	2.946	2.1	0.1977	1.6	0.78	1163	17	1394	16	1769	24	34.3
Spot 36	2064	14.4	4661	0.1135	2.0	2.920	2.6	0.1866	1.7	0.66	1103	18	1387	20	1857	36	40.6
Spot 48	3047	12.7	3289	0.1073	1.1	2.307	2.7	0.1560	2.4	0.92	934	21	1214	19	1754	19	46.7
Spot 38	3019	18.7	4069	0.1077	1.1	2.303	2.1	0.1551	1.8	0.86	930	16	1213	15	1761	20	47.2
Spot 37	2581	17.4	5187	0.1074	0.9	2.088	1.6	0.1411	1.3	0.81	851	10	1145	11	1756	17	51.6
Spot 51	2941	13.0	2745	0.1226	1.0	2.056	2.1	0.1217	1.8	0.87	740	13	1134	14	1994	18	62.9
Spot 57	33	26.2	26,300	0.1168	1.7	1.883	2.5	0.1170	1.9	0.76	713	13	1075	17	1908	30	62.6
Spot 47	2495	11.7	2618	0.1194	1.1	1.876	1.7	0.1141	1.3	0.77	696	8	1073	11	1947	19	64.2
Spot 45	2403	5.7	4537	0.1138	0.8	1.750	1.9	0.1115	1.8	0.92	682	11	1027	12	1861	14	63.4
Spot 50	2919	13.1	2112	0.1253	1.1	1.566	2.2	0.0907	1.9	0.86	560	10	957	14	2034	20	72.5
Spot 46	2649	5.8	2922	0.1100	1.2	1.243	2.1	0.0820	1.7	0.81	508	9	820	12	1799	23	71.8
Spot 56	2119	0.5	2922	0.1138	1.1	1.197	1.8	0.0763	1.5	0.80	474	7	799	10	1862	20	74.6
Wissota Tonalite (Figs. 14 & 15)																	
LPIG_3c				0.1136	0.7	4.740	1.6	0.3026	1.0	0.95	1774	13	1704	15	1858	13	4.5
LPIG_3a				0.1139	0.7	4.683	1.6	0.2982	1.0	0.95	1764	13	1682	15	1863	13	5.3
LPIG_3b				0.1133	0.7	4.675	1.6	0.2992	1.0	0.95	1763	13	1688	15	1853	13	4.9
LPIG_1e				0.1103	0.7	4.506	1.6	0.2963	1.0	0.95	1732	13	1673	15	1804	13	4.0
LPIG_1d				0.1091	0.7	4.257	1.6	0.2829	1.0	0.95	1685	13	1606	14	1785	13	5.6
LPIG_1b				0.1115	0.7	4.240	1.6	0.2757	1.0	0.95	1682	13	1569	14	1825	13	7.8
LPIG_1c				0.1107	0.7	3.991	1.6	0.2616	1.0	0.95	1632	13	1498	14	1810	13	9.8
Veedum Quartzite (Site 50)																	
004A				0.1684	1.0	11.35	0.03	0.4885	0.01	0.96	2543	5.1	2552	24	2564	26	−0.8
005A				0.3006	1.9	28.48	0.08	0.6973	0.02	0.96	3473	5.0	3436	27	3372	33	2.9
014A (rim)				0.0873	0.4	2.04	0.04	0.1890	0.04	0.96	1153	5.2	1128	16	1116	11	3.2
006A				0.2978	1.8	27.84	0.08	0.6780	0.08	0.96	3459	4.7	3414	27	3336	33	3.5
008A				0.1673	1.0	10.61	0.38	0.4598	0.01	0.96	2531	5.2	2489	25	2439	25	3.6
010A				0.1843	0.1	12.36	0.35	0.4867	0.01	0.96	2692	5.4	2633	26	2556	27	5.0
012A				0.1703	0.07	10.32	0.20	0.4395	0.01	0.96	2561	3.3	2464	18	2349	18	8.3
003A (rim)				0.0778	0.05	1.879	0.05	0.1752	0.00	0.96	1142	7.0	1074	18	1040	12	8.9
017A (rim)				0.0772	0.06	1.822	0.04	0.1712	0.00	0.96	1126	7.6	1053	15	1019	10	9.6
001A				0.0889	0.06	2.650	0.07	0.2163	0.01	0.96	1401	6.4	1315	20	1262	14	9.9
018A				0.3166	0.17	28.038	0.73	0.6423	0.02	0.96	3553	4.2	3420	25	3198	31	10.0

Notes:
1. Discordance is based on [($^{206}Pb/^{207}Pb$ date − $^{206}Pb/^{238}U$ date)/$^{206}Pb/^{207}Pb$ date].
2. All uncertainties are reported at the 1-sigma level, and include only measurement errors.
3. Systematic errors are as follows (at 2-sigma level): [2.5% ($^{206}Pb/^{238}U$) & 1.4% ($^{206}Pb/^{207}Pb$)].
4. Analyses conducted by LA-MC-ICPMS, as described by Gehrels et al. (2008).
5. U concentration and U/Th are calibrated relative to Sri Lanka zircon standard and are accurate to ~20%.
6. Common Pb correction is from measured ^{204}Pb with common Pb composition interpreted from Stacey and Kramers (1975).
7. Common Pb composition assigned uncertainties of 1.5 for $^{206}Pb/^{204}Pb$, 0.3 for $^{207}Pb/^{204}Pb$, and 2.0 for $^{208}Pb/^{204}Pb$.
8. U decay constants and composition as follows: $^{238}U = 9.8485 \times 10^{-10}$, $^{235}U = 1.55125 \times 10@^{-10}$, $^{238}U/^{235}U = 137.88$.

(continued on next page)

Table 4 (*continued*)

U-Pb Isotopic Data for Apatite

			Corrected Isotopic Ratios				^{207}Pb-Corrected Isotopic Date	
Grain	U ppm	% Pbc	^{238}U/^{206}Pb	% err	^{207}Pb/^{206}Pb	% err	^{206}Pb/^{238}U	±
Gabbro (Lake Arbutus; Figs. 16–18)								
Spot 13	1.24	36.0	1.8406	2.4	0.5164	1.5	1593	57
Spot 5	0.63	34.2	1.9566	2.8	0.4846	1.8	1607	62
Spot 2	1.09	26.8	2.0924	2.4	0.4039	1.2	1768	61
Spot 1	1.11	23.3	2.2550	2.5	0.3585	1.5	1770	63
Spot 15	2.27	13.1	2.6757	2.4	0.2415	2.3	1773	68
Spot 18	1.38	20.0	2.3711	2.5	0.3208	1.6	1786	64
Spot 6	1.26	31.5	1.7641	2.6	0.4871	1.1	1798	63
Spot 8	1.02	26.4	2.0481	2.5	0.4056	2.0	1804	67
Spot 7	1.00	22.1	2.2425	2.7	0.3488	1.2	1810	65
Spot 16	1.14	21.8	2.2341	2.5	0.3471	1.1	1822	62
Spot 14	0.80	30.1	1.7588	2.7	0.4759	1.7	1851	69
Spot 4	1.65	18.1	2.3277	2.4	0.3067	2.2	1861	70
Spot 3	1.18	21.1	2.1967	2.5	0.3439	2.2	1865	71
Spot 17	1.67	19.7	2.1420	4.2	0.3368	8.8	1938	170
Spot 11	0.85	24.5	1.8753	2.8	0.4090	4.9	1975	107
Spot 12	0.87	22.7	1.9579	2.5	0.3825	1.7	1977	71
Spot 10	0.61	25.3	1.7536	2.6	0.4343	1.9	2028	74
Spot 21	0.50	16.0	1.1851	3.0	0.5264	2.9	2733	113
Spot 20	7.75	0.4	1.5996	2.4	0.2451	0.2	3113	91
Wissota Dike (Figs. 14 & 15)								
Spot 2	2.38	35.1	3.6880	4.5	0.3979	3.8	987	60
Spot 6	2.32	31.6	3.2937	1.5	0.3787	2.7	1151	44
Spot 1	1.74	26.5	3.5673	1.4	0.3274	3.5	1163	50
Spot 3	2.20	26.2	3.4614	1.9	0.3274	2.6	1199	47
Spot 8	2.16	26.6	3.2863	2.0	0.3353	6.0	1247	79
Spot 9	2.69	23.5	3.2833	1.1	0.3086	4.5	1305	64
Spot 7	1.58	27.0	3.0262	1.6	0.3484	5.8	1326	79
Spot 11	1.44	27.7	2.2204	1.3	0.4006	5.3	1668	90
Spot 5	1.31	20.8	2.2766	2.0	0.3345	3.3	1824	76

Notes:
1. All uncertainties are reported at the 1-sigma level, and include only measurement errors.
2. Systematic errors are as follows (at 2-sigma level): [2.5% (^{238}U/^{206}Pb) & 1.4% (^{206}Pb/^{207}Pb)].
3. Analyses conducted by LA-MC-ICPMS, as described by Thomson et al. (2012).
4. U concentration and U/Th are calibrated relative to MAD apatite standard and are accurate to ~20%.
5. Common Pb corrected date is from ^{207}Pb/^{206}Pb – ^{238}U/^{206}Pb age concordance.
6. U decay constants and composition as follows: $^{238}U = 9.8485 \times 10^{-10}$, $^{235}U = 1.55125 \times 10^{-10}$, $^{238}U/^{235}U = 137.88$.

1988) and metamorphic xenotime and monazite (Tohver et al., 2007; Vallini et al. 2007) have revealed that the metamorphism is Yavapai (1750 Ma) in age, a result also reported in Huronian sediments (1738 Ma; Rasmussen et al. 2013, Fig. 24). Garnet growth rates in Animikie strata are Yavapai in age and consistent with a short-lived Proterozoic orogen (Holm and Selverstone, 1990). The Wisconsin Magmatic and Marshfield terranes did not experience widespread Yavapai metamorphism, only rocks ~120 km north of the Yavapai margin and in-board for another ~200 km where plutons intruded (Holm et al., 2007). Kyanite-sillimanite assemblages are found in Animikie BIFs and turbidites near the margin and grade north to assemblages of biotite and Fe-silicates (i.e., greenschist). Studies of quartz microstructures and dislocation densities in the Mesnard Quartzite in the Republic metamorphic node preserve Yavapai stress gradients that are −33 to −77 MPa and highest in the low-grade metamorphic assemblages . There is no metamorphic or structural overprint in Penokean rocks caused by the Mazatzal orogen. The Penokean hinterland did experience widespread metamorphism during intrusion of anorogenic Wolf River magmas (Medaris and Singer, 2004), also represented by the 1450 Ma aged zircon rims in our Veedum, WI quartzite. The Veedum Quartzite also has Keweenaw (Grenville) zircon rim ages, ~100 km southeast of the rift margin.

5.4. Penokean pseudotachylite

The Superior province was surrounded by accretionary, convergent tectonism by the Penokean, Trans-Hudson (including Cape Smith) and New Quebec orogens ~1850 Ma. We have observed numerous

Table 5
CA-TIMS U-Th-Pb isotopic data, Granite Falls, MN Granite (Site 48).

	Compositional Parameters						Radiogenic Isotope Ratios							Isotopic Dates							
Sample	Th	$^{206}Pb^*$	mol %	Pb^*	Pb_c	^{206}Pb	^{208}Pb	^{207}Pb		^{207}Pb		^{206}Pb		corr.	^{207}Pb		^{207}Pb		^{206}Pb	
	U	$\times 10^{-13}$ mol	$^{206}Pb^*$	Pb_c	(pg)	^{204}Pb	^{206}Pb	^{206}Pb	% err	^{235}U	% err	^{238}U	% err	coef.	^{206}Pb	±	^{235}U	±	^{238}U	±
(a)	(b)	(c)	(c)	(c)	(c)	(d)	(e)	(e)	(f)	(e)	(f)	(e)	(f)		(g)	(f)	(g)	(f)	(g)	(f)
MRV14-1																				
z4	**0.463**	**76.033**	**99.96%**	**716**	**2.85**	**35,717**	**0.129**	**0.172681**	**0.040**	**11.7085**	**0.089**	**0.491764**	**0.055**	**0.949**	**2583.80**	**0.67**	**2581.38**	**0.83**	**2578.30**	**1.18**
z2	**0.336**	**66.401**	**99.98%**	**1514**	**1.15**	**80,331**	**0.094**	**0.172635**	**0.040**	**11.7052**	**0.098**	**0.491755**	**0.069**	**0.942**	**2583.35**	**0.67**	**2581.11**	**0.91**	**2578.26**	**1.46**
z6	**0.401**	**69.752**	**99.94%**	**454**	**4.07**	**22,834**	**0.112**	**0.172676**	**0.039**	**11.7076**	**0.089**	**0.491740**	**0.056**	**0.955**	**2583.75**	**0.66**	**2581.31**	**0.83**	**2578.20**	**1.20**
z3	**0.388**	**31.007**	**99.97%**	**1193**	**0.69**	**65,074**	**0.108**	**0.172644**	**0.040**	**11.7000**	**0.088**	**0.491508**	**0.054**	**0.949**	**2583.45**	**0.68**	**2580.70**	**0.83**	**2577.20**	**1.16**
z5	0.479	68.405	99.96%	709	2.60	35,333	0.133	0.172466	0.040	11.6687	0.093	0.490702	0.062	0.945	2581.72	0.67	2578.19	0.87	2573.71	1.32
z1	0.412	53.942	99.97%	1115	1.29	57,829	0.115	0.172481	0.040	11.6641	0.091	0.490467	0.058	0.946	2581.86	0.67	2577.83	0.85	2572.70	1.23

(a) z1, z2 etc. are labels for single zircon grain fragments annealed and chemically abraded after Mattinson (2005); bold indicates results used in weighted mean calculations.
(b) Model Th/U ratio iteratively calculated from the radiogenic 208Pb/206Pb ratio and 206Pb/238U age.
(c) Pb^* and Pbc represent radiogenic and common Pb, respectively; mol % $^{206}Pb^*$ with respect to radiogenic, blank and initial common Pb.
(d) Measured ratio corrected for spike and fractionation only. Fractionation estimated at 0.10 ± 0.03%/a.m.u. for Faraday analyses, based on analysis of NBS-981 and NBS-982.
(e) Corrected for fractionation, spike, and common Pb. Up to 0.5 pg of common Pb was allocated to procedural blank: 206Pb/204Pb = 18.042 ± 0.61%; 207Pb/204Pb = 15.537 ± 0.52%; 208Pb/204Pb = 37.686 ± 0.63% (all uncertainties 1-sigma). The remainder was assigned a model Pb composition of Stacey and Kramers (1975) at 2.6 Ga.
(f) Errors are 2-sigma, propagated using the algorithms of Schmitz and Schoene (2007).
(g) Calculations are based on the decay constants of Jaffey et al. (1971). 206Pb/238U and 207Pb/206Pb ages corrected for initial disequilibrium in 230Th/238U using Th/U [magma] = 3.

occurrences of pseudotachylite in Archean crust generally in proximity to terrane boundaries (Figs. 19, 20). Radiometric age control is poor but field crosscutting relations all point toward Paleoproterozoic formation ages (Fig. 23, inset, with location details in Table 6).

5.5. The Marshfield terrane

The tonalite at Wissota dam is younger (1813 Ma) than the included gabbro (1846 Ma) xenolith (Figs. 14 and 15). The host tonalite is weakly foliated and all of the complex brittle and ductile structures in the dike are discordant with the host rock supporting the xenolith interpretation. The granite dike is a Yavapai intrusion (1760 Ma) and has a post Yavapai U-Pb apatite reheating age. Map view shortening of the gabbro xenolith is ~20%, like a S-C kinematic structure oriented WSW-ENE (see inset, Fig. 14a), which is consistent with Yavapai shortening strain axes (Fig. 21). Uplift at Wissota at ~1100 Ma is supported by the U-Pb apatite cooling age and the xenolith explanation better aligns with the paleomagnetic results of Chan (1991).

The Hatfield gneiss exposed below Arbutus dam near Black River Falls, WI has a crystallization age of ~2900 Ma and was intruded by gabbro ~20 Ma later. Deformation is localized in the gneiss between the two gabbro intrusions on the north and south (Fig. 16) with remarkable kinematic complexity of both brittle and ductile shearing (Figs. 16 and 18; Dean and Craddock, 1993). Apatite in the gabbro suggest a Yavapai cooling age which may correlate with the brittle structures. The Wissota and Arbutus sites are separated by ~80 km within the Archean Marshfield terrane and have very different petrologic and structural histories and the U-Pb apatite ages suggest differential uplift histories. Curiously, the Hatfield gneiss age is identical to the ages of gneisses in the Bighorn Mountains in the Wyoming province, a piece of Archean crust that rifted away from the Superior province at 2150 Ma (Ernst and Bleeker, 2010). Perhaps the Marshfield terrane is a portion of the Wyoming province that was accreted back to the Superior province at 1850 Ma?

5.6. Sudbury impact layer deformation

Jirsa (2011) described in detail the Sudbury impact deformation 800 km from the impact near Gunflint Lake, MN which is the most distal exposure of impact-related deformation (Fig. 10). The Gunflint Fm. preserves a consistent up-section depositional AMS fabric (K_{max} parallel to bedding and oriented NW-SE) which is ~parallel to the Penokean shortening direction in other foreland samples (Fig. 20). This AMS fabric is disrupted and rotated by the folding associated with the propagation of impact-related seismic energy through the area; the impact layer fold axes are oriented normal to the propagation direction of surface ~E-W seismic waves from Sudbury. The K_{max} orientation constrains the SIL folding dynamics as K_{max} is rotated from being ~horizontal (layer-parallel) and N-S in orientation before the impact to being horizontal and E-W (layer-normal) as bedding changed from being horizontal into N-S isoclinal fold shapes (Figs. 10c, 11). The Gunflint Fm. paleopole (0°, 60°S) below the impact layer is not preserved upsection at the impact layer (Fig. 11) and also reflects this chaotic change. Additional AMS and paleopole data from the Thunder Bay area (Figs. 8 and 9) would help resolve the origin of the N-S folds in the Gunflint Fm. as being tectonic or related to the Sudbury impact.

6. Conclusions

Accretion of the Wisconsin Magmatic and Marshfield terranes to the southern margin of the Archean Superior province formed the north-vergent Penokean thrust belt in Huron and Animikie basins. Near the margin, Archean crystalline rocks were faulted, north-vergent nappes formed and a thin-skinned fold-and-thrust belt formed the 200 km wide belt now identified on the south and north sides of the Keweenaw rift and Lake Superior. Penokean shortening strains are generally layer-

Table 6
Locations of Presumed Penokean Pseudotachylite.

Sample	Latitude	Longitude	Terrane	Orientation	Age (Ma)
1	52° 43′ 55.23 N	95° 16′ 26.54 W	Sachigo Superterrane	Foliation-parallel	< 2650
2	49°45.463 N	94°38.307 W	Wabigoon-Winnipeg River	N70°E	< 2630
3	48°47.105 N	93°3.323 W	Wabigoon-Quetico	N70°E	1947 ± 23
4	48° 36′ 3.69 N	93° 12′ 6.41 W	Quetico-Wawa	N70°E	< 2630
5	48° 41′ 22.55 N	85° 57′ 30.52 W	Wawa (Abitibi)	N70°E	< 2630
6	48° 8′ 15.18 N	82° 36′ 44.85 W	Wawa (Abitibi); Kapuskasing	N45°E	> 1720
7	48° 8′ 15.18 N	82° 36′ 44.85 W	MRV	N25°E	< 2610
8	44° 48′ 10.75 N	95° 32′ 48.42 W	MRV	N60°E	< 2067
9	46° 25′ 15.57 N	87° 24′39.89 W	MRV/Watersmeet gneisses	N70°E	< 2600 Ma
10	45°0.579198 N	88°0.134511 W	Pembine-Wausau Terrane	E-W, 90°	< 1862 Ma

parallel and parallel to the thrust shortening direction and there is no Yavapai or Mazatzal strain overprint. Vertical strain overprints are found in a zone 50–60 km from the Penokean margin and are consistent with strains associated with the stacking of nappes. Shortening strains across the belt and foreland are roughly parallel so the Penokean orogen was collisional, like the Appalachians, with no rotations of thrust sheets during shortening. Strains in Archean terranes north of the Penokean thrust belt are unique and unaffected by far-field Penokean, Yavapai or Mazatzal deformation. Pseudotachylite of Penokean age is common in Archean rocks and may be related to the uniform orogenic convergence around the Superior province in the Paleoproterozoic. Metamorphism across the Penokean belt was related to accretion of Yavapai crust (1750 Ma) although the metamorphism is 120 km inboard of the Yavapai margin, and there is a SW-NE shortening strain fabric across the Penokean margin and hinterland that is of Yavapai origin, i.e., post-Penokean and pre-Mazatzal, found only in Yavapai intrusions in Animike sediments (Site 25). Mazatzal shortening (1630 Ma) is preserved as layer-parallel and layer-normal shortening oriented at ~N20°W and no strain overprint is preserved in Huron-Animikie sediments. Deformation in the accreted Archean crust of the Marshfield terrane is complex (Wissota and Arbutus sites) but has no anorogenic (1450 Ma) metamorphic overprint.

Acknowledgements

The project is the result of many decades of field excursions to better understand the Penokean deformation in the Huron and Animikie sections. This was aided by Dave Southwick, G.B. Morey, Jerry Webers, Cam Craddock, Dick Ojakangas, John Klasner, Bill Cannon, Daniel Holm, Rob Rainbird, Peter Jangawaard, Phil Fralik and Mike Easton. Mark Jirsa kindly provided some images used in Figures 3 and 10. Understanding the complex folds in the Gunflint Fm. near Thunder Bay was made possible by Mary-Louise Hill, Mark Smyk and Jordan Baird. Research efforts at the Wissota and Arbutus sites benefited from the efforts of Macalester undergraduates Erin Beutel and Mike Dean, respectively. Bernhard Schulz aided with dating attempts on the Veedum quartzite monazites. The Arizona Laserchron folks were awesome, as always, as was Mike Jackson's crew at the Institute for Rock Magnetism, University of Minnesota. Dave Corrigan and an anonymous review improved the clarity of the manuscript.

Appendix 1-Methods

Calcite twin analysis

The calcite strain-gage technique (CSGT) of Groshong (1972) allows investigation of intraplate stresses as constrained by intracrystalline twinning of rock-forming calcite grains. Although the result is actually a strain tensor (3-D strain ellipsoid), a similar orientation of the stress tensor appears likely in case of coaxial deformation (Turner, 1953, 1962). The CSGT has been used to constrain strain tensor directions in veins (Kilsdonk and Wiltschko, 1988), limestone (e.g. Craddock and van der Pluijm, 1988; Craddock et al., 2000) and marble (Craddock and Craddock, 2012; Craddock et al., 2017a).

Under temperatures of ca. 200 °C intracrystalline deformation of calcite results in the formation of e-twins. The formation of calcite e-twins requires a shear stress exceeding ca. 10 MPa (Wenk et al., 1987; Lacombe and Laurent, 1996). Calcite offers three glide systems for e-twinning. From U-stage measurements of width, frequency and orientation of twins, and the crystallographic orientation of the host crystals, a strain tensor can be calculated using a least-squares technique (Groshong, 1972). In order to remove "noise" from the dataset, a refinement of the calculated strain tensor can be achieved by stripping 20% twins with highest deviations (Groshong et al., 1984). In cases where the data appear to be inhomogeneous, the separation of incompatible twins ("NEV" = negative expected values) from compatible twins ("POS" = positive expected values) of the initial dataset allows separate calculation of two or more least-squares deviatoric strain tensors. Thus, the CSGT can be used to obtain information on superimposed deformations (Groshong, 1972; 1974) and differential stress magnitudes.

Measurements of about 50 grains on one thin-section or 25 grains on two mutually perpendicular thin-sections yield the best results (Groshong

et al., 1984; Evans and Groshong, 1994). Application of the CSGT requires the following assumptions to be valid: (1) low temperatures (dominance of Type I and Type II twins), (2) random c-axis orientations of calcite, (3) homogenous strain, (4) coaxial deformation, (5) volume constancy, (6) low porosity materials and (7) low strain (< 15%). These conditions are met throughout our sample suite.

Finite strains

Where twinned calcite was absent in the study area we used ellipsoidal elements (quartz grains in quartzites, ashfall lapilli, etc.) in the sediments to resolve an oriented strain ellipsoid using center-to-center methods from three mutually perpendicular thin sections as described in Craddock and McKiernan (2007).

X-ray fluorescence

Two N–S lamprophyre dikes exposed in Saganaga Lake, MN were analyzed for major and trace element compositions using X-ray fluorescence. Samples were split with a vise wedge and only pieces lacking weathered or saw-marked edges were used in XRF analyses. Details of XRF sample preparation, analyses, analytical precision, and detection limits are provided in Vervoort et al. (2007).

$^{40}Ar/^{39}Ar$ analyses by laser heating

$^{40}Ar/^{39}Ar$ incremental heating experiments using a defocused CO_2 laser beam were performed at the University of Wisconsin Rare Gas Geochronology Laboratory, following procedures described in Smith et al (2006). A few milligrams of lamprophyre biotite single crystals, each optically clear and fresh, were hand-picked and then irradiated in the CLICIT facility (cadmium-shielded) of the Oregon State University nuclear reactor for 40 h. The conversion efficiency of ^{39}K to ^{39}Ar was monitored using sanidine from the 28.34 Ma Taylor Creek Rhyolite (Renne et al., 1998). Final data reduction was via ArArCalc (Koppers, 2002). The uncertainties of all reported ages are at the 2σ level.

U-Pb geochronology (LA-ICPMS) of zircon and apatite

Zircon and apatite crystals were extracted from samples by traditional methods of crushing and grinding, followed by separation by panning, heavy liquids, and a Frantz magnetic separator. Zircons were incorporated into a 1″ epoxy mount together with fragments of our Sri Lanka standard zircon. The mounts are sanded down to a depth of ~20 μm, polished, imaged, and cleaned prior to isotopic analysis.

Zircon and apatite U-Pb ages were determined by laser ablation–multicollector–inductively coupled plasma mass spectrometry (LA-MC-ICPMS) at the Arizona LaserChron Center (Gehrels et al., 2008, 2011; Thomson et al., 2012). The analyses involve ablation of zircon with a Photon Machines Analyte G2 Excimer laser. Seven new U-Pb ages were acquired (Hatfield gneiss and Arbutus gabbro, U-Pb zircon; Arbutus gabbro, U-Pb apatite; Wissota tonalite, Wissota Granite, and Wissota gabbro, U-Pb zircon; and Wissota gabbro, U-Pb apatite) for rocks within the Marshfield terrane. The data are presented in Table 4. The resulting interpreted ages are shown on Pb/U concordia diagrams (Stacey and Kramers, 1975) and weighted mean diagrams using the routines in Isoplot (Ludwig, 2008). For the Concordia plots, only the data used to calculate the Concordia and weighted mean ages are included. Those ages that are clearly xenocrysts or outside of the 2 sigma error and acceptable MSWD ranges are not included.

U-Pb geochronology (TIMS) of zircon

U-Pb dates were obtained by the chemical abrasion isotope dilution thermal ionization mass spectrometry (CA-TIMS) method from analyses composed of single zircon grains from a granite along the Yellow Medicine shear zone (Fig. 1). These zircon crystals were analyzed via chemical abrasion isotope dilution thermal ionization mass spectrometry (CA-IDTIMS) at Boise State University. The details of chemical separations, mass spectrometry and data analysis are described in Schmitz and Schoene (2007).

Paleomagnetism

The Kappa Bridge is an AC susceptibility bridge with an automated sample handler for determining *aniso*tropy of low-field magnetic susceptibility (AMS) at room temperature at the Institute for Rock Magnetism, University of Minnesota. The AMS technique has been used as a proxy for strains in foreland strata (Sun et al., 1993; Evans et al., 2003) and magmatic flow in dikes (Ernst and Baragar, 1992) and plutons (Bouchez, 1997). An alternating current in the external “drive” coils produces an alternating magnetic field in the sample space with a frequency of 680 Hz and amplitude of up to 1mT. The induced magnetization of a sample is detected by a pair of “pickup” coils, with a sensitivity of 1.2E – 6SI volume units. For anisotropy determination, a sample is rotated about three orthogonal axes, and susceptibility is measured at 1.8◦ intervals in each of the three measurement planes. The vibrating-sample magnetometer was used to characterize the magnetic susceptibility of the lamprophyre dikes and Gunflint Fm. by generating hysteresis curves in order to identify the magnetic mineral(s) in each rock type. Fourteen cores from 2 sample sites were demagnetized to determine a paleopole signature for the Gunflint Fm., ten by stepwise alternating field (AF) methods, and four by thermal methods using Schoenstedt demagnetizers. Initially, one specimen from each site was demagnetized by each method, in five steps, and the results were used to determine the optimum demagnetization sequence for the remaining specimens. The magnetic carrier mineral(s) was determined using the vibrating-sample magnetometer (VSM), generating a hysteresis loop plot.

Saganaga Lake Lamprophyre $^{40}Ar/^{39}Ar$ Incremental Heating Results

Sample ID File #		Laser Power (%)	$^{40}Ar/^{39}Ar$ ± 1σ	$^{37}Ar/^{39}Ar$ ± 1σ	$^{36}Ar/^{39}Ar$ ± 1σ	F[a] ± 1σ	$^{40}Ar^{*}$ (%)	^{39}Ar (%)	K/Ca	Apparent Age ± 2σ Ma[b]
CG9										
Laser Incremental heating			groundmass			J = 0.0004923 ± 0.09% (1σ)[c]			μ = 1.0049 ± 0.02% (1σ)[d]	
BE7078	#	2.3	263.7028 ± 1.4144	0.4216 ± 0.0114	0.8645 ± 0.0058	8.2802 ± 1.1598	3.14	3.49	1.020	7.34 ± 2.05
BE7079	#	2.9	213.4437 ± 0.9202	0.8961 ± 0.0162	0.6909 ± 0.0034	9.3717 ± 0.6054	4.39	6.96	0.480	8.30 ± 1.07
BE7081	#	3.4	67.9560 ± 0.2133	1.9251 ± ± 0.0333	0.2003 ± 0.0014	8.9193 ± 0.3987	13.11	8.75	0.223	7.90 ± 0.71
BE7082	#	3.9	22.4534 ± 0.0708	1.8740 ± 0.0327	0.0456 ± 0.0004	9.1280 ± 0.1214	40.60	14.02	0.229	8.09 ± 0.21
BE7084	#	4.6	12.1258 ± 0.0432	1.3803 ± ± 0.0236	0.0100 ± 0.0002	9.2984 ± 0.0758	76.61	18.42	0.311	8.24 ± 0.13
BE7085	#	5.5	10.0620 ± 0.0458	0.9831 ± 0.0176	0.0027 ± 0.0002	9.3348 ± 0.0651	92.71	18.95	0.437	8.27 ± 0.12
BE7087	#	8.0	10.3906 ± 0.0497	0.9693 ± 0.0173	0.0038 ± 0.0002	9.3601 ± 0.0782	90.02	20.31	0.443	8.29 ± 0.14
BE7088	#	13.0	13.1308 ± 0.1117	2.2287 ± 0.0408	0.0133 ± 0.0005	9.3869 ± 0.1800	71.38	7.18	0.193	8.32 ± 0.32
BE7090	#	25.0	26.7032 ± 0.4374	3.6988 ± 0.0765	0.0595 ± 0.0022	9.4400 ± 0.7277	35.26	1.93	0.116	8.36 ± 1.29
Weighted Mean from 9 of 9 steps:					MSWD	0.60			Weighted Mean age:	**8.25 ± 0.07**
Inverse Isochron from 9 of 9 Steps:	$^{40}Ar/^{36}Ar$ ± 2σ:	294.8 ± 1.4		MSWD	0.53			Isochron age:	**8.26 ± 0.07**	
CG352										
Laser Incremental heating			plagioclase			J = 0.0004923 ± 0.09% (1σ)[c]			μ = 1.0049 ± 0.02% (1σ)[d]	
BE7120		3.0	68.8093 ± 0.2812	0.4780 ± 0.0106	0.2165 ± 0.0018	4.8729 ± 0.4849	7.08	13.66	0.899	4.32 ± 0.86
BE7121		4.0	36.6459 ± 0.1558	1.7705 ± 0.0325	0.0974 ± 0.0011	8.0139 ± 0.3019	21.84	14.98	0.243	7.10 ± 0.53
BE7123		5.0	26.3464 ± 0.1092	3.8513 ± 0.0721	0.0520 ± 0.0017	11.3106 ± 0.4968	42.82	10.12	0.111	10.02 ± 0.88
BE7124		6.0	19.1718 ± 0.1370	5.3429 ± 0.1036	0.0211 ± 0.0013	13.4042 ± 0.3997	69.67	8.16	0.080	11.87 ± 0.71
BE7126	#	7.5	17.1297 ± 0.0965	6.1054 ± 0.1147	0.0120 ± 0.0008	14.1155 ± 0.2519	82.06	7.78	0.070	12.49 ± 0.44
BE7127	#	10.0	16.2911 ± 0.1049	6.5935 ± 0.1279	0.0101 ± 0.0016	13.8781 ± 0.4947	84.81	6.16	0.065	12.28 ± 0.87
BE7129	#	14.0	15.0378 ± 0.0691	7.0924 ± 0.1269	0.0075 ± 0.0008	13.4436 ± 0.2320	88.97	10.56	0.060	11.90 ± 0.41
BE7130	#	18.0	14.6185 ± 0.0874	7.0122 ± 0.1307	0.0053 ± 0.0010	13.6613 ± 0.3030	93.01	9.83	0.061	12.09 ± 0.53
BE7132	#	25.0	15.1236 ± 0.0848	7.3679 ± 0.1337	0.0067 ± 0.0008	13.7732 ± 0.2419	90.62	10.80	0.058	12.19 ± 0.43
BE7133	#	40.0	15.4459 ± 0.1091	6.9157 ± 0.1365	0.0085 ± 0.0012	13.5410 ± 0.3707	87.26	7.95	0.062	11.99 ± 0.65
Weighted Mean from 5 of 9 steps:					MSWD	0.82			Weighted Mean age:	**12.13 ± 0.20**
Inverse Isochron from 5 of 9 Steps:	$^{40}Ar/^{36}Ar$ ± 2σ:	309.7 ± 55.8		MSWD	0.93			Isochron age:	**12.04 ± 0.41**	
CG331										
Laser Incremental heating			groundmass			J = 0.0004923 ± 0.09% (1σ)[c]			μ = 1.0049 ± 0.02% (1σ)[d]	
BE7106		2.3	59.2878 ± 0.1646	0.2021 ± 0.0057	0.1573 ± 0.0009	12.8162 ± 0.2526	21.61	1.48	2.128	11.35 ± 0.45
BE7107		2.9	41.7819 ± 0.0889	0.2180 ± 0.0042	0.0990 ± 0.0005	12.5521 ± 0.1387	30.04	3.91	1.972	11.11 ± 0.24

BE7109		3.4	24.2452 ± 0.0492	0.2604 ± 0.0046	0.0389 ± 0.0003	12.7651 ± 0.0914	52.64	6.64	1.651	11.30 ± 0.16
BE7110		3.9	17.1552 ± 0.0310	0.2145 ± 0.0039	0.0130 ± 0.0001	13.3288 ± 0.0426	77.68	10.08	2.004	11.80 ± 0.08
BE7112	#	4.6	15.2905 ± 0.0311	0.1501 ± 0.0028	0.0054 ± 0.0001	13.7156 ± 0.0369	89.69	14.14	2.864	12.14 ± 0.07
BE7113	#	5.5	14.4736 ± 0.0159	0.1141 ± 0.0022	0.0024 ± 0.0001	13.7597 ± 0.0237	95.06	16.49	3.768	12.18 ± 0.04
BE7115	#	8.0	14.4669 ± 0.0173	0.1057 ± 0.0020	0.0026 ± 0.0001	13.7095 ± 0.0225	94.76	28.89	4.066	12.14 ± 0.04
BE7116	#	13.0	14.5790 ± 0.0133	0.1562 ± 0.0028	0.0031 ± 0.0000	13.6857 ± 0.0175	93.86	13.85	2.753	12.11 ± 0.03
BE7118	#	25.0	14.6966 ± 0.0241	0.1636 ± 0.0031	0.0034 ± 0.0001	13.7148 ± 0.0334	93.31	4.51	2.628	12.14 ± 0.06
Weighted Mean from 5 of 9 steps:					MSWD	1.59			Weighted Mean age:	**12.14 ± 0.03**
Inverse Isochron from 5 of 9 Steps:	$^{40}Ar/^{36}Ar$ ± 2σ:	289.0 ± 39.8		MSWD	2.05			Isochron age:	**12.15 ± 0.11**	

[a]F is the ratio of radiogenic ^{40}Ar to K-derived ^{39}Ar.
[b]All ages calculated using the decay constants of Steiger and Jäger ($\lambda_{40K} = 5.543 \times 10^{-10} yr^{-1}$) and corrected for ^{37}Ar and ^{39}Ar decay, half lives of 35.2 days and 269 years, respectively.
[c]J-value calculated relative to 28.02 Ma for the Fish Canyon sanidine.
[d]μ: mass discrimination per atomic mass unit.
[#]indicates increments that have been included in weighted mean and isochron calculations.

Summary of $^{40}Ar/^{39}Ar$ experiments

		K/Ca	Total fusion		Weighted Mean Analysis		
Sample #	Material	total	Age (Ma) ± 2σ	N	^{39}Ar %	MSWD	Age (Ma) ± 2 σ
Sag Lake	biotite	9.22	2085 ± 5	19 of 26	97.5	1.30	**2094 ± 5**

J-value calculated relative to 28.201 Ma for the Fish Canyon sanidine.
Age in bold is preferred.

Appendix A. Supplementary data

Supplementary data to this article can be found online at https://doi.org/10.1016/j.precamres.2018.09.004.

References

Addison, W.D., Brumpton, G.R., Vallini, D.A., McNaughton, N.J., Davis, D.W., Kissin, S.A., Fralick, P.W., Hammond, A.L., 2005. Discovery of distal ejecta from the 1850 Ma Sudbury impact event. Geology 33, 193–196.

Baird, J., 2015. Fold analyses in the Gunflint Fm.: working towards a characterization of regional deformation in the Animikie Group near Thunder Bay, Ontario: H. B. Sc. Thesis. Lakehead University, Thunder Bay, Ontario, pp. 40.

Bauer, R.L., 1985. Correlation of early recumbent and younger upright folding across the boundary between an Archean gneiss belt and greenstone terrane, northeasrtn, Minnesota. Geology 13, 657–660.

Bauer, R.L., Hudleston, P.J., Southwick, D.L., 1992. Deformation across the western Quetico subprovince and adjacent boundary regions in Minnesota. Canadian J. Earth Sci. 29, 2087–2103.

Bennett, G., Dressler, B.O., Robertson, J.A., 1991. The Huronian Supergroup and associated intrusive rocks, Ontario Geological Survey Special Volume 4, part 1, p. 549–592.

Bickford, M.E., Van Schmus, W.R., Zietz, I., 1986. Proterozoic history of the midcontinent region of North America. Geology 14, 492–496.

Bickford, M.E., Wooden, J.L., Bauer, R.L., 2006. SHRIMP study of zircon grains from Early Archean rocks in the Minnesota River Valley: implications for the tectonic history of the Superior Province. Geol. Soc. Am. Bull. 118, 94–108.

Bouchez, J.L., 1997. Granite is never isotropic: an introduction to AMS studies of granitic rocks. In: Bouchez, J.-L. (Ed.), Granite: From Segregation Melt to Emplacement Fabrics. Kluwer Academic Publishers, Dordrecht, Netherlands, pp. 95–112.

Boyd, N.K., Smithson, S.B., 1994. Seismic profiling of Archean crust: Crustal structure in the Morton block, Minnesota River Valley subprovince. Tectonophysics 232, 211–224.

Brocum, S.J., Dalziel, I.W.D., 1974. The Sudbury basin, the Southern province, the Grenville front and the Penokean orogen. Geol. Soc. Am. Bull. 85, 1571–1580.

Cannon, W.F., Schulz, K.J., Horton Jr., J.W., Kring, D.A., 2009. The Sudbury impact layer in the Paleoproterozoic iron ranges of northern Michigan, USA. Geol. Soc. Am. Bull. 122, 50–75.

Card, K.D., 1990. A review of the Superior province of the Canadian Shield, a product of Archean accretion. Precambr. Res. 48, 99–156.

Carr, S.D., Easton, R.M., Jamieson, R.A., Culshaw, N.G., 2000. Geologic transect across New York and Ontario. Can. J. Earth Sci. 37, 193–216.

Carter, P.J., 1989. Finite Strain Estimates in Archean Mona Schist Pillow Basalt and Enchantment Lake Fm. Metawackes in the Eastern Upper Peninsula of Michigan. Michigan State University M.S. thesis, pp. 97.

Chan, L.S., 1991. Paleomagnetism of Central Wisconsin Dike Swarm: Constraints on Thermomechanical Model of the Midcontinent rift. 37th Institute on Lake Superior Geology, pp. 23.

Chandler, V.W., 1991. Aeromagnetic Anomaly Map of Minnesota. University of Minnesota, Minnesota Geological Survey.

Chapple, W.M., 1978. Mechanics of thin-skinned fold and thrust belts. Geol. Soc. Am. Bull. 89, 1189–1198.

Corfu, F., Andrews, A.J., 1986. A U–Pb age for mineralized. Nipissing Diabase, Gowganda, Ontario. Canadian J. Earth Sci. 23, 107–109.

Corrigan, D., Pehrsson, S., Wodicka, N., De Kemp, E., 2009. The Paleoproterozoic Trans-Hudson orogeny: a prototype of the modern accretionary process. Geological Society of London Special Publications 327, 457–479.

Craddock, J.P., 1992. Transpression during tectonic evolution of the Idaho-Wyoming fold-and-thrust belt. In: Link, P.K., Kuntz, M.A., Platt, L.B. (Eds.), Regional Geology of Eastern Idaho and Western Wyoming. Geological Society of America, pp. 125–139.

Craddock, J.P., van der Pluijm, B., 1988. Kinematic analysis of an en echelon-continuous vein complex. J. Struct. Geol. 10, 445–452.

Craddock, J.P., van der Pluijm, B.A., 1989. Late Paleozoic deformation of the cratonic carbonate cover of eastern North America. Geology 17, 416–419.

Craddock, J.P., Moshoian, A., 1995. Continuous Proterozoic Strike-Slip Fault-En Echelon Fracture Arrays in Archean Rocks: implications for Fault Propagation Mechanics and Dike Injection: Basement. Tectonics 10, 379–407.

Craddock, J.P., Magloughlin, J.F., 2005. Calcite strains, kinematic indicators, and magnetic flow fabric of a Proterozoic pseudotachylyte swarm, Minnesota River valley, USA. Tectonophysics 402, 153–168.

Craddock, J.P., McKiernan, A.W., 2007. Tectonic implications of finite strain variations in Baraboo-interval quartzites (ca. 1700Ma), Mazatzal orogen, Wisconsin and Minnesota, USA. Precambr. Res. 156, 175–194.

Craddock, S.D., Craddock, J.P., 2012. Strain Variations in Carbonates across the Proterozoic Grenville Orogen: 58th ILSG (Thunder Bay), p. 21.

Craddock, J.P., Neilson, K.J., Malone, D.H., 2000. Calcite twinning strain constraints on Heart Mountain detachment kinematics, Wyoming. J. Struct. Geol. 22, 983–991.

Craddock, J.P., Anziano, J., Wirth, K.R., Vervoort, J.D., Singer, B., Zhang, X., 2007. Structure, geochemistry and geochronology of a lamprophyre dike swarm, Archean Wawa terrane, Michigan, USA. Precambr. Res. 157, 50–70.

Craddock, J.P., Rainbird, R.H., Davis, W.J., Davidson, C., Vervoort, J.D., Konstantinou, A., Lundquist, B., 2013a. Detrital zircon geochronology and provenance of the Paleoproterozoic Huron (~ 2.4–2.2 Ga) and Animikie (~2.2–1.8 Ga) basins, southern Superior Province. J. Geol. 121, 623–644.

Craddock, J.P., Vervoort, J.D., Wirth, K.R., Davidson, C., Konstantinou, A., Finley-Blasi, L., Juda, N., Walker, E., 2013b. Detrital Zircon Provenance of the Mesoproterozoic Midcontinent Rift, Lake Superior region, USA. J. Geol. 121, 57–73.

Craddock, J.P., Craddock, S.D., Konstantinou, A., Kylander-Clark, A., Malone, D.H., 2017a. Calcite Twinning Strain Variations across the Proterozoic Grenville Orogen and Keweenaw-Kapuskasing Inverted Foreland, USA and Canada. Geosci. Front. https://doi.org/10.1016/j.gsf.2017.01.006.

Craddock, J.P., Malone, D.H., Porter, R., Compton, J., Luczaj, J., Konstantinou, A., Day, J.E., Johnson, S.T., 2017b. Paleozoic reactivation structures in the Appalachian-Ouachita-Marathon foreland: Far-field deformation across Pangea. Earth Sci. Rev. 169, 1–27.

Dean, M.C., Craddock, J.P., 1993. Outcrop offsets and microscopic kinematic indicators in a Proterozoic mafic dike-strike slip fault array. In: 39th Annual Proceedings of the Lake Superior Institute, Black River Falls, WI, p. 27–28.

Dott Jr., R.H., 1983. The Proterozoic red quartzite enigma in the north-central United States: Resolved by plate collision? In: Medaris, L.G. (Ed.), Early Proterozoic Geology of the Great Lakes Region. Geological Society of America, Boulder, Colorado, pp. 129–141.

Easton, R.M., 2006, Complex folding and faulting history in Huronian Supergroup rocks located north of the Murray fault zone, Southern Province, Ontario: 52nd Institute on Lake Superior Geology, Proceedings, v. 52, p. 15–16.

Ernst, R.E., Baragar, W.R.A., 1992. Evidence from the magnetic fabric for the flow of magma in the Mackenzie giant radiating dyke swarm. Nature 356, 511.

Ernst, R., Bleeker, W., 2010. Large igneous provinces (LIPs), giant dyke swarms, and mantle plumes: significance for breakup events within Canada and adjacent regions from 2.5 Ga to the Present. Can. J. Earth Sci. 47, 695–739.

Evans, M.A., Groshong, R.H., 1994. A Computer Program for the Calcite Strain-Gage Technique. J. Struct. Geol. 16, 277–281.

Evans, M.A., Lewchuk, M.T., Elmore, R.D., 2003. Strain partitioning of deformation mechanisms in limestones: examining the relationship of strain and anisotropy of magnetic susceptibility. J. Struct. Geol. 25, 1525–1550.

Fralick, P., Davis, D.W., Kissin, S.A., 2002. The age of the Gunflint Formation, Ontario, Canada: single zircon U-Pb age determinations from reworked volcanic ash. Can. J. Earth Sci. 39, 1085–1091.

Gehrels, G.E., Blakey, R., Karlstrom, K.E., Timmons, J.M., Dickinson, B., Pecha, M., 2011. Detrital zircon U-Pb geochronology of Paleozoic strata in the Grand Canyon, Arizona. Lithosphere 3, 183–200.

Gehrels, G.E., Valencia, V., Ruiz, J., 2008. Enhanced precision, accuracy, efficiency, and spatial resolution of U-Pb ages by laser ablation–multicollector–inductively coupled plasma–mass spectrometry. Geochem. Geophys. Geosystems 9, Q03017. https://doi.org/10.1029/2007GC001805.

Gibbs, A.K., Payne, B., Setzer, T., Brown, L.D., Oliver, J.E., Kaufman, S., 1981. Seismic reflection study of the Precambrian crust of central Minnesota. Geol. Soc. Am. Bull. 95, 280–294.

Goldich, S.S., Hedge, C.E., 1962. Dating of the Precambrian of the Minnesota River Valley, Minnesota. J. Geophys. Res. 67, 3561–3562.

Green, J.C., Bornhorst, T.J., Chandler, V.W., Mudrey, M.G., Myers, P.E., Pesonen, L.J., Wilband, J.T., 1987. Keweenawan dykes of the Lake Superior region: evidence for the evolution of the middle Proterozoic Midcontinent Rift of North America in Mafic Dyke Swarms, In: Halls, H.C., Fahrig, W.F. (Eds.), Geologic Association Canada Special Paper, v. 34, pp. 289–302.

Greenberg, J.K., Brown, B.A., 1984. Cratonic sedimentation during the Proterozoic: an orogenic connection in Wisconsin and the upper Midwest. J. Geol. 92, 159–171.

Gross, A., Holm, D.K., Schneider, D.A., 2006. Kinematic analysis and monazite geochronology of the Eau Plaine and Niagara shear zones, Wisconsin: 52nd Institute on Lake Superior Geology, p. 20.

Groshong Jr., R.H., 1972. Strain calculated from twinning in calcite. Geol. Soc. Am. Bull. 83, 2025–2038.

Groshong Jr., R.H., 1974. Experimental test of least-squares strain calculations using twinned calcite. Geol. Soc. Am. Bull. 85, 1855.

Groshong Jr, R.H., Teufel, L.W., Gasteiger, C.M., 1984. Precision and accuracy of the calcite strain-gage technique. Bull. Geol. Soc. Am. 95, 357–363.

Halls, H.C., Davis, D.W., Stott, G.M., Ernst, R.E., Hamilton, M.A., 2008. The Paleoproterozoic Marathon Large Igneous Province: new evidence for a 2.1 Ga long-lived mantle plume event along the southern margin of the N. American Superior province. Precambr. Res. 162, 327–353.

Hill, M.L., Smyk, M., 2005. Penokean fold-and-thrust deformation of the Paleoproterozoic Gunflint Fm. near Thunder Bay, Ontario: 51st Institute on Lake Superior Geology, p. 26.

Himmelberg, G.R., 1968. Geology of Precambrian Rocks, Granite Falls–Montevideo Area, southwestern Minnesota. Minn. Geol. Surv. Publ. SP-5.

Hnat, J.S., van der Pluijm, B.A., 2011. Foreland signature of indenter tectonics: insights from calcite twin analysis in the Tennessee salient of the southern Appalachians, USA. Lithosphere 3, 317–327.

Hoffman, P.F., 1988. United Plates of America, the birth of a craton: early Proterozoic assembly and growth of Laurentia. Annu. Rev. Earth Planet. Sci. 16, 543–603.

Holm, D.K., Selverstone, J., 1990. Rapid growth and strain rates inferred from synkinematic garnets, Penokean orogeny, Minnesota. Geology 18, 166–169.

Holm, D.K., Lux, D.R., 1996. Core complex model proposed for gneiss dome development during collapse of the Paleoproterozoic Penokean orogen, Minnesota. Geology 24, 343–346.
Holm, D.K., Holst, T.B., Ellis, M., 1988. Oblique subduction, footwall deformation, and imbrication: a model for the Penokean orogen in east-central Minnesota. Geol. Soc. Am. Bull. 100, 1811–1818.
Holm, D.K., Darrah, K.S., Lux, D.R., 1998. Evidence for widespread ~1760 Ma metamorphism and rapid crustal stabilization of the early Proterozoic (1870–1820 Ma) Penokean orogen, Minnesota. Am. J. Sci. 298, 60–81.
Holm, D.K., Schneider, D., Chandler, V.W., 2007. Proterozoic and tectonic evolution of the Upper Great Lakes region. N. America: Precambr. Res. 157, 1–14.
Holst, T.B., 1982. Evidence for multiple deformation during the Penokean orogeny in the middle Precambrian Thomson Formation, Minnesota. Can. J. Earth Sci. 19, 2043–2047.
Holst, T.B., 1984. Evidence for nappe development during the early Proterozoic Penokean orogeny, Minnesota. Geology 12, 135–138.
Holst, T.B., 1985. Implications of a large flattening strain for the origin of a bedding-parallel foliation in the early Proterozoic Thomson Formation, Minnesota. J. Struct. Geol. 7, 375–383.
Holst, T.B., 1993. The Penokean orogeny in Minnesota and Upper Michigan- a comparison of structural geology. U.S. Geol. Survey Bull. 1904-D.
James, H.L., 1955. Zones of regional metamorphism in the Precambrian of northern Michigan. Geol. Soc. Am. Bull. 66, 1455–1488.
Jirsa, M.A., Chandler, V.W., Lively, R.S., 2005. Bedrock geology of the Mesabi Iron Range. Minnesota: Minnesota Geological Survey Miscellaneous Map Series M-163, I sheet, scale 1:100,000.
Jirsa, M.A., 2011. M-191 Bedrock Geology of the Western Gunflint Trail Area, Northeastern Minnesota, scale 1:24,000.
Kalliokoski, J., Lynott, J.S., 1987, Huron River: Precambrian Unconformities and Alteration at and near Big Eric's Crossing, Michigan : North-Central Section of the Geological Society of America, Centennial Field Guide, v. 3, p. 273–276.
Kappmeyer, J., Wiltschko, D.V., 1984. Quartz deformation in the Marquette and Republic troughs, Upper Peninsula of Michigan. Can. J. Earth Sci. 21, 793–801.
Ketchum, K.Y., Heaman, L.M., Bennett, G., Hughes, D.J., 2013. Age, petrogenesis and tectonic setting of the Thessalon volcanic rocks, Huronian Supergroup, Canada. Precambr. Res. 233, 144–172.
Kilsdonk, W., Wiltschko, D.V., 1988. Deformation mechanisms in the southeastern ramp region of the Pine Mountain block, Tennessee. Geol. Soc. Am. Bull. 100, 644–653.
Klasner, J.S., Ojakangas, R.W., Schulz, K.J., LaBerge, G.L., 1993. Nature and style of deformation in the foreland of the early Proterozoic Penokean orogen, northern Michigan. U.S. Geol. Survey Bull. 1904-K, 1–22.
Konstantinou, A., Wirth, K.R., Vervoort, J.D., Davidson, C., Malone, D.H., Craddock, J.P., 2014. Detrital zircon geochronology of early Paleozoic Midcontinent region, supermature quartz arenites: Implications for paleogeography, erosion and sedimentation patterns. J. Geol. 122, 201–216.
Koppers, A.A.P., 2002. ArArCALC—software for 40Ar/39Ar age calculations. Comput. Geosci. 28, 605–619.
Kusky, T.M., Hudleston, P.J., 1999. Growth and demise of an Archean carbonate platform, Steep Rock Lake, Ontario, Canada. Can. J. Earth Sci. 36, 565–584.
LaBerge, G.L., Ojakangas, R.W., Licht, K.J., 1992. Archean and early Proterozoic geology of the Gogebic district, northern Michigan and Wisconsin: 38th Institute on Lake Superior Geology, Trip #1, p. 1–40.
Lacombe, O., Laurent, P., 1996. Determination of deviatoric stress tensors based on inversion of calcite twin data from experimentally deformed monophase samples: preliminary results. Tectonophysics 255, 189–202.
Long, D.G.F., 1995. Huronian sandstone thickness and paleocurrent trends as a clue to the tectonic evolution of the Southern Province. Can. Mineral. 33, 922–923.
Ludwig, K.R., 2008. Isoplot 3.00, a Geochronological Took-kit for Excel. Berkeley Geochronology Center Special Publication 4, pp. 67.
Maas, R.S., Brown, B.A., 1987. Archean gneiss at Lake Arbutus dam, Jackson County, Wisconsin: Geological Society of America Centennial Field Guide, Northcentral Section, p. 189–190.
Malone, D.H., Stein, C.A., Craddock, J.P., Kley, J., Stein, S., Malone, J.E., 2016. Maximum depositional age of the Neoproterozoic Jacobsville Sandstone, Michigan: implications for the evolution of the Midcontinent Rift. Geosphere 12, 1–12.
McSwiggen, P.L., Morey G.B., Cleland, J.M., 1995. Iron-formation protolith and genesis, Cuyuna Range, MN: Minnesota Geologic Survey Report of Investigations 45, 54 p.
Medaris, L.G., and Singer, B., 2004, Geochronology of Precambrian rocks in central Wisconsin: a review of 40Ar/39Ar analyses. In: 50th Institute on Lake Superior Geology, p. 113–114.
Medaris Jr., L.G., Singer, B.S., Dott Jr., R.H., Naymark, A., Johnson, C.M., Schott, R.C., 2003. Late Paleoproterozoic climate, tectonics, and metamorphism in the southern Lake Superior region and Proto-North America: evidence from Baraboo Interval Quartzites. J. Geol. 111, 243–257.
Medaris, L.G., Jr., Jicha, B.S., Dott, R.H., Jr., Singer, B.S., 2009, A 1465 Ma 40Ar/39Ar age for the Seeley Slate: implications for metamorphism and deformation in the Baraboo Range, Wisconsin: in 55th Annual Meeting of the Institute on Lake Superior Geology Proceedings, Volume 55, Part 1—Program and Abstracts, p. 59–60.
Medaris Jr, L.G., Dott Jr, R.H., Craddock, J.P., Marshak, S., 2011. The Baraboo District—A North American classic. Archean to Anthropocene: Field Guides to the Geology of the Mid-Continent of North America. Geol. Soc. Am. Field Guide 24, 63–82.
Meyer, R., 1983. A Strain Study in the Kona Fm., Marquette County, Michigan. Michigan State University, pp. 65 M.S. thesis.
Myers, P.E., Cummings, M.L., Wurdinger, S.R., 1980. Precambrian geology of the Chippewa valley: 26th Annual Institute on Lake Superior Geology, Eau Claire, WI, 123 p.
Morey, G.B., 1999. High-grade iron ore deposits of the Mesabi Range, Minnesota-product of a continental-scale Proterozoic growndwater flow system. Econ. Geol. 94, 133–142.
NICE (Northern Interior Continental Evolution), 2006. Geologic terrane map of Precambrian basement rocks in Minnesota, Wisconsin and Iowa. http://www.mngs.umn.edu/nicegeo/niceimgs.htm.
Ojakangas, R.W., 1994. Sedimentology and provenance of the early Proterozoic Michigamme Fm. and Goodrich Quartzite, N. Michigan-regional stratigraphic implications and suggested correlations. U.S. Geol. Survey Bull. 1904-R.
Ojakangas, R.W., Morey, G.B., Southwick, D.L., 2001. Paleoproterozoic basin development and sedimentation in the Lake Superior region, North America. Sedimentary Geol. 141–142, 319–341.
Peterman, Z.E., Day, W.C., 1989. Early Proterozoic activity on Archean faults in the western Superior Province: evidence from pseudotachylyte. Geology 17, 1089–1092.
Pettijohn, F.J., 1943. Basal Huronian conglomerates of the Menomonee and Calumet districts, Michigan. J. Geol. 51, 387–397.
Percival, J.A., Sanborn-Barrie, M., Skulski, T., Stott, G.M., Helmstaedt, H., White, D.J., 2006. Tectonic evolution of the western Superior province from NATMAP and Lithoprobe studies. Can. J. Earth Sci. 43, 1085–1117.
Percival, J.A., 2007,4. Eo-to Mesoarchean Terranes of the Superior Province and Their Tectonic Context. Developments Precambr. Geol. v. 15, 1065–1085.
Pufahl, P.K., Hiatt, E.E., Stanley, C.R., Morrow, J.R., Nelson, G.J., Edwards, C.T., 2007. Physical and chemical evidence of the 1850 Ma Sudbury impact event in the Baraga Group, Michigan. Geology 35, 827–830.
Rasmussen, B., Bekker, A., Fletcher, I.R., 2013. Correlation of Paleoproterozoic glaciations based on U-Pb zircon ages for tuff beds in the Transvaal and Huronian Supergroups. Earth Planet. Sci. Lett. 382, 173–180.
Riley, N.A., 1947. Structural petrology of the Baraboo quartzite. J. Geol. 55, 453–475.
Renne, Paul R., et al., 1998. Intercalibration of standards, absolute ages and uncertainties in 40Ar/39Ar dating. Chem. Geol. 145, 117–152.
Romano, D., Holm, D.K., Foland, K.A., 2000. Determining the extent and nature of Mazatzal-related overprinting of the Peokean orogenic belt in the southern Lake Superior region, north-central USA. Precambr. Res. 104, 25–46.
Roscoe, S.M., 1969. Huronian rocks and uraniferous conglomerates. Geol. Surv. Can. Pap. 68–40, 205 p.
Roscoe, S.M., Card, 1993. The reappearance of the Huronian in Wyoming: rifting and drifting of ancient continents. Canadian J. Earth Sci. 30, 2475–2480.
Schmitz, M.D., Schoene, B., 2007. Derivation of isotope ratios, errors and error correlations for U-Pb geochronology using ^{205}Pb-^{235}U-(^{233}U)-spiked isotope dilution thermal ionization mass spectrometric data. Geochem. Geophys. Geosystems (G^3) 8, Q08006. https://doi.org/10.1029/2006GC001492.
Schmitz, M.D., Wirth, K.R. and Craddock, J.P., 1995. Major and trace element geochemistry of early Proterozoic mafic dykes of northern Minnesota and southwestern Ontario: Physics and Chemistry of Dykes, G. Baer & A. Heimann (Eds.), p. 219–236.
Schmitz, M.D., Southwick, D.L., Bowring, S.A., Boerboom, T.R., Wirth, K.R., 2006. High-precision U-Pb geochronology in the Minnesota River Valley subprovince and its bearing on the Neoarchean to Paleoproterozoic evolution of the southern Superior Province. Geol. Soc. Am. Bull. 118, 82–93.
Schneider, D.A., Holm, D.K., Lux, D.R., 1996. On the origin of early Proterozoic gneiss domes and metamorphic nodes, northern Michigan. Can. J. Earth Sci. 33, 1053–1063.
Schneider, D.A., Holm, D.K., O'Boyle, C., Hamilton, M., Jercinovic, M., 2004. Paleoproterozoic development of a gneiss dome corridor in the southern Lake Superior region, USA. Geol. Soc. Am. Spec. Pap. 380, 339–357.
Schultz, K.J., Cannon, W.F., 2007. The Penokean orogeny in the Lake Superior region. Precambr. Res. 157, 4–25.
Schultz-Ela, D.D., Hudleston, P.J., 1991. Strain in an Archean greenstone belt of Minnesota. Tectonophysics 190, 233–268.
Schwartz, G.M., 1942. Concretions of the Thomson Fm., Minnesota. Am. J. Sci. 240, 491–499.
Sims, P.K., Card, K.D., Morey, G.B., Peterman, Z.E., 1981. The Great Lakes tectonic zone-a major crustal structure in central North America. Geol. Soc. Am. Bull. 91, 690–698.
Sims, P.K., 1990, Geologic map of Precambrian rocks of Neillsville-Stevens Point area, central Wisconsin: U.S. Geological Survey Map I-1926, (1:100,000).
Smith, M.E., Singer, B.S., Carroll, A.R., Fournelle, J.H., 2006. High resolution calibration of Eocene strata: 40Ar/39Ar geochronology of biotite in the Green River Formation. Geology 34, 393–396.
Southwick, D.L., Day, W.C., 1983. Geology and petrology of Proterozoic mafic dykes, north-central Minnesota and western Ontario. Can. J. Earth Sci. 20, 622–638.
Southwick, D.L., Halls, H.C., 1987. Compositional characteristics of the Kenora-Kabetogama dyke swarm (Early Proterozoic), Minnesota and Ontario. Can. J. Earth Sci. 24, 2197–2205.
Southwick, D.L., Chandler, V.M., 1996. Block and shear-zone architecture of the Minnesota River Valley sub-province: implications for late Archean accretionary tectonics. Can. J. Earth Sci. 26, 2145–2158.
Southwick, D.L., Morey, G.B., McSwiggen, P.L., 1988. RI-37 Geologic Map (Scale 1: 250, 000) of the Penokean Orogen, Central and Eastern Minnesota, and Accompanying Text.
Stacey, J.S., Kramers, J.D., 1975. Approximation of terrestrial lead isotope evolution by a two-stage model. Earth Planet. Sci. Lett. 26, 207–221.
Stein, C.A., Stein, S., Merino, M., Keller, G.R., Flesch, L.M., Jurdy, D.M., 2014. Was the Midcontinent Rift part of a successful seafloor-spreading episode? Geophys. Res. Lett. 41, 1465–1470.
Sun, W.W., Jackson, M., Craddock, J.P., 1993. Relationship between remagnetization, magnetic fabric and deformation in Paleozoic carbonates. Tectonophysics 221 (3), 61–366.

Thomson, S.N., Gehrels, G.E., Ruiz, J., Buchwaldt, R., 2012. Routine low-damage U-Pb dating of apatite using laser ablation-multicollector-ICPMS. Geochem. Geophys. Geosyst. 13, Q0AA21. https://doi.org/10.1029/2011GC003928.
Tohver, E., Holm, D.K., van der Pluijm, B.A., Essene, E.J., Cambray, F.W., 2007. Late Proterozoic (geon 18 and 17) reactivation of the Neoarchean Great Lakes tectonic zone, northern Michigan: evidence from kinematic analysis, thermobarometry and Ar/Ar geochronology. Precambr. Res. 157, 144–168.
Turner, F.J., 1953. Nature and dynamic interpretation of deformation lamellae in calcite of three marbles. Am. J. Sci. 251, 276–298.
Turner, F.J., 1962. Compression and tension axes deduced from (0112) Twinning in calcite. J. Geophys. Res. 67, 1660.
Vallini, D.A., Cannon, W.F., Schulz, K.J., McNaughton, N.J., 2007. Thermal history of low metamorphic grade Paleoproterozoic sedimentary rocks of the Penokean orogen, Lake Superior region: evidence for a widespread 1786 Ma overprint based on xenotime geochronology. Precambr. Res. 157, 169–187.
van der Pluijm, B.A., Craddock, J.P., Graham, B.R., Harris, J.H., 1997. Paleostress in cratonic North America: Implications for deformation of continental interiors. Science 277, 794–796.
Van Hise, C.R., Leith, C.K., 1911. The Geology of the Lake Superior Region (No. 52). Government Printing Office, US.
Van Schmus, R., 1976. Early and Middle Proterozoic history of the Great Lakes area, North America. Royal Soc. London Philosophical Trans. 280, 605–628.
Van Schmus, W.R., 1980. Chronology of igneous rocks associated with the Penokean orogen on Wisconsin. Geol. Soc. Am. Spec. Pap. 182, 159–168.
Van Schmus, W.R., Bickford, M.E., 1981. Proterozoic chronology and evolution of the mid-continent region, North America. In: Kroner, A. (Ed.), Precambrian Plate Tectonics. Elsevier, Amsterdam, pp. 261–296.
Van Wyck, N., Johnson, C.M., 1997. Common lead, Sm-Nd, and U-Pb constraints on petrogenesis, crustal architecture, and tectonic setting of the Penokean orogeny (Paleoproterozoic) in Wisconsin. Geol. Soc. Am. Bull. 109 (7), 799–808.
Van Wyck, N., Norman, M., 2004. Detrital zircon ages from early Proterozoic quartzites, Wisconsin, support rapid weathering and deposition of mature quartz arenites. J. Geol. 112, 305–315.
Vervoort, J.D., Wirth, K., Kennedy, B., Sandland, T., Harpp, K.S., 2007. The magmatic evolution of the Midcontinent Rift: new geochronologic and geochemical evidence from felsic magmatism. Precambr. Res. 157, 235–268.
Wartman, Jakob, Craddock, J.P., Wirth, K.W., Medaris, G., Vervoort, J.D., Davidson, C., 2007. Detrital zircon provenance and structural geology of the Hamilton Mound inlier, central WI: 53rd Institute on Lake Superior Geology, p. 87.
Wenk, H.-R., Takeshita, T., Bechler, E., Erskine, B.G., Matthies, S., 1987. Pure Shear and Simple Shear Calcite Textures. Comparison of Experimental, Theoretical and Natural Data. J. Struct. Geol. 9, 731–745.
Westjohn, D.B., 1978. Finite Strain Study in the Precambrian Kona Fm., Marquette County. Michigan State University, Michigan, pp. 72 M.S. thesis.
Whitmeyer, S.J., Karlstrom, K.E., 2007. Tectonic model for the Proterozoic growth of North America. Geosphere 3, 220–259.
Wilks, M.E., Nisbet, E.G., 1988. Stratigraphy of the Steep Rock Group, northwest Ontario: a major Archaean unconformity and Archaean stromatolites. Can. J. Earth Sci. 25, 370–391.
Wunderman, R.L., Wannamaker, P.E., Young, C.T., 2018. Architecture of the hidden Penokean terrane suture and Midcontinent rift system overprint in eastern Minnesota and western Wisconsin from magnetotelluric profiling. Lithosphere 10, 291–300.
Young, G.M., 1973. Tillites and aluminous orthoquartzites as possible time markers for middle Precambrian (Aphebian) rocks of North America. In: Huronian Stratigraphy and Sedimentation. Geological Association of Canada Special Paper 12, pp. 97–128.
Young, G.M., 1983. Tectono-sedimentary history of early Proterozoic rocks of the northern Great Lakes Region. In: Medaris, L.G. (Ed.), Early Proterozoic Geology of the Great Lakes Region. Geological Society of America, pp. 15–32.